M.Sc. Huajie Yin

Thermal and Dynamic Glass Transition in Ultrathin Films of Homopolymers and a Miscible Polymer Blend

BAM-Dissertationsreihe • Band 117
Berlin 2014

Die vorliegende Arbeit entstand an der BAM Bundesanstalt für Materialforschung und -prüfung.

Impressum

Thermal and Dynamic Glass Transition in Ultrathin Films of Homopolymers and a Miscible Polymer Blend

2014

Herausgeber:
BAM Bundesanstalt für Materialforschung und -prüfung
Unter den Eichen 87
12205 Berlin
Telefon: +49 30 8104-0
Telefax: +49 30 8112029
E-Mail: info@bam.de
Internet: www.bam.de

Layout: BAM-Referat Z.8

ISSN 1613-4249
ISBN 978-3-9816380-5-9

THERMAL AND DYNAMIC GLASS TRANSITION IN ULTRATHIN FILMS OF HOMOPOLYMERS AND A MISCIBLE POLYMER BLEND

vorgelegt von
Master of Polymer Science
Huajie Yin
aus Shanghai, VR China

von der Fakultät III − Prozesswissenschaften
der Technischen Universität Berlin
zur Erlangung des akademischen Grades

Doktor der Naturwissenschaften
Dr. rer. nat.

genehmigte Dissertation

Promotionsausschuss:
Vorsitzender: Prof. Dr. rer. nat. Walter Reimers
Gutachter: Prof. Dr.-Ing. Manfred H. Wagner
Gutachter: Prof. Dr. rer. nat. Andreas Schönhals

Tag der wissenschaftlichen Aussprache: 26. März 2014

Berlin 2014
D 83

TABLE OF CONTENTS

ACKNOWLEDGMENTS

First and foremost, I would like to express my sincere gratitude to Prof. Dr. rer. nat Andreas Schönhals (BAM Federal Institute for Materials Research and Testing) for giving me the opportunity to work on the fantastic research topic. His guidance, support, encouragement and patience throughout my Ph.D. study have greatly helped me develop my scientific attitude, knowledge and skills. I also want to acknowledge the financial support from the German Science Foundation (DFG SCHO-470/20-1).

I would also like to thank Prof. Dr.-Ing. Manfred H. Wagner (Technische Universität Berlin) for being my supervisor and giving me a lot of valuable suggestions and comments on my research work.

I would like to thank Prof. Dr. Christoph Schick (Universität Rostock), Dr. Heiko Huth (Universität Rostock), Prof. Dr. Friedrich Kremer (Universität Leipzig) and Dr. Martin Tress (Universität Leipzig) for the helpful experimental assistance and fruitful discussions. They have provided me a lot of useful suggestions and guidance that helped me overcome many difficulties in the experimental work.

During my Ph.D. study, several researchers coming from different countries visited our lab. Special thanks to Prof. Dr. Simone Napolitano (Université Libre de Bruxelles), Dr. Daniele Cangialosi (Centro de Física de Materiales) and Dr. Mohammed M. Kummali (Centro de Física de Materiales) for the valuable discussions which have enriched my scientific knowledge and also for the pleasant and successful cooperation.

I would like to thank all former and current colleagues at BAM. I appreciate the help from Prof. Dr. Jörg F. Friedrich, Prof. Dr. Heinz Sturm, Dr. R. Mix, Dr. R.-D. Schulze, Mr. D. Neubert, Mrs. G. Hidde, Mr. F. Milczewski, Mr. B. Audi, Dr. D. Silbernagl and Dr. C. Brunero. I would like to thank Purv, Alaa, Christina, Marieke, Jing, Korinna, Anne, Sherif, Ning, Maalolan, Kishore, Kirti and Ranjit for advices and laughter over the years.

I would like to thank all my friends in China, Germany and some other countries for giving me encouragement to move forwards.

Finally, I am extremely grateful to my parents, Yajun Yin and Minhong Su for their love, sacrifice and support throughout my life. I would also like to sincerely thank my parents-in-law for their encouragement and belief in me. Most importantly, I would like to express my heartfelt thanks to my beloved wife, Wenjing Huang, who has patiently supported me to

achieve my goals and brought me so much happiness, courage and strength. I must also thank my adorable son, Jiawei Yin, for bringing me joy every day and giving me one more reason to keep strong. The thesis would not have been accomplished without the love, dedication and encouragement from my family.

ABSTRACT

Nowadays nanoscale thin polymer films are widely used in many fields like coatings, membranes, sensors, electronic devices and so on. Meanwhile, a lot of research work has evidenced the fact that many physical properties (glass transition, crystallization, dewetting, physical aging, etc.) of ultrathin polymer films show strong deviations from their bulk behavior. Since the aforementioned properties of polymer are closely related to their application and functionality, the discrepancies motivated us to obtain a more complete understanding of how nanoscale confinement affects the physical properties of polymer.

The research work presented in this thesis is focused on understanding how the free surface (air-polymer interface), the polymer-substrate interface and the film thickness influence the glass transition temperature (T_g) and the related segmental dynamics (α-relaxation process) in both homopolymers and miscible polymer blends of thin films. Complementary experimental techniques including Differential Scanning Calorimetry (DSC), Capacitive Scanning Dilatometry (CSD), Broadband Dielectric Spectroscopy (BDS) and Specific Heat Spectroscopy (SHS) have been used to investigate the glass transition of thin polymer films from both the thermodynamic and the kinetic point of view.

In the thesis the film thickness dependence of T_g and segmental dynamics of different thin polymer films have been investigated. For ultrathin polycarbonate (PC) films capped between two aluminum (Al) layers an increase of both the glass transition temperature (T_g) and Vogel temperature (T_0) with decreasing film thickness (d) was observed when the thickness became lower than 20 nm. The segmental relaxation time at a fixed temperature was found to increase for the ultrathin PC film of 19 nm measured by BDS, whereas no thickness dependency of the segmental dynamics was detected within the experimental error limit for the PC films supported on silicon dioxide (SiO_2) (10-192 nm) in the SHS measurements. These properties are discussed in terms of the thin film geometry and the relevant interfacial interaction between the polymer and the substrate. In the case of thin polystyrene (PS) films with high molecular weight (M_w), T_g is decreasing with reducing film thickness while the segmental dynamics is independent of film thickness. Moreover, the effects of the M_w and the annealing protocol performed on thin PS films on their T_g and segmental dynamics is studied. In the part of thin poly(vinyl methyl ether) (PVME) films, no thickness dependence of the segmental dynamics was observed in the SHS measurements. The last part of the thesis was concentrated on the thin films of a miscible polymer blend, PS/PVME with the weight fraction of 50/50. It

was observed that the segmental dynamics became faster with reducing the film thickness. This phenomenon is explained in terms of surface enrichment of PVME in the polymer blend system where PVME has a lower surface energy than PS. The segmental dynamics of the PVME-enriched free surface layer are faster than the bulk dynamics. Such free surface effect becomes so predominant with reducing the film thickness that it affects the segmental dynamics of the whole films detected by SHS using differential AC chip-based calorimetry. X-ray photoelectron spectroscopy (XPS) was used to probe the surface composition in order to confirm such surface enrichment phenomena.

ZUSAMMENFASSUNG

Dünne Polymerschichten im nanoskaligen Bereich finden heute in vielen Gebieten z. B. für Beschichtungen, als Membranen, für Sensoren oder in diversen elektronischen Geräten ihre Anwendung. Wissenschaftliche Studien belegen, dass viele physikalische Eigenschaften (Glasübergang, Kristallisation, Entnetzung, Alterung etc.) von ultradünnen Polymerschichten (Polymere in 1-dimensionaler räumlicher Begrenzung) stark von dem Verhalten im Volumen abweichen. Da die Eigenschaften eng mit der Verwendung und Funktionalität von Polymeren verknüpft sind, müssen die beobachteten Unterschiede in nanoskaliger Begrenzung genauer untersucht werden.

Die vorliegende Arbeit beschäftigt sich damit, wie die Oberfläche (Luft-Polymer-Grenzfläche), die Polymer-Substrat-Wechselwirkung und die Schichtdicke die Glasübergangstemperatur (T_g) und die segmentale Dynamik (α-Relaxationsprozess) in Homopolymeren und mischbaren Polymer-Blends in dünnen Schichten beeinflussen. Komplementäre experimentelle Methoden, wie Differential Scanning Calorimetry (DSC), Capacitive Scanning Dilatometry (CSD), Breitbandige Dielektrische Spektroskopie (BDS) und Spezifische Wärme Spektroskopie (SHS) wurden angewendet, um den Glasübergang der dünnen Polymerschichten aus der thermodynamischen und kinetischen Sicht zu untersuchen.

In dieser Arbeit werden die Glasübergangstemperatur und die segmentale Dynamik von ultradünnen Polymerschichten in Abhängigkeit der Schichtdicke untersucht. Für ultradünne Polycarbonatschichten (PC-Schichten, dünner als 20 nm) zwischen zwei Aluminiumschichten wurde ein Anstieg von der Glasübergangstemperatur (T_g) als auch der Vogel Temperatur (T_0) mit abnehmender Schichtdicke beobachtet. BDS-Messungen zeigten einen Anstieg der segmentalen Relaxationszeit für ultradünne PC-Schichten. In den SHS-Messungen für die Siliciumdioxid (10-192 nm) basierten PC-Schichten konnte unter Einbeziehung des experimentellen Fehlers keine Abhängigkeit der segmentalen Dynamik von der Schichtdicke festgestellt werden. Diese Eigenschaften werden im Hinblick auf die Geometrie der dünnen Schichten und die relevanten Wechselwirkungsenergien zwischen dem Polymer und dem Substrat diskutiert. Im Falle von dünnen Polystyrolschichten (PS-Schichten) mit hohem Molekulargewicht (M_w) sinkt die Glasübergangstemperatur T_g mit Verringerung der Schichtdicke. Die segmentale Dynamik hängt jedoch nicht von der Stärke der Schichtdicke ab. Darüber hinaus werden für dünne PS-Schichten die Auswirkungen des Molekulargewichts M_w und Temperbedingungen auf T_g und die segmentale Dynamik untersucht. Im Bereich der

dünnen Polyvinylmethyletherschichten (PVME-Schichten) konnte mittels SHS keine Abhängigkeit der segmentalen Dynamik von der Schichtdicke aufgezeigt werden. Der letzte Teil dieser Arbeit beschäftigt sich mit dünnen Schichten mischbarer Polymer-Blends mit einem Gewichtsteil von 50/50 PS/PVME. Es wurde eine Beschleunigung der segmentalen Dynamik mit geringerer Schichtdicke beobachtet. Dieses Phänomen wird mit der Oberflächenanreicherung von PVME, welches eine niedrigere Oberflächenenergie als PS aufweist, in das Polymer-Blend-System erklärt. Die segmentale Dynamik der mit PVME angereicherten freien Oberflächenschicht ist schneller als die Volumen-Dynamik. Durch die Verringerung der Schichtdicke werden diese freien Oberflächeneffekte so dominant, dass sie die gesamte segmentale Dynamik der Schichten von SHS (differenzieller AC Chip-basierten Kalorimetrie) erkennbare beeinflussen. Mittels Röntgenphotoelektronenspektroskopie (XPS) konnte die Oberflächenzusammensetzung des Films ermittelt und so die Phänomene der Oberflächenanreicherung verifiziert werden.

1 INTRODUCTION

Nowadays a lot of research work has been carried out on thin polymer films, which is motivated in multiple ways. From the technological point view, thin polymer films are widely used in coating industry, microelectronic devices driven by the potential benefit of miniaturization and also innovative organic devices like organic field-effect transistor [1,2]. From the scientific point of view, many properties of thin polymer films with thickness comparable to the radius of gyration of the polymer show strong deviation from their bulk properties like the crystallization behavior [3], the dewetting phenomenon [4], the glass transition temperature [5,6], the physical aging [7], the compliance [8], the relaxation dynamics [9], etc. A simple scaling down assumption is limited. If a more complete understanding of the structure and dynamics in thin polymer films is achieved, the functionality of many innovative devices can be further developed. In spited of the large amount of data, a general theory to describe the effects of 1-dimensional spatial confinement (film thickness at the nanoscale) on the properties of polymers has not been developed yet.

The glass transition as one of the deepest and most interesting unsolved problems in solid state physics [10] is of great scientific interest and critical technical importance. The research work discussed in this thesis will be specifically focused on understanding how the surface/interface and the film thickness influence the glass transition temperature (T_g) and the related segmental dynamics (α-relaxation process) in both homopolymers and miscible polymer blends of thin films. Complementary experimental techniques including Differential Scanning Calorimetry (DSC), Capacitive Scanning Dilatometry (CSD), Broadband Dielectric Spectroscopy (BDS) and Specific Heat Spectroscopy (SHS) have been employed to investigate the influence of the film thickness on the glass transition behavior of polymers from both the thermodynamic and the kinetic point of view. The glass transition temperature (T_g) at which a polymer changes from the equilibrium rubbery state to the out-of-equilibrium glassy state was measured by DSC and CSD. The segmental dynamics of a polymer in the equilibrium state was characterized by BDS and SHS.

After an introduction as Chapter 1, an overview of the glass transition and the related relaxation behavior in both homopolymers and miscible polymer blends is provided in Chapter 2. It begins with the discussion of bulk polymers, covering the topics of the glass transition temperature, the segmental dynamics, the dynamic heterogeneity and some models of the glass transition in both homopolymers and binary miscible polymer blends. Following

this, a review of the thickness dependence of T_g and segmental dynamics in thin polymer films is presented, regarding different geometries (substrate supported and freely standing) and different materials (homopolymers and miscible polymer blends).

Chapter 3 provides fundamental information about the main experimental techniques, not only CSD and DSC which measure T_g but also BDS and SHS which probe the segmental dynamics of polymers.

Chapter 4 briefly introduces the methods and conditions to prepare and characterize the samples, the materials used in the study and the detailed description of sample preparation for the measurements.

Chapter 5 presents the main results and discussion of different polymeric systems under investigation. The first part addresses the influence of film thickness on the glass transition temperature and segmental dynamics of ultrathin polycarbonate (PC) films by using BDS, CSD and SHS. For ultrathin PC films capped between two aluminum (Al) layers an increase of T_0 as well as T_g with decreasing film thickness was observed when the thickness became lower than 20 nm. Moreover, the segmental relaxation time at a fixed temperature was found to increase for ultrathin PC films in the dielectric measurements, whereas no thickness dependency of the segmental dynamics was detected within the experimental error limit for the PC films supported on SiO_2 (10-192 nm) in the calorimetric measurements. These properties are discussed in terms of the thin film geometry as well as the relevant interfacial interaction between the polymer and the substrate. In the second part it is demonstrated that in thin polystyrene (PS) films with high molecular weight (M_w) the glass transition temperature is decreasing with reducing film thickness while the segmental dynamics is independent of the film thickness. Moreover, the influence of the M_w and the annealing protocol performed on thin PS films on their T_g and segmental dynamics is investigated. The third part provides the study on the segmental dynamics in thin poly(vinyl methyl ether) (PVME) films investigated by SHS. No thickness dependence of the segmental dynamics was observed. The last part is focused on the thin films of miscible polymer blend, PS/PVME with the weight fraction of 50/50. It was observed that the segmental dynamics became faster with reducing the film thickness. This phenomenon is explained in terms of surface enrichment of PVME in the polymer blend system where PVME has a lower surface energy than PS. The segmental dynamics of the PVME-enriched free surface layer are faster than the bulk dynamics. Such free surface effect becomes so predominant with the reduction of film thickness that it has

great influence on the segmental dynamics of the whole films detected by SHS using differential AC chip-based calorimetry. X-ray photoelectron spectroscopy (XPS) was used to probe the surface composition in order to confirm such surface enrichment phenomena.

Finally, Chapter 6 summarizes the work related to the investigation of the glass transition temperature and segmental dynamics in thin polymer films.

2 BACKGROUNDS

2.1 Glass Transition and Segmental Dynamics in Bulk Homopolymers

2.1.1 Glass Formation and the Glass Transition Temperature

Upon cooling a glass-forming liquid or polymer to lower temperature without crystallizing, its density and viscosity increase, and the molecules move more and more slowly. At some temperature the characteristic time of molecular motions responsible for structural rearrangements becomes much longer than the timescale of the experiment. The liquid falls out of equilibrium. The resulting material is a glass in a non-equilibrium state without long-range order. The transition from the equilibrium liquid state to the solid-like glassy state is called thermal glass transition. It occurs over a given temperature range called the glass transition region. The temperature at the mid-point of this region is often defined as the glass transition temperature, T_g, which is generally determined as the temperature at the intersection of extrapolated tangent lines from the glassy region at lower temperatures and the liquid region at higher temperatures where the slope of the temperature dependence of characteristic thermodynamic quantities such as specific volume and enthalpy changes abruptly (but continuously) (Fig. 1). It is noteworthy to mention that the glass transition is not a true thermodynamic phase transition because the behavior as depicted in Fig. 1 does not involve discontinuous changes in any physical property [11,12]. Rather, it is a kinetic phenomenon. Moreover, T_g depends on the cooling rate. Upon faster cooling a glass-forming liquid falls out of the equilibrium state at a higher temperature than that observed in the case of slower cooling as shown in Fig. 1. Consequently, T_g increases with higher cooling rate.

Methods like differential scanning calorimetry (DSC) [13, 14], ellipsometry [15, 16], capacitive scanning dilatometry (CSD) [17,18], fluorescence technique [19], etc, can be used to measure the T_g at which a thermodynamic quantity (heat capacity, volume, density, etc.) undergoes a change in its temperature dependence. In the following discussion, T_g defined from such a thermodynamic point of view is called thermal T_g to differentiate it from dynamic T_g which is defined from a kinetic point of view. The dynamic T_g is directly related to the segmental dynamics of polymers. It will be discussed in the following Section 2.1.2 in detail.

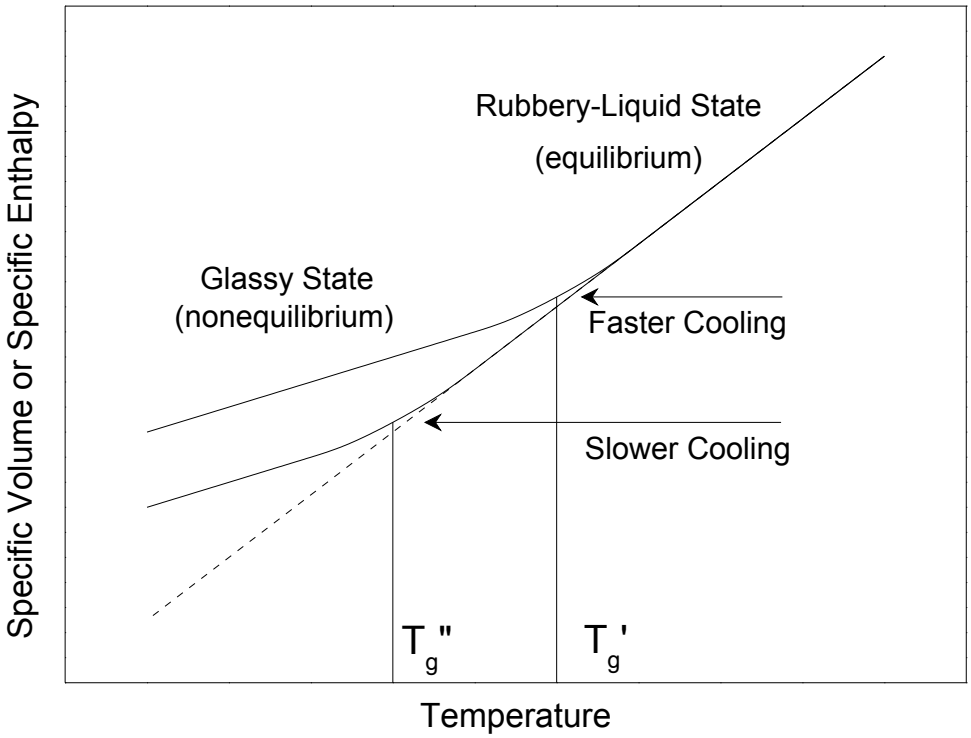

Fig. 1 *The general temperature dependence of specific volume or enthalpy for an amorphous polymer. The vertical lines denote T_g' and T_g'' for different cooling rates.*

2.1.2 Segmental Dynamics

It is well known that in the bulk a polymeric system can behave as an elastic solid, as a rubbery (viscoelastic) material which is highly deformable or as a melt in dependence on temperature. This is illustrated in Fig. 2 where the temperature dependence of the shear modulus is given schematically for an amorphous polymer. The polymeric system behaves like a glassy solid at low temperatures where the shear modulus is in the order of magnitude of 10^9 Pa. At the glass transition, the shear modulus drops down to the order of magnitude of 10^6 Pa. The step-like change is attributed to the glass transition and T_g can be estimated from it. For temperatures higher than T_g, the system shows rubberlike (viscoelastic) properties. The rubberlike plateau is due to chain entanglements that are formed for molecular weights higher than a critical value M_c. At even higher temperatures, the system flows like an ordinary liquid with the shear modulus of approximately zero. The complex mechanical behavior is due to different motional processes on a molecular level within the system such as localized fluctuations, segmental dynamics and collective chain motions involving the whole macromolecule.

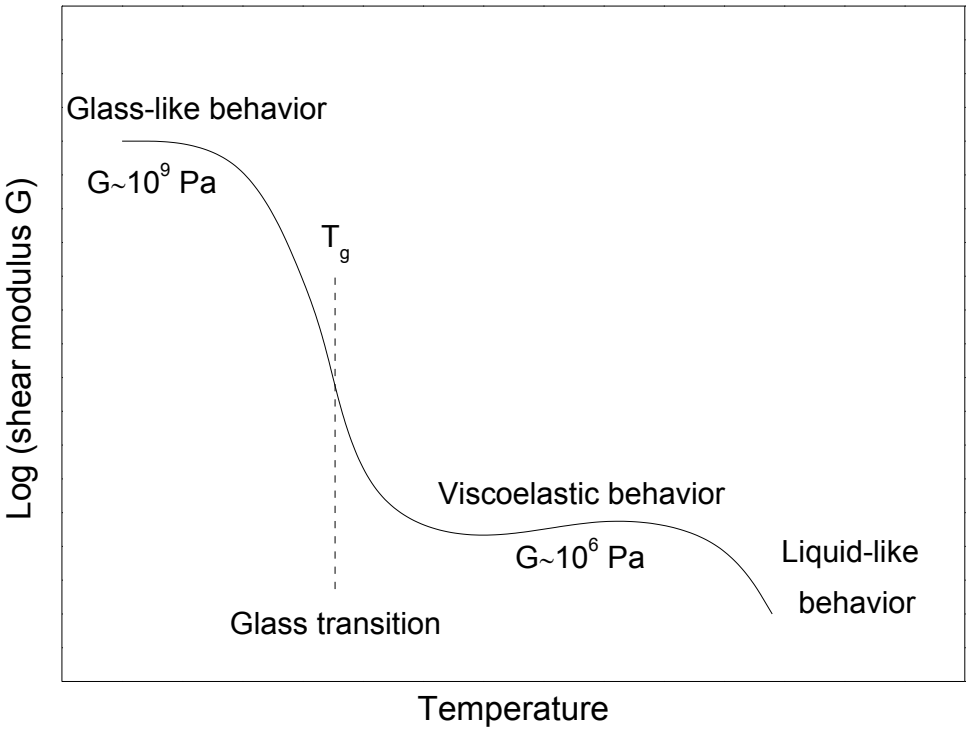

Fig. 2 *Schematic temperature dependence of the shear modulus for an amorphous polymer with a molecular weight higher than M_c. This figure was taken from Ref. 20.*

From the dynamic point of view, the thermal T_g is often alternatively identified as the temperature at which the viscosity reaches a value of $\eta = 10^{13}$ Poise or the segmental relaxation time is $\tau = 10^2$ s. Below thermal T_g, segmental motion is more or less frozen. Above T_g, the segmental dynamics get faster and faster with increasing temperature and the glass transition is regarded as a dynamic phenomenon in the equilibrium liquid. In the following discussion the term "dynamic glass transition" is associated with the segmental mobility- (relaxation time-) temperature behavior at constant pressure. A dynamic T_g corresponding to a known relaxation time can be determined by a variety of methods like dynamic mechanical analysis [21], light scattering [22], neutron scattering [23], nuclear magnetic resonance [24], specific heat spectroscopy [25] and especially broadband dielectric spectroscopy [26].

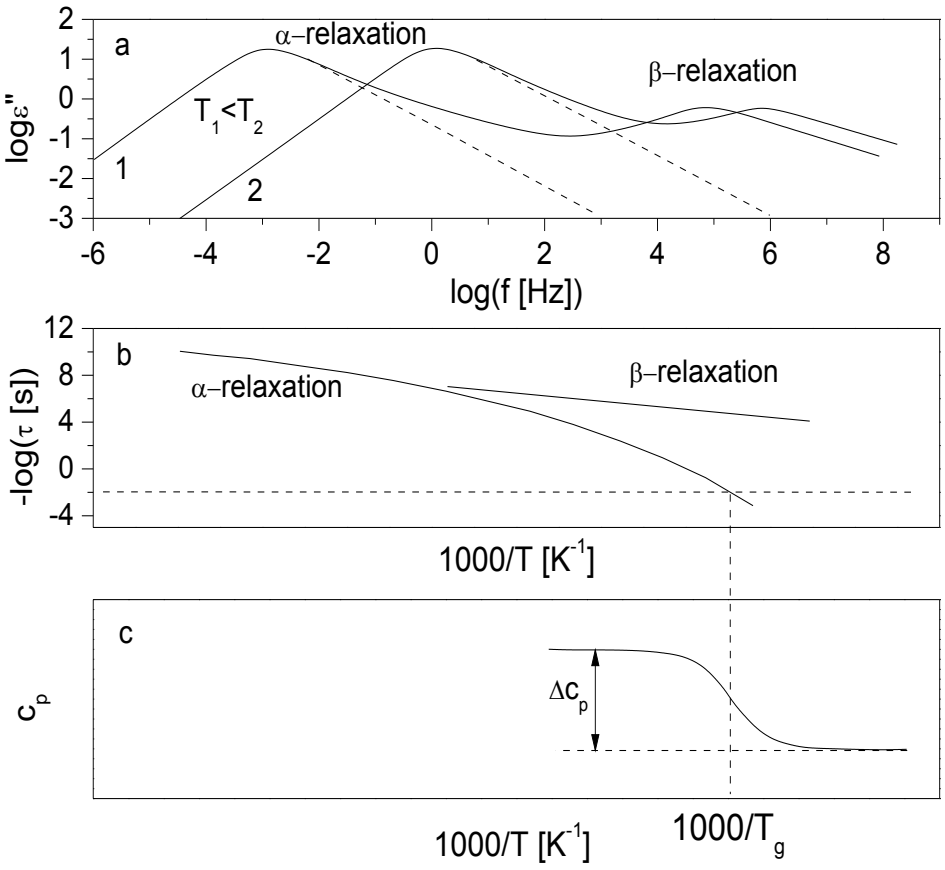

Fig. 3 *Schematic illustrations of the molecular dynamics of amorphous polymers at the glass transition. (a): Dielectric loss vs. frequency for two temperatures T_1 and T_2. Two relaxation processes, the α-relaxation (dynamic glass transition) and the β-relaxation, are indicated. (b): Relaxation map (relaxation rate vs. inverse temperature) for the α- and the β-relaxation processes. The former can be described by the VFT-equation (Equ. 1) and the latter follows the Arrhenius function (Equ. 3). (c): Specific heat capacity is plotted vs. inverse temperature. Thermal T_g is determined as the middle point temperature of the steplike change in the specific heat capacity. This figure was taken from Ref. 27.*

Fig. 3a gives a schematic overview about the different dynamical processes taking place in amorphous polymers using the dielectric loss as an example. At lower frequencies the alpha- (α-) relaxation process is observed, which is also called structural (primary) relaxation or dynamic glass transition [28]. In the case of amorphous polymers, the dynamic glass transition is related to segmental fluctuations. In the high temperature limit the segmental relaxation time τ has a typical value of about $\tau_\infty \approx 10^{-13}$ s. With decreasing temperature the relaxation time τ (frequency $f=(2\pi\tau)^{-1}$) increases strongly and its temperature dependence can be described by the empirical Vogel-Fulcher-Tammann- (VFT-) equation [29-31] (Fig. 3b):

$$f_{p,\alpha}(T) = \frac{1}{2\pi\tau_{p,\alpha}(T)} = f_\infty \exp\left(-\frac{DT_0}{T - T_0}\right) \quad (1)$$

where f_∞ is the frequency in the high temperature limit ($f_\infty=(2\pi\tau_\infty)^{-1}$) and T_0 denotes the Vogel temperature which is found 30-70 K below the thermal T_g. The frequency of maximal loss related to α-relaxation is defined as the α-relaxation rate $f_{p,\alpha}$ or α-relaxation time $\tau_{p,\alpha}=1/(2\pi f_{p,\alpha})$. D is the so-called fragility parameter and provides among others a useful quantity to classify glass-forming systems [32,33]. Polymers are called "fragile" if their $f_{p,\alpha}(T)$ dependence deviates strongly from Arrhenius-type behaviour and "strong" if $f_{p,\alpha}(T)$ is close to the latter. At the thermal T_g, $f_{p,\alpha}(T_g)$ has reached a typical value of ~10^{-2} Hz (Fig. 3b-c).

An analogous representation of the VFT-equation for the temperature dependence of the α-relaxation time of amorphous polymers is the Williams-Landel-Ferry- (WLF-) equation [34]:

$$\log(\alpha_T) = \log\left[\frac{\tau(\mathrm{T})}{\tau(\mathrm{T_R})}\right] = -\log\left[\frac{f(\mathrm{T})}{f(\mathrm{T_R})}\right] = -\frac{C_1(T - T_R)}{C_2 + T - T_R} \quad (2)$$

where α_T is a shift factor, C_1 and C_2 are constants and $\tau(T_R)$ is the relaxation time at a reference temperature T_R, which is often taken to be T_g with a typical value of $\tau(T_R)$~100 s. This equation is valid generally in a temperature range from T_g to T_g + 100 K [35]. Values of C_1 = 17.44 and C_2 = 51.6 K have been observed to approximately predict the temperature dependence of the relaxation times of a large number of glass formers [34-36]. The WLF equation can well describe the temperature dependence of the dielectric relaxation process in polymers [34]. The parameters in the WLF- and VFT- equations are related by $T_0 = T_g - C_2$, $DT_0 = C_1C_2/\log_{10}e$ and $f_\infty = \tau(T_g) \exp(-C_1/\log_{10}e)$ [36].

In addition to the α-relaxation process, a beta- (β-) relaxation process can be observed in the higher frequency range in Fig. 3a. The temperature dependence of the β-relaxation rate $f_{p,\beta}$ follows an Arrhenius-type equation (Fig. 3b):

$$f_{p,\beta}(T) = \frac{1}{2\pi\tau_{p,\beta}(T)} = f_\infty \exp\left(-\frac{E_A}{k_B T}\right) \quad (3)$$

where E_A is the activation energy and k_B is the Boltzmann constant. The β-relaxation in amorphous polymers is often assigned to rotational fluctuations of side group or other intramolecular fluctuations.

2.1.3 Models of the Glass Transition

Although the glass transition of glass-forming materials, including amorphous polymers, is a topical problem of condensed matter physics for a long time [10,11], there is no general accepted theoretical approach that can describe all aspects of the glass transition. Theories based on thermodynamic and kinetic arguments will be briefly introduced in order to discuss this phenomenon.

2.1.3.1 Free Volume Concept

The concept of free volume was proposed by Doolittle and Cohen [37-39]. The amount of free space in an amorphous polymer due to insufficient packing of the disordered chain segments in the amorphous state results in the free volume. Based on the concept of free volume (V_f), which is defined by

$$V_f = V - V_0 \tag{4}$$

where V is the actual volume and V_0 is the theoretical volume based on actual chemical structure and van der Waals radii, Doolittle developed following equation to describe the relation between viscosity and free volume [37]:

$$\eta = A\exp[\frac{B(V-V_f)}{V_f}] \tag{5}$$

where A and B are fitting parameters and η is viscosity. Further assuming that free volume increases linearly with temperature:

$$f = f_g + \Delta\alpha(T - T_g) \tag{6}$$

where f is the fractional free volume, $f=V_f/(V_f+V_0)$, f_g is the fractional free volume at T_g and Δα is the difference in thermal expansion coefficients above and below T_g. The Doolittle Equation (Equ. 5) can be used to rationalize the WLF-equation (Equ. 2) in the frame of free volume theory:

$$\log(\alpha_T) = \log[\frac{<\tau(\mathrm{T})>}{<\tau(\mathrm{T_R})>}] \approx \log[\frac{\eta(T)}{\eta(T_g)}] = \frac{B}{(1/\log(e))}(\frac{1}{f} - \frac{1}{f_g}) \quad (7)$$
$$= \frac{-(B/2.303 f_g)(T - T_g)}{f_g/\Delta\alpha + T - T_g} = \frac{-C_1(T - T_g)}{C_2 + T - T_g}$$

where C_1=B/2.303f_g and C_2=f_g/Δα.

The free volume model can be used to describe the temperature dependence of relaxation mechanisms like the α-relaxation time or viscosity. However, the fractional free volume cannot be determined a priori. It is noteworthy to mention that in such a qualitative model no characteristic length scale is involved.

2.1.3.2 Adam-Gibbs Theory

Adam and Gibbs developed a model of dynamic glass transition based on the central idea of cooperatively rearranging region (CRR) [40]. A CRR is defined as the smallest volume that can change its configuration independently from the neighboring regions. The temperature dependence of the relaxation process is related to the temperature dependence of the size of a CRR. The length scale of this cooperative dynamics region will increase with decreasing temperature and eventually reach the sample size at temperature T_2. The relaxation time of the system is given by

$$\frac{1}{\tau(T)} = A\exp(-\frac{S_C^*\Delta E}{k_B T S_C}) \quad (8)$$

where ΔE is a free energy barrier for a conformational change of a segment, S_C is the total configurational entropy and S_C^* is the critical configurational entropy related to the lower limit of the size of a CRR having at least two configurations, capable of performing a rearrangement from one configuration to another. The configurational entropy S_C can be related to the change of the specific heat capacity Δc_p at T_g by

$$S_c(T) = \int_{T_2}^{T} \frac{\Delta c_p}{T} dT \quad (9)$$

At lower temperature the size of CRRs is larger and the relaxation time of the system is also larger. It is worth mentioning that the Adam-Gibbs model does not provide information about the absolute size of a CRR at T_g.

In the frame of a fluctuation approach, the theory of Adam and Gibbs was extended by Donth [12,41]. A correlation length ξ or volume V_{CRR} of a CRR can be calculated from the height of the step in c_p and the temperature fluctuation δT of a CRR at T_g according to the following equation:

$$\xi^3 \sim V_{CRR} = \frac{k_B T_g^2 \Delta(\frac{1}{c_P})}{\rho \delta T^2} \tag{10}$$

where ρ is the density and $\Delta(1/c_p)$ is the step of the reciprocal specific heat capacity assuming $c_v \approx c_p$. δT can be extracted experimentally from the width of the glass transition [42,43]. Recently it is possible to estimate δT from broadband heat capacity spectroscopy [44,45]. Employing DSC [46] and SHS [47,48], the size of a CRR was estimated for several polymers to be in the range of 1-3 nm, which corresponds to 10-200 segments [28].

2.1.4 Dynamic Heterogeneity

Many experimental and theoretical studies [49-51] showed that the relaxation function of many complex systems deviates strongly from the simple exponential law [52]:

$$\Phi(t) = \exp[-\frac{t}{\tau_D}] \tag{11}$$

with a characteristic relaxation time τ_D, and often follows the stretched exponential or Kohlrausch-Williams-Watts- (KWW-) equation [53,54]:

$$\Phi(t) = \exp[-(\frac{t}{\tau_{KWW}})^{\beta_{KWW}}] \tag{12}$$

where τ_{KWW} is a characteristic time and β_{KWW} is the stretching parameter ($0 < \beta_{KWW} \leq 1$). For a typical fragile glass former, β_{KWW} decreases from near 1 at high temperature to about 0.5 near T_g [50].

Two different scenarios have been suggested to explain the nonexponential relaxation behavior. In the spatially homogeneous case, each molecule is assumed to relax nearly identically in an intrinsically non-exponential manner. In the case of heterogeneous dynamics, every local relaxation might be nearly exponential, while the relaxation time varies significantly among each other.

In the past 20 years, many experimental methods have been developed to test the two explanations. Dynamic heterogeneity has been widely studied using different experimental techniques like dielectric spectroscopy [55,56], nuclear magnetic resonance [57], second harmonic generation measurements [58,59], differential scanning calorimetry [42,60,61], fluorescence recovery after photobleaching [62] or translational and rotational probe diffusion [63], etc. Dynamic heterogeneity was observed through molecular dynamics simulation as well [64,65]. Most experiments show that the heterogeneous picture is more appealing [50].

2.2 Glass Transition and Segmental Dynamics in Bulk Miscible Polymer Blends

2.2.1 Miscibility of Binary Polymer-Polymer Blends

Miscible polymer blends are of practical importance. Compared to the difficulty of synthesizing new polymer species, blending is a simple and low-cost way to produce polymeric material with tunable properties. Polymer blend miscibility is one of the crucial factors which decide the final properties of the products.

The blend miscibility governed by the Gibbs free energy of mixing (ΔG_M) is defined as

$$\Delta G_M = \Delta H_M - T\,\Delta S_M \tag{13}$$

where ΔH_M and ΔS_M are the enthalpy and the entropy of mixing, respectively. In the frame of the classical Flory-Huggins theory of polymer miscibility based on a lattice model, the expression for the Gibbs free energy of mixing is proposed as [66]

$$\frac{\Delta G_M}{\mathrm{RT}} = \frac{\phi_A}{M_A}\ln\phi_A + \frac{\phi_B}{M_B}\ln\phi_B + \chi\phi_A\phi_B \tag{14}$$

where M_A and M_B are the molecular weights of polymer A and B, ϕ_A and ϕ_B are the volume fractions of component A and B, respectively, and χ is the interaction parameter between

component A and B. R is the universal gas constant and T is the absolute temperature. Polymer miscibility can be achieved if

$$\frac{\Delta G_M}{\mathrm{RT}} < 0 \tag{15}$$

and

$$\frac{\partial^2 \Delta G_M}{\partial \phi_{\mathrm{A}}^2} = \frac{\partial^2 \Delta G_M}{\partial \phi_{\mathrm{B}}^2} = \mathrm{RT}[\frac{1}{M_A \phi_A} + \frac{1}{M_B \phi_B} - 2\chi] > 0 \tag{16}$$

2.2.2 Dynamic Heterogeneity in Miscible Polymer Blends

Thermodynamically miscible polymer blends are known to be dynamically heterogeneous due to the presence of distinct dynamics in the regions very close to each other. The signatures of dynamic heterogeneities in miscible polymer blends are dual relaxation processes that reflect the component's segmental dynamics and additionally broadening of the relaxation spectra with respect to homopolymers. Increasing the dynamic asymmetry, i.e., by increasing the difference in the glass transition temperatures (ΔT_g) of the blend components, enhances the dynamic heterogeneity.

2.2.2.1 Dual Relaxation Processes

Many experimental techniques have been used to investigate the polymer miscibility. Among them, DSC is the most often used method and the criteria of the polymer miscibility is a single glass transition temperature, whose value is between the glass transition temperatures of the pure components in the blend. As discussed in Section 2.1, the α-relaxation process is correlated with the glass transition behavior. A single α-relaxation peak also indicates miscibility. From this point of view, experimental techniques capable of monitoring the relaxation processes like broadband dielectric spectroscopy are expected to provide valuable information on the local fluctuations of concentrations and on the local miscibility. In general both the α- and the β-relaxation processes will be modified in miscible polymer blends. The most sensitive process with regard to blending is the α-relaxation. The relaxation map for a miscible blend system is shown in Fig. 4a as an ideal case. A single α-relaxation process is located between the traces obtained for each component. The position of the relaxational trace of the polymer blend with the miscibility on the segmental level depends on the composition.

There are several models like the Fox [67] or the Gordon/Taylor equation [68] to describe the dependence of the glass transition temperature on the composition for a spatially homogeneous blend at such length scales, which can be found in standard textbooks of polymer science [69,70]. The correlation between a single DSC T_g and a single α-relaxation peak for a miscible polymer blend exists in some cases [71-80] where the α-relaxation dynamics of each component is close to each other which means the local segmental environment for both components is similar.

However, this is not always the case. Despite a single T_g determined by DSC for a polymer blend, two α-relaxation processes are observed in many cases. The segmental dynamics in a thermodynamically miscible polymer blend show dual relaxation processes in the relaxation map (Fig. 4b), with the fast mode reflecting relaxations of the lower-T_g component and the slow one reflecting relaxations of the higher-T_g component. The location of both processes depends on the macroscopic composition of the blend. Poly(vinylethylene)/polyisoprene (PVE/PI) blend system is miscible according to DSC measurements, while two α-relaxation processes have been probed by means of dielectric spectroscopy [81]. The dielectric loss curve in the blend is clearly bimodal, as indicated in Fig. 5. The faster process is discussed to originate from the lower T_g component (PI) and its relaxation rate is very close to that of the corresponding neat polymer at the same temperature. The slower process is related to the higher T_g component (PVE) and is much faster than the α-relaxation of the corresponding homopolymer in the unblended state. This effect has been observed for a variety of miscible binary polymer blends [82-95].

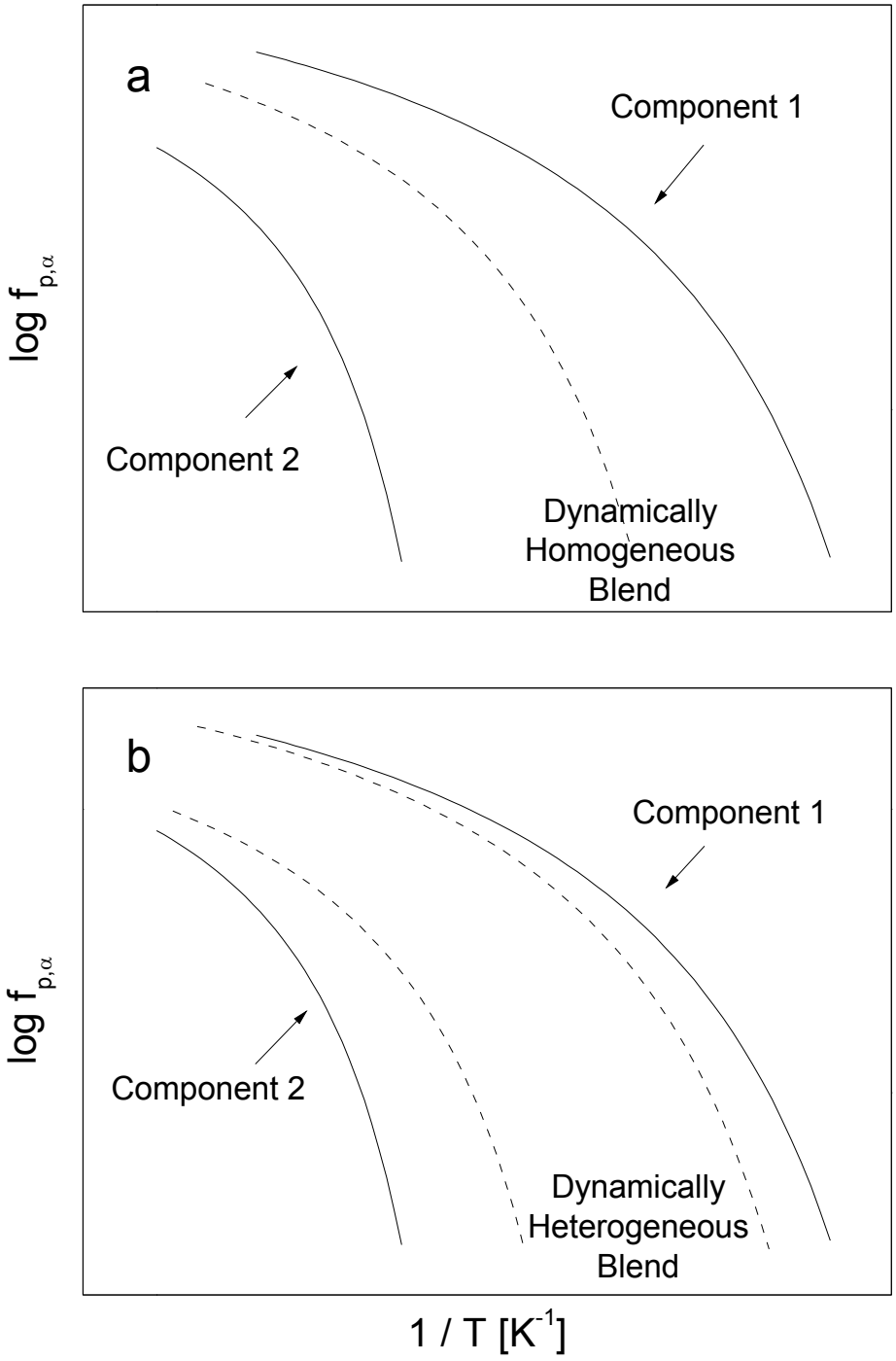

Fig. 4 *Schematic representation (relaxation map) of the temperature dependence of the α-relaxation rate for a thermodynamically miscible binary polymer-polymer blend: (a) Dynamically homogeneous blend with a single α-relaxation process as an ideal case. (b) Dynamically heterogeneous blend with dual relaxation processes reflecting component's segmental dynamics. This figure was reproduced from Ref. 96.*

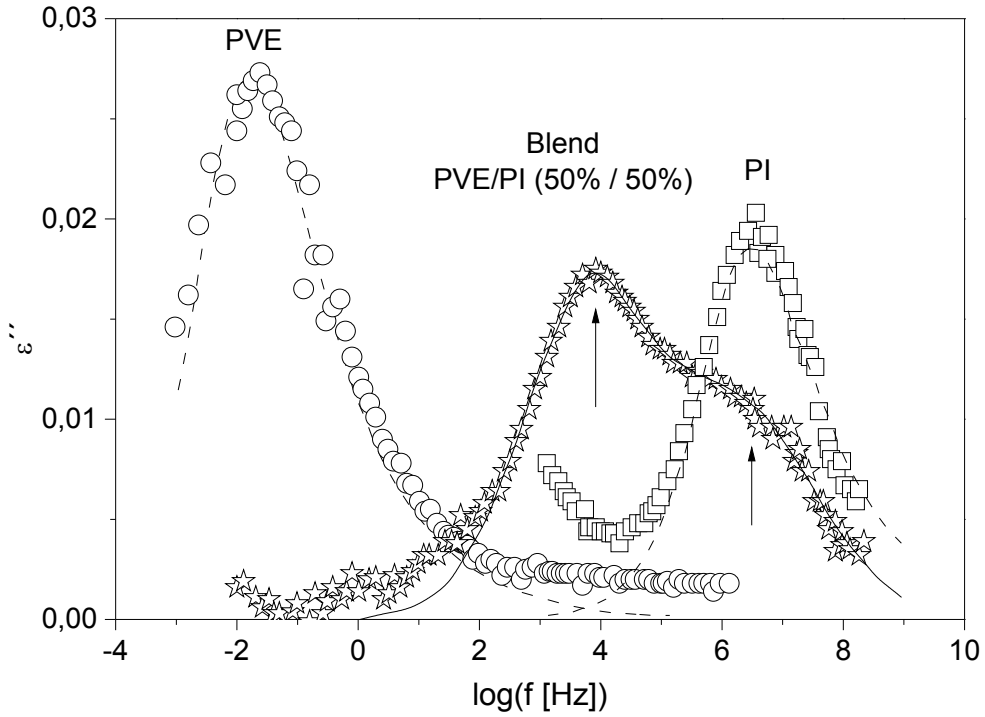

Fig. 5 *Frequency dependence of the dielectric loss at 270 K for PI, PVE and their blend, PVE/PI, at a composition of 50/50: pure PVE (circles); pure PI (squares); blend PVE/PI (stares). Lines are estimated contributions of the dynamic glass transition. Two segmental relaxation processes can be resolved in the PI/PVE blend, which exhibit only one T_g in DSC measurement. This figure was taken from Ref. 97. The original data were taken from Ref. 81.*

2.2.2.2 Broadening of Dielectric Spectra

It is known for a long time that the relaxation function measured for a miscible blend is considerably broadened compared to the spectra of the pure polymers [76,98]. This is shown for a miscible blend of polystyrene (PS) and poly(vinyl methyl ether) (PVME) in Fig. 6 as an example [99-101]. Compared to PVME the dipole moment of PS is weak and therefore the contribution of PS to the dielectric loss of the blend is negligible. In other words the fluctuations of PVME are selectively monitored by dielectric spectroscopy whereas the fluctuations of the PS segments are dielectrically invisible. For the blend (Fig. 6a) the loss peak is much broader than that for the single component PVME (Fig. 6b). The broadening of relaxation spectra as compared to the homopolymers is not only observed for the PS/PVME system. This further demonstrated by many other experimental work performed on different polymer blend systems [94,102]. Such broadening effects can be explained in terms of concentration fluctuation [101], which will be discussed in Section 2.2.4.

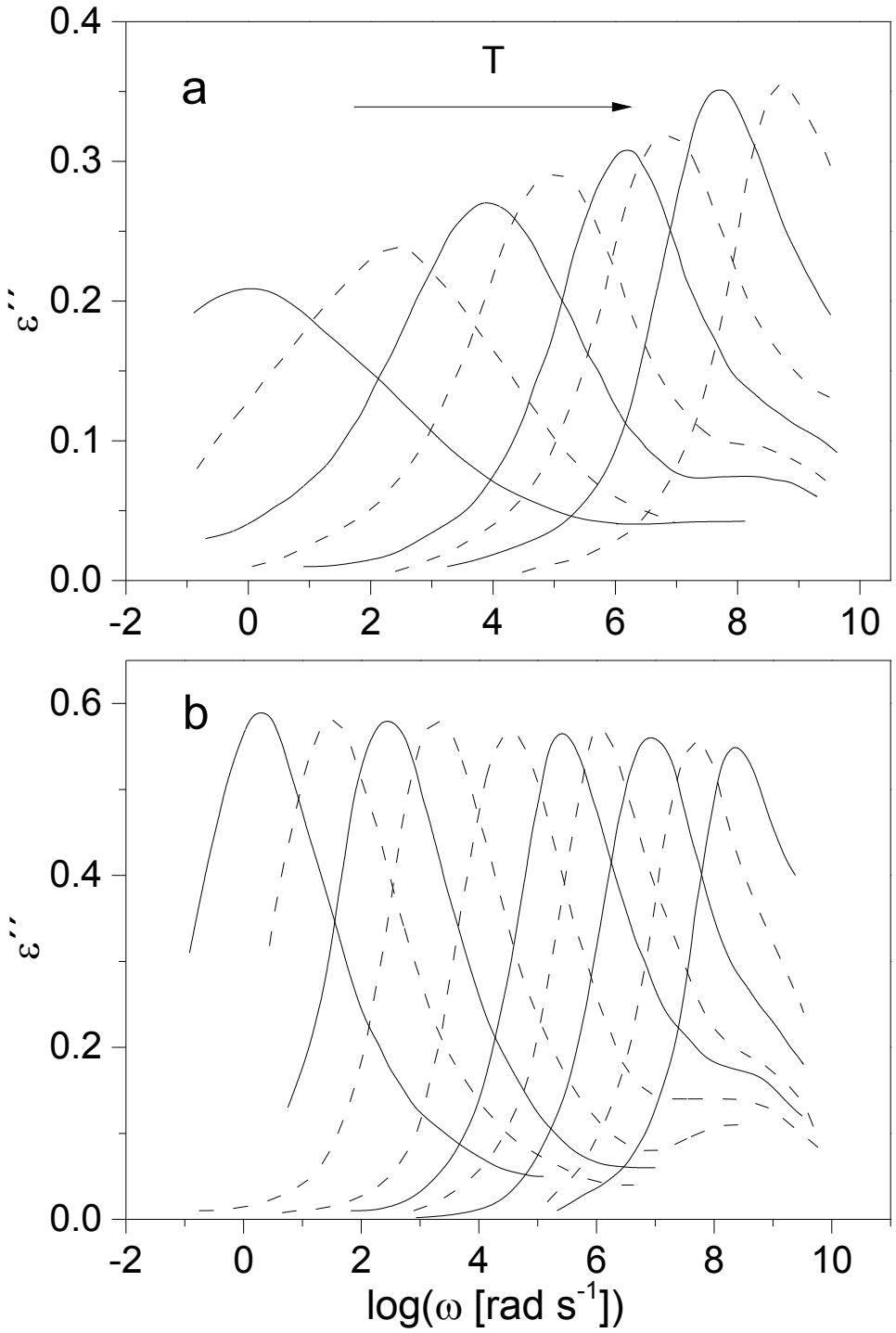

Fig. 6 *Dielectric loss for the PVME/PS blend at a composition of 65% PVME / 35% PS. (a) Dielectric loss versus frequency for PVME/PS blend: (T=263 K, 273 K, 283 K, 293 K, 308 K, 318 K, 338 K, 368 K). (b) Dielectric loss versus frequency for pure PVME: (T=253 K, 258K, 263 K, 268 K, 278 K, 288 K, 298 K, 308 K, 328 K, 348 K). This figure was taken from Ref. 103. The original data were taken from Ref. 104.*

2.2.3 Surface Enrichment

In a binary polymer blend system, the compositions at the interfaces are generally different from that in the bulk due to the different surface energies of the two components. The component with lower surface energy will be enriched at the surface to minimize the total free energy of the system. A schematic diagram of a surface of a polymer blend is shown in Fig. **7**.

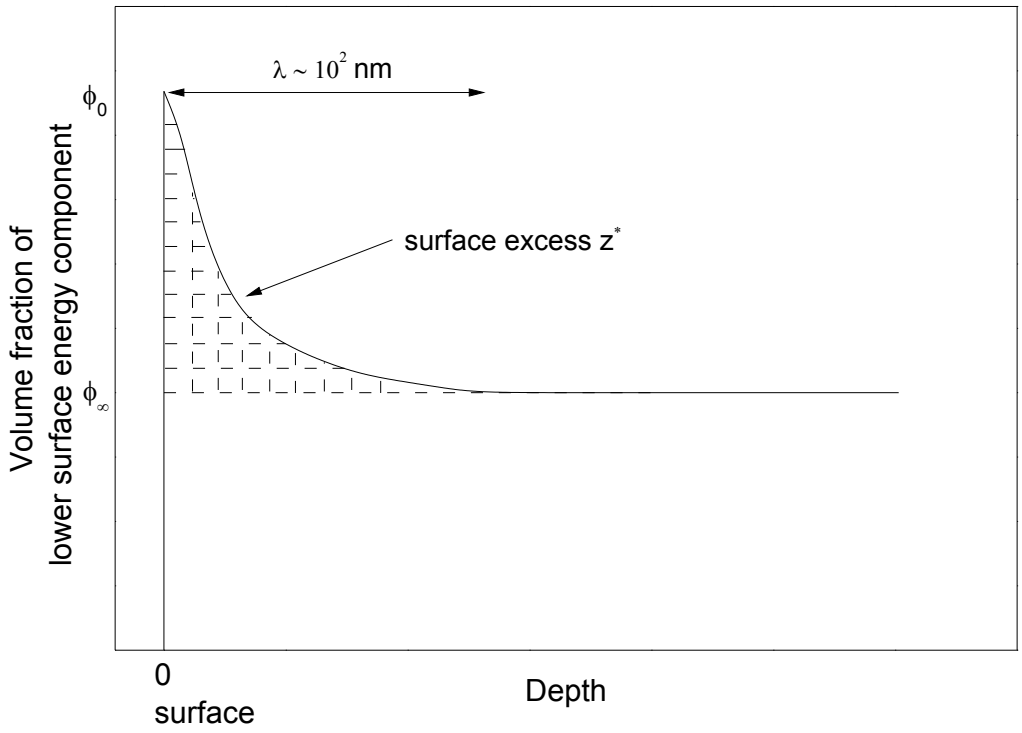

***Fig.** 7 Schematic diagram of the surface composition profile in a binary polymer blend. This figure was reproduced from Ref. 105.*

In general, the composition profile ϕ(z) which describes the way in which the composition changes from the surface composition (ϕ_0) to the bulk composition (ϕ_∞) over some characteristic length λ in the order of magnitude of 10^2 nm. The tendency for the lower surface energy component to preferentially segregate at the air-polymer surface can be quantified using the quantity called integrated surface excess, Z*, which is defined once the system reaches thermodynamic equilibrium as [105]

$$Z^* = \int_0^\infty [\phi(\mathrm{z}) - \phi_\infty] dz \qquad (17)$$

When Z*=0 there is no segregation. A positive value of Z* indicates that the investigated component has segregated to the surface preferentially. A negative value indicates that the component is depleted from the surface.

2.2.4 Theories of Segmental Dynamics in Miscible Polymer Blends

The molecular origins of distinct segmental dynamics in miscible polymer blends (A and B binary system) have been the subject of considerable debate in recent years. Most researchers agree that the molecular fluctuations of a segment of polymer A in binary blend is controlled by the local composition in some volume around the selected segment. This local concentration might be quite different from the macroscopic blend composition which will give rise to a relaxation time different from the mean relaxation time.

Different models have been developed to describe such effects in miscible polymer blends. In the following section, temperature driven concentration fluctuations (TCF) and self-concentration (SC) models will be briefly introduced.

2.2.4.1 Temperature Driven Concentration Fluctuations

Zetsche and Fischer [101, 106] assumed that there are many dynamically heterogeneous domains in polymer blends and different domains have different compositions, which follow a Gaussian distribution centered around the global composition. Size of the heterogeneous domains is related to a length scale ξ characterized by the global composition in the Donth model [12,41]. Kumar et al. modified Fischer's TCF model by correlating the size of heterogeneous nanodomains with their local composition in a self-consistent manner [107-109].

The TCF models are able to describe the broadening of the relaxation function as temperature approaches the average glass transition temperature $<T_g>$. The main problem of that approach is that these models have no explanation for the heterogeneous behaviour. Moreover the estimated length scales for glass transition $\xi \sim V_{CRR}^{1/3}$ grows too strongly as temperature decreases towards $<T_g>$ and can reach larger than 10 to 20 nm. This is much too large than expected for the glass transition. A more detailed discussion can be found for instance in Ref. 98.

2.2.4.2 Self-Concentration

The idea of self-concentration in polymer blends was mainly developed by Lodge and McLeish [110] based on earlier works of Kornfield et al. [111,112]. In a miscible binary polymer-polymer blend (A and B components), a local region around an A segment is always somewhat enriched in A segments compared to the bulk composition, ϕ, and similarly for B. This is due to chain connectivity effects. Each segment experiences a different average local environment. As a result, the local dynamics of each polymer exhibit different dependences on temperature and overall composition. In the LM model for a binary blend with A and B components, the effective local concentration can be described by $\phi_{eff,A}$ and $\phi_{eff,B}$.

$$\phi_{eff,A} = \phi_{self,A} + (1-\phi_{self,A}) < \phi_A > \tag{18}$$

$$\phi_{eff,B} = \phi_{self,B} + (1-\phi_{self,B}) < \phi_B > \tag{19}$$

where $\phi_{self,A}$ and $\phi_{self,B}$ are termed the "self-concentration"; ϕ_A and ϕ_B are the bulk volume fractions of A and B, respectively. The self-concentration is determined from the volume fraction occupied by monomers in one Kuhn length (l_K) inside a volume $V_K = l_K^3$ as

$$\phi_{self} = \frac{C_\infty M_0}{k \rho N_A V_K} \tag{20}$$

where C_∞ is the characteristic ratio, ρ is the density, M_0 is the molar mass of the repeating unit, N_A is Avogadro number and k counts the number of backbone bonds per repeat unit of one component. The effective local glass transition temperature is associated with the average local concentration of each component by

$$T_{g,eff}^{A} = < T_g > (\phi = \phi_{eff,A}) \tag{21}$$

$$T_{g,eff}^{B} = < T_g > (\phi = \phi_{eff,B}) \tag{22}$$

$T_{g,eff}^{A}$ and $T_{g,eff}^{B}$ can be calculated from any theoretical or empirical equations which describe the relationship between glass transition temperature and composition (e.g. the Fox equation [67] or the Gordon/Taylor equation [68]), using $\phi_{eff,A}$ or $\phi_{eff,B}$ as the input concentration.

2.3 Glass Transition and Segmental Dynamics in Thin Polymer Films

2.3.1 The Glass Transition Temperature of Thin Polymer Films

2.3.1.1 The Glass Transition Temperature of Substrate Supported Polymer Films

The first systematic study of the film thickness impact on the T_g values in thin polymer films supported by substrates was reported by Keddie et al. in 1994 [15, 113]. They applied ellipsometry to measure T_g as a function of film thickness in spin-coated films of PS and poly(methyl methacrylate) (PMMA). A T_g reduction with decreasing film thickness was observed in ultrathin PS films supported on silica and ultrathin PMMA films supported on gold, as shown is Fig. 8. In their study of PS films supported on silica, they further proposed the following empirical equation to describe the thickness dependence of T_g values in thin polymer films.

$$T_g(h) = T_g(\text{bulk})[1 - (\frac{a}{h})^d] \qquad (23)$$

where T_g(bulk) is the bulk T_g, a and d are fitting parameters (3.2 nm and 1.8 in the study, respectively) and h is the thickness of the film. Keddie et al. hypothesized that the presence of a liquid-like layer at the free surface of thin polymer films with enhanced molecular mobility compared to the bulk leads to the reduction of T_g [15].

Using a fluorescence/multilayer method, Ellison and Torkelson carried out the first direct measurement on the T_g of an ultrathin 14-nm-thick PS layer with one free surface [19]. The ultrathin layer next to the free surface showed a dramatic decrease in T_g, which extends several tens of nm into the film. Yang et al. measured the viscosity of unentangled, short-chain PS films on silicon at different temperatures and found that the transition temperature for the viscosity decreases with reducing the film thickness. By applying the hydrodynamic equations to the films, the data can be explained by the presence of a highly mobile surface liquid layer. T_g depression was further reported in thin polymer films supported on non-attractive substrates using different characterization methods, including PS [5,6,16,114-118], PMMA [116,119-122] and some other polymers [123-125].

Keddie et al. further performed measurements on PMMA films supported on silica, which exhibits attractive interactions due to hydrogen bonding [113]. In contrast, an increase of T_g

with reducing film thickness was observed, as shown in Fig. 8b. They proposed that the effects of attractive interactions (hydrogen bonding) between PMMA and silica overwhelmed the effects of the free surface and resulted in an overall increase in T_g [113]. In addition to PMMA supported on silica, many other systems show an increase in T_g with reducing film thickness due to an attractive interaction [116,120-122,126-133].

Since the interfacial interaction plays an important role in the T_g deviation of thin polymer films, Frey systematically investigated the dependence of the glass transition temperature of PS and PMMA films on interfacial energy and thickness [119]. The polymer films are supported on octadecyltrichlorosilane (OTS) deposited silica. X-rays were used to modify the OTS layer by incorporating oxygen-containing groups on the surface to obtain tunable interfacial energy between the polymer and the substrate. The T_g values of the films were characterized by three complementary techniques: local thermal analysis, ellipsometry, and X-ray reflectivity. At low interfacial energies between the polymer and the substrate, T_g decreased with reducing the film thickness while at high interfacial energies, T_g increased with reducing the film thickness. For a film thickness ca. 20 nm, ΔT_g scaled linearly with the interfacial energy between the polymer and the substrate, indicating the importance of interfacial energy, as shown in Fig. 9.

In the recent studies of Al-capped polymer thin films by CSD, PS films show T_g depression [132], while an increase of T_g was observed for PC films [133]. The interfacial energy of PS/Al is estimated to be 5.6 mJ m^{-2} [134], which is much higher than that of PC/Al with the value of 2.5 mJ m^{-2} [133]. Moreover, Grohens et al. found that PMMA stereoregularity had great effect on its T_g in the vicinity of an attractive substrate. Different chain rearrangements (conformation) and density changes occurred at interfaces for i-PMMA and s-PMMA [135]. Glynos et al. further demonstrated the important role of the chain structure of the macromolecule on the thickness dependence of T_g by changing the molecular architecture, going from linear chains to star-shaped macromolecules [136]. All these findings indicate that the interfacial energy alone is not the only relevant parameter to describe thickness dependence of thermal T_g in thin polymer films. The change of the local density due to the chain adsorption, which propagated from the irreversibly adsorbed layer to the interior part of the film, is assumed to be a further important parameter to describe the thickness dependence of T_g.

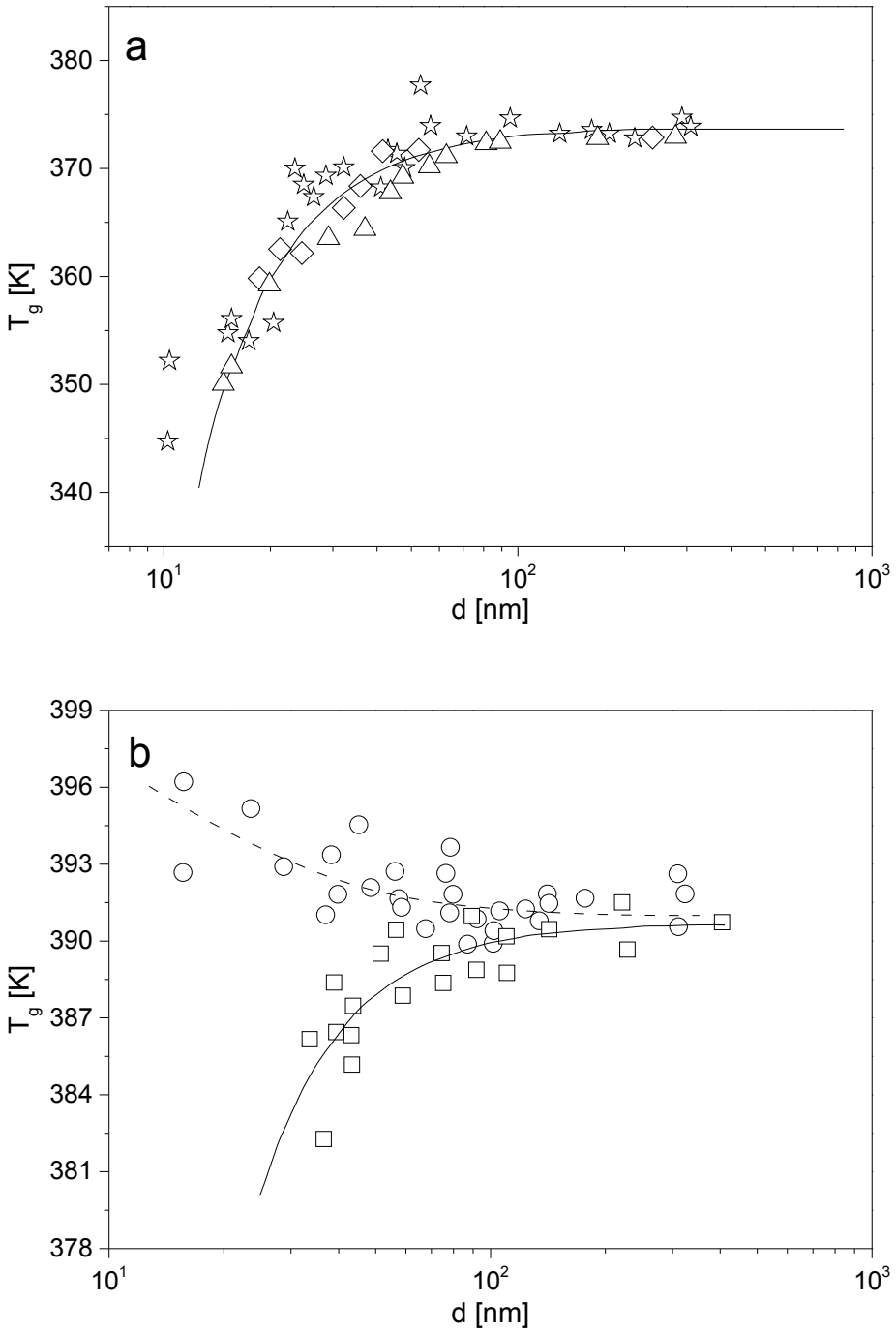

Fig. 8 *T_g vs. film thickness of PS and PMMA supported on different substrates. (a): Thin PS films supported on silicon with different molecular weights: M_w=2900 kg/mol (stars), M_w=500.8 kg/mol (triangles) and M_w=120 kg/mol (diamonds). The solid line is best fit to Equ. 23. Data for PS were reproduced from Ref. 15. (b): Thin PMMA films (M_w=100.25 kg/mol) supported on gold-coated silicon (squares). The solid line is best fit to Equ. 23. Thin PMMA films (M_w=100.25 kg/mol) supported on silicon covered by a native oxide layer (circles). The dashed line is a guide for the eyes. Data for PMMA were taken from Ref. 113.*

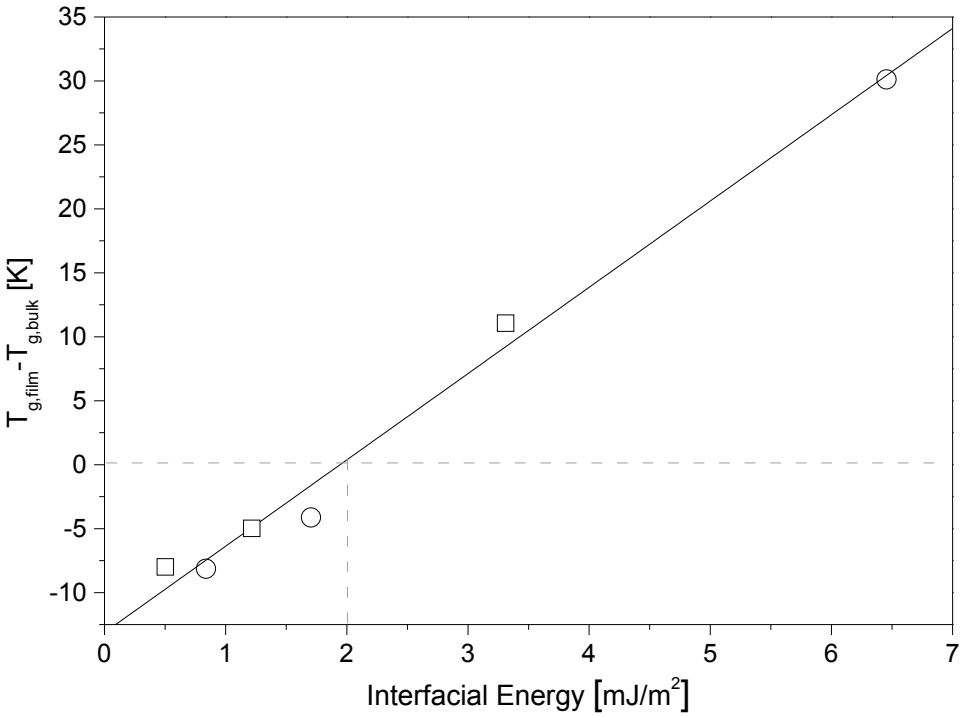

Fig. 9 *The difference in T_g values between bulk and ultrathin films (ca. 20 nm) of PS (circles) and PMMA (squares) is plotted as a function of the interfacial energy, respectively. The solid line is a linear fitting of the data for two polymers. At an interfacial energy of ca. 2 mJ/m^2, the T_g in a 20-nm-film does not show significant T_g deviation from the bulk value. Data in the plot were taken from Ref. 119.*

In summary, T_g of thin polymer films is significantly affected by the film thickness and the interfacial interaction between the polymer and the substrate layers. A depression of T_g compared to the bulk value with decreasing film thickness has been widely observed for both supported and metal-capped thin polymer films having a lack of attractive interaction with the substrates. The existence of a highly mobile surface layer was suggested to explain the phenomenon of T_g depression in thin polymer films. Since the T_g deviation in thin films from the bulk value is strongly related to the surfaces and interfaces modifying the relevant thermal T_g in the outermost layer of the polymer film, an increase of T_g can be observed when polymer-substrate interactions are sufficiently strong. Further evidence also showed that the interfacial energy as a parameter is not enough to describe the effects of interfacial interactions on the T_g of thin polymer films.

2.3.1.2 The Glass Transition Temperature in Freestanding Polymer Films

Compared to many investigations of T_g in supported polymer films, relatively few studies have been carried out on freestanding polymer films. The first study of T_g in freestanding films was conducted by Forrest et al. using brillouin light scattering and transmission ellipsometry [115,137,138]. A much greater T_g depression was observed in freely standing films compared to substrate supported films. The trend have been observed by many other researchers with different experimental methods [115,138-148]. It was also found that there is a strong M_w dependence of the T_g reduction in freely standing PS films of high M_w. In the low M_w regime, the thickness dependence of T_g is M_w independent. The molecular weight dependence of thermal T_g for freestanding films is presented in Fig. 10.

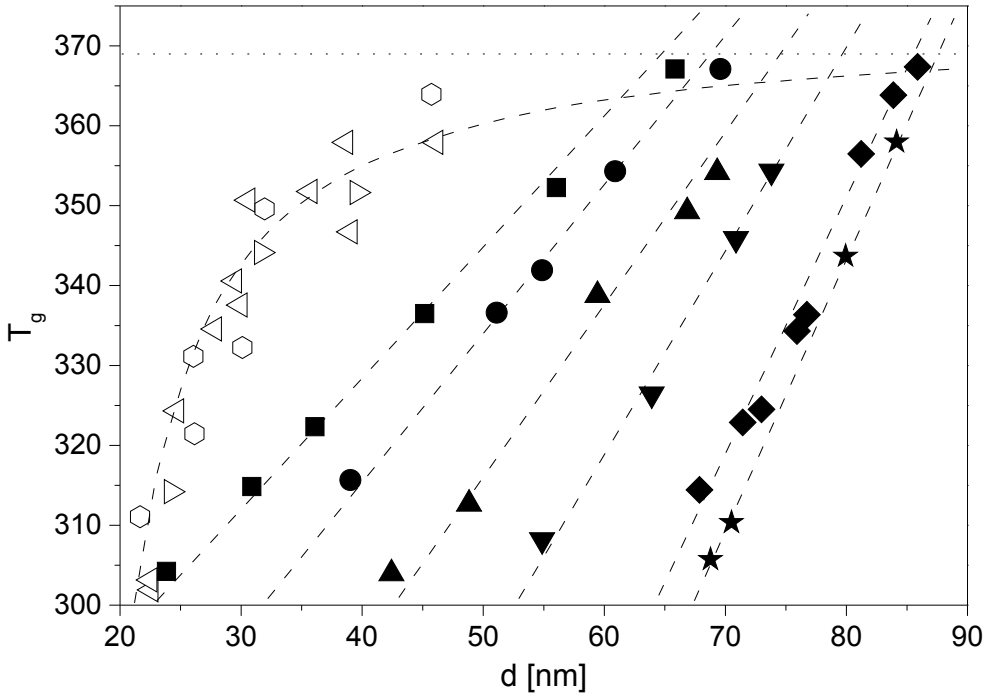

Fig. 10 *Thermal T_g is plotted as a function of film thickness for freestanding films with different molecular weights: M_w=116 kg/mol (hollow left-pointing triangles), M_w=197 kg/mol (hollow right-pointing triangles), M_w=347 kg/mol (hollow hexagons), M_w=575 kg/mol (solid squares), M_w=767 kg/mol (solid circles), M_w=1250 kg/mol (solid up-pointing triangles), M_w=2240 kg/mol (solid down-pointing triangles), M_w=6680 kg/mol (solid diamonds), M_w=9100 kg/mol (solid stars). The hollow symbols are obtained using BLS and taken from Ref. 143. The solid symbols are obtained with ellipsometry and taken from Ref. 140.*

2.3.2 The Segmental Dynamics in Thin Polymer Films

It is known that the α-relaxation dynamics due to cooperative segmental motions in thin polymer films show strong deviation from their bulk behavior. One of the first measurements on the α-relaxation time of polymers confined in thin films was done by Hall et al. by using second harmonic generation [9]. It was reported that there was a substantial broadening in the α-relaxation time distribution in poly(isobutyl methacrylate) films. Fukao and Miyamoto applied BDS to investigate the confinement effects on the α-relaxation dynamics of PS films [149,150]. A broadening of the distribution of α-relaxation times was observed. In addition, it was found that the average α-relaxation time decreases with reducing the film thickness, indicating faster dynamics under confinement. The onset film thickness at which dynamic T_g began to exhibit deviation from bulk value was dependent on the frequency. At lower frequency, larger onset thickness was observed. Similar observations were also reported by other groups [17,18,151,152]. Recently several studies also showed that the average α-relaxation time increased due to the presence of reduced mobility layer at the interface resulting from the strong interaction between the polymer and substrate [133,153,154]. The dielectric measurements mentioned above were performed on polymers capped between two Al layers. Serghei and Kremer developed a new experimental approach which enables BDS to measure the segmental dynamics in thin polymer films having a free surface [155-157]. They demonstrated that down to film thicknesses of ~10 nm no shift in the average relaxation time and no broadening of the dynamic glass transition are detected.

Recently nanocalorimetric measurements were carried out to investigate the glass transition behavior of thin supported films. Allen et al. first employed nanocalorimetry to study the glass transition of thin polymer films supported by platinum coated SiN substrates with ultrahigh heating/cooling rates [158-161]. No thickness dependence of T_g in thin polymer films was observed. Schick et al. further developed specific heat spectroscopy by using differential AC chip-based calorimetry in a broad frequency range (ca. 1-4000 Hz) combined with a high sensitivity of pJ/K to study the dynamic glass transition of polystyrene (PS), poly(methyl methacrylate) (PMMA) and poly(2,6-dimethyl-1,5-phenylene oxide) (PPO) thin films supported by SiO_2 covered SiN substrates [162-164]. For all investigations no thickness dependence of dynamic T_g was observed down to thicknesses of several nm. The relatively high frequency used in differential AC chip-based calorimetry and high heating/cooling rate employed in thin film calorimetry developed by Allen et al. were empirically used to explain

the discrepancy between the nanocalorimetry results and those showing T_g depressions. Evidence for a cooling rate dependence of the T_g depression was shown by Fakhraai and Forrest [16]. In this work, ellipsometry was to probe the fast and slow relaxation dynamics associated with thermal T_g via various cooling rates. T_g of PS films decreases with decreasing thickness upon slow cooling (~1 K/min) while T_g is independent of thickness upon fast cooling (~90 K/min). These results indicated that the confinement effect on thermal T_g in thin polymer films is cooling-rate dependent. The slow dynamics are affected more by confinement.

Quite recently Paeng et al. [165] used a photobleaching method to measure the reorientation of dilute probe molecules in freestanding PS films. It was demonstrated that these probes are good reporters of segmental dynamics of polymers. Two subsets of probes with distinct dynamics were observed. The slower subset of probe molecules exhibits bulk-like dynamics. The more mobile subset of probes is consistently associated with a mobile surface layer, and the thickness of the mobile surface layer is shown to increase with temperature. Near thermal T_g, the time scale of the slow process becomes comparable to that of the fast process.

2.3.3 The Glass Transition Temperature and Segmental Dynamics in Miscible Polymer Blend Films

In spite of a large body of literature on the glass transition behavior of bulk miscible polymer blend, there are only several studies of T_g in miscible polymer blend of thin films [166-171]. Pham and Green investigated the influence of film thickness and composition on the effective T_g of PS/tetramethylbisphenol-A Polycarbonate (TMPC) blend films spin-coated on SiO_x/Si substrates using spectroscopic ellipsometry. It was revealed that the effective T_g of thin film mixtures of PS and TMPC decreased with decreasing film thickness while the T_g of TMPC films increased with decreasing film thickness [166]. In a recent study, Frieberg et al. used X-ray photon correlation spectroscopy (XPCS) to detect the dynamics of poly(vinyl methyl ether) (PVME) chains at the free surface of PS/PVME thin film mixtures which is found to be orders of magnitude larger than the PVME chains in the bulk. These dynamics manifest from differences between the local compositions of the blend at the free surface and the bulk, as well as film thickness constraints [167].

3 PRINCIPLES OF EXPERIMENTAL TECHNIQUES

3.1 Broadband Dielectric Spectroscopy

The broadband dielectric spectroscopy is a very useful tool to study the molecular dynamics of polymers. This is due to the fact that a broad dynamical range from 10^{-3} to 10^{9} Hz can be covered by this method in its modern form [172]. Therefore motional processes which take place for polymeric systems on extremely different time scales can be investigated in a broad frequency and temperature range.

In this section, the theory of broadband dielectric spectroscopy is discussed. In the first part the essential points of electrostatics are reviewed. The dielectric relaxation behavior is discussed at an infinite time after applying an outer electric field. In the second part the formalism of time dependent dielectric processes is developed in the frame of linear response theory. In the third part different model functions to analyze the dielectric relaxation processes are discussed.

3.1.1 Electrostatics

For a small electric field with field strength **E**, the dielectric displacement **D** can be expressed as:

$$\boldsymbol{D} = \varepsilon * \varepsilon_0 \boldsymbol{E} \qquad (24)$$

where ε_0 is the dielectric permittivity of vacuum (ε_0 = 8.854 10^{-12} As V^{-1} m^{-1}) and ε* is the complex dielectric function. ε* is time (or frequency) dependent if time dependent processes take place within the sample [173]. In general, time dependent processes within a material lead to a difference of the time dependencies of the outer electrical field **E**(t) and the resulting dielectric displacement **D**(t). In the simple case of a periodical field $\boldsymbol{E}(t) = \boldsymbol{E_0} \exp(-i\omega t)$ (ω-angular frequency, ω=2πf, f-frequency of the outer electric field, $i = \sqrt{-1}$ -imaginary unit) the complex dielectric function ε* is defined by

$$\varepsilon^*(\omega) = \varepsilon'(\omega) - i\varepsilon''(\omega) \qquad (25)$$

where ε'(ω) is the real part and ε''(ω) the imaginary part of the complex dielectric function. In the stationary state the difference in the time dependence of **E**(t) and **D**(t) is a phase shift.

The polarization **P** describes the dielectric displacement which originates from the response only of a material to an external field. It is defined as

$$\boldsymbol{P} = \boldsymbol{D} - \boldsymbol{D}_0 = (\varepsilon^* - 1)\varepsilon_0 \boldsymbol{E} \tag{26}$$

The macroscopic polarization **P** can have a permanent or an induced character. For molecules containing only one kind of permanent dipoles **μ**, the polarization **P** can be expressed by

$$\boldsymbol{P} = \frac{1}{V}\sum \boldsymbol{\mu}_i + \boldsymbol{P}_\infty = \frac{N}{V}\langle \boldsymbol{\mu} \rangle + \boldsymbol{P}_\infty \tag{27}$$

where N denotes the whole number of dipoles in the system, N/V is the number density of dipoles involved in the relaxation process and <**μ**> is the mean dipole moment. The permanent polarization is caused by the orientation of the permanent dipoles $\boldsymbol{\mu}_i$ induced by an electrical field. Permanent dipole moments can be oriented by an electrical field. This is called orientational polarization. The induced polarization $\mathbf{P}_\infty$ is caused by the local electric field, which distorts a neutral distribution of charges. The induced polarization includes different contributions:

1. Electronic polarization: This resonant process occurs when the electron cloud of an atom (or molecule) is shifted with respect to the positive nucleus.
2. Atomic polarization: This process is observed when an agglomeration of positive and negative ions is deformed under the force of the applied field.

When the dipoles are assumed to be not interacting with each other and the field of a permanent dipole polarizes its environment (surrounding particles) (local field effects) is negligible, one can derive the contribution of the orientational polarization to the dielectric function as

$$\Delta\varepsilon = \varepsilon_S - \varepsilon_\infty = \frac{1}{3\varepsilon_0}\frac{\mu^2}{k_B T}\frac{N}{V} \tag{28}$$

where $\varepsilon_S = \lim_{\omega \to 0} \varepsilon'(\omega)$. $\varepsilon_\infty = \lim_{\omega \to \infty} \varepsilon'(\omega)$ covers all contributions to the dielectric function which are due to induced polarization $\mathbf{P}_\infty$ [174]. In the following Δε is also called dielectric strength.

A more general approach was proposed by Onsager by considering the local field effects [175]:

$$\varepsilon_S - \varepsilon_\infty = \frac{1}{3\varepsilon_0} F \frac{\mu^2}{k_B T} \frac{N}{V} \quad \text{with } F = \frac{\varepsilon_S(\varepsilon_\infty + 2)^2}{3(2\varepsilon_S + \varepsilon_\infty)} \tag{29}$$

The Onsager Equation can be used to estimate dipole moments for non-associating organic liquids. It does not work for polar associating liquids. Kirkwood [176-178] and Fröhlich [179] introduced the correlation factor g to model the interaction between dipoles with respect to the ideal case of non-interacting dipoles. The formal definition of the Kirkwood/Fröhlich correlation factor is given by

$$g = \frac{<\sum_i \boldsymbol{\mu}_i \sum_j \boldsymbol{\mu}_j>}{N\mu^2} = 1 + \frac{<\sum_i \sum_{i<j} \boldsymbol{\mu}_i \boldsymbol{\mu}_j>}{N\mu^2} = \frac{\mu^2_{Interact.}}{\mu^2} \tag{30}$$

where μ^2 is the mean square dipole moment for non-interacting, isolated dipoles which can be measured for instance in diluted solutions. Furthermore, Kirkwood and Fröhlich extended Onsager's function to the following form:

$$\varepsilon_S - \varepsilon_\infty = \frac{1}{3\varepsilon_0} F g \frac{\mu^2}{k_B T} \frac{N}{V} \tag{31}$$

3.1.2 Dielectric Relaxation

The dielectric relaxation theory for small electric field strengths is a special case of linear response theory [180,181]. The time dependent response of an isotropic system which follows an external disturbance can be described by a linear equation. In the case of a dielectric relaxation process, the disturbance is the time dependent external electrical field **E**(t), while the response of the system is the polarization **P**(t) [182]:

$$\boldsymbol{P}(t) = \boldsymbol{P}_\infty + \varepsilon_0 \int_{-\infty}^{t} \varepsilon(t-t') \frac{d\boldsymbol{E}(t')}{dt'} dt' \tag{32}$$

where ε(t) denotes the time dependent dielectric function and $\mathbf{P}_\infty$ covers all contributions arising from induced polarization. When a dielectric system applied by a step-like change of the outer electrical field, $d\mathbf{E}(t)/dt = \mathbf{E}_0\delta(t)$, ε(t) can be directly measured as response of the system, $\varepsilon(t) = (\mathbf{P}(t) - \mathbf{P}_\infty)/\mathbf{E}_0\varepsilon_0$. The relationship between the time dependence of the electric

field, the polarization and the time dependent relaxation function for a step-like change of the outer electric field is shown in Fig. 11.

When a stationary periodical outer electric field is applied to the dielectric material, $\boldsymbol{E}(\omega) = \boldsymbol{E}_0 \exp(-i\omega t)$, Equ. 32 becomes

$$\boldsymbol{P}(\omega) = \varepsilon_0 (\varepsilon^*(\omega) - 1)\boldsymbol{E}(\omega) \tag{33}$$

The relationship between the time dependent dielectric function ε(t) and the complex dielectric function ε*(ω) is provided in the following equation:

$$\varepsilon^*(\omega) = \varepsilon'(\omega) - i\varepsilon''(\omega) = \varepsilon_\infty - \int_0^\infty \frac{d\varepsilon(t)}{dt} \exp(-i\omega t)\, dt \tag{34}$$

Generally speaking, ε'(ω) shows a stepwise decrease with frequency and is related to the energy stored reversibly during the relaxation. The imaginary part ε''(ω) has a peak-like structure in the frequency domain and is proportional to the energy dissipated in each period due to the relaxation. For these reasons, the real and imaginary parts are called the dielectric storage and dielectric loss in the literatures as well.

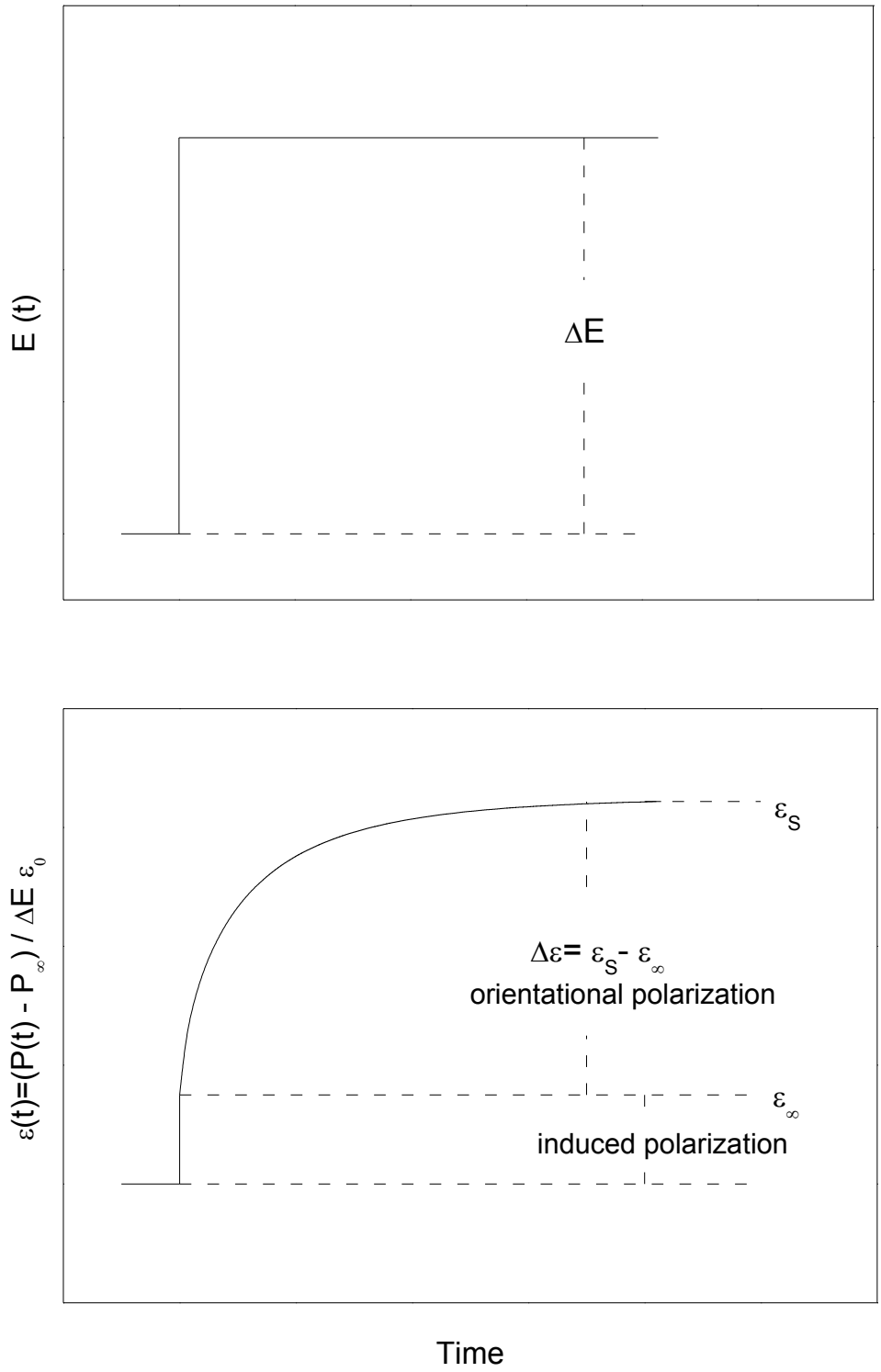

Fig. 11 *Schematic relationship between the time dependence of the electric field ΔE (upper panel), the polarization P(t) and the time dependent dielectric relaxation function ε(t) (lower panel). For sake of simplicity the vector sign is omitted in the figure. This figure was taken from Ref. 183.*

3.1.3 Analysis of Dielectric Relaxation Spectra

3.1.3.1 Debye Relaxation Process

The dielectric relaxation processes are generally analyzed by different model functions. The simplest approach to calculate the time dependence of the dielectric behavior is to assume that the change in polarization is proportional to its actual value [52,179]:

$$\frac{d\,\boldsymbol{P}(t)}{d\,t} = -\frac{1}{\tau_D}\boldsymbol{P}(t) \quad . \tag{35}$$

The solution of this first order differential equation leads to an exponential decay for the correlation function Φ(t) (Equ. 11)

Debye relaxation function in the frequency domain is obtained:

$$\varepsilon^*(\omega) = \varepsilon' - i\varepsilon'' = \varepsilon_\infty + \frac{\Delta\varepsilon}{1 + i\omega\tau_D} \tag{36}$$

where the real and the imaginary parts are given as follows.

$$\varepsilon' = \varepsilon_\infty + \frac{\Delta\varepsilon}{1 + (\omega\tau_D)^2} \tag{37}$$

$$\varepsilon'' = \frac{\Delta\varepsilon\,\omega\tau_D}{1 + (\omega\tau_D)^2} \tag{38}$$

The frequency dependence of the real and the imaginary part of the Debye function is shown in Fig. 12. In general, the real part shows a stepwise decrease, while the imaginary part presents a symmetric peak with a maximum. The symmetric loss peak is with a half width of 1.14 decades. The frequency of maximal loss is related to the relaxation rate $f_p=\omega_p/2\pi$ or relaxation time $\tau_D=1/(2\pi f_p)=1/\omega_p$. The dielectric strength Δε of a relaxation process can be determined either from the area under the loss peak ε''(ω) or from the step in the real part ε'(ω).

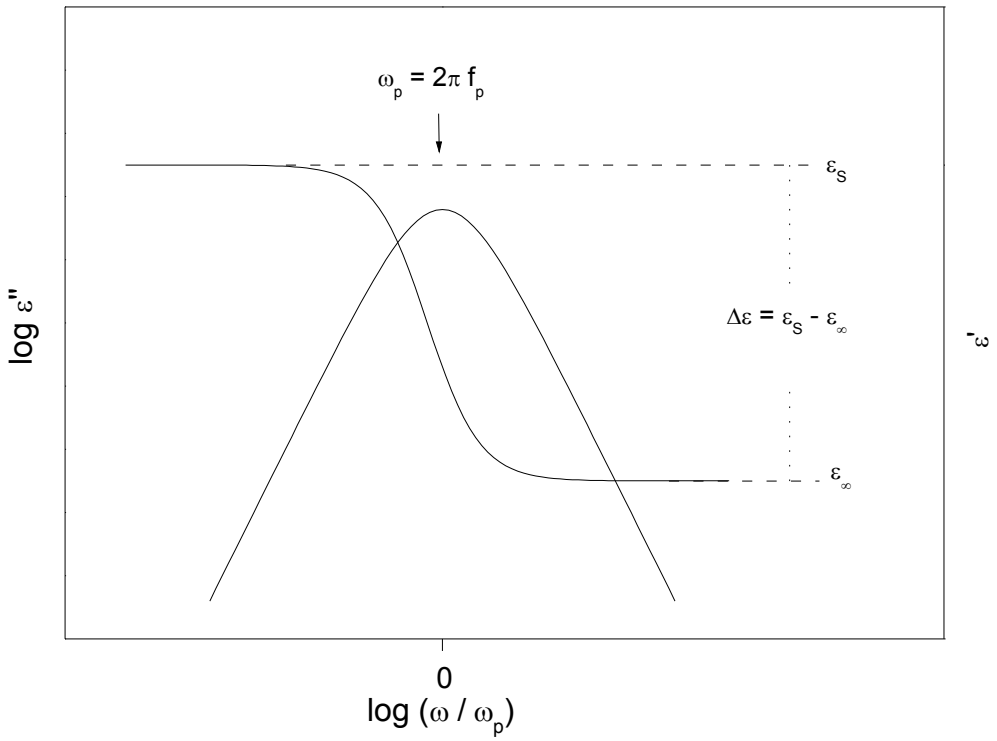

Fig. 12 *Frequency dependence of the real part ε′ and imaginary part ε′′ of the complex dielectric function according to the Debye function. This figure was taken from Ref. 184.*

3.1.3.2 Non-Debye Relaxation Process

In practice, the Debye function is not sufficient to describe the experimental results obtained for complex systems like amorphous polymers. In most cases the half width of measured loss peaks is much broader than predicted by Equ. 36 and additionally their shapes are asymmetric with a high frequency tail. This is called non-Debye relaxation behavior.

The broadening of the symmetric relaxation peak is described by the Cole/Cole (CC) function [185]:

$$\varepsilon^*_{CC}(\omega) = \varepsilon_\infty + \frac{\Delta\varepsilon}{1+(i\omega\tau_{CC})^\beta} \qquad (39)$$

where the β value characterizes the symmetric broadening of the relaxation peaks ($0<\beta\leq 1$) and τ_{CC} is the characteristic relaxation time.

The complex dielectric function can have an asymmetric broadening as well, which can be described by the Cole/Davidson (CD) function [186,187]:

$$\varepsilon^*_{CD}(\omega) = \varepsilon_\infty + \frac{\Delta\varepsilon}{(1+i\omega\tau_{CD})^\gamma} \tag{40}$$

where γ (0< γ ≤1) describes an asymmetric broadening of the relaxation function and τ_{CD} is the characteristic relaxation time.

The majority of cases of non-Debye dielectric spectrum are well described by the so-called Havriliak/Negami (HN) relationship:

$$\varepsilon^*_{HN}(\omega) = \varepsilon_\infty + \frac{\Delta\varepsilon}{(1+(i\omega\tau_{HN})^\beta)^\gamma} \tag{41}$$

where β and γ (0<β≤1 and 0<βγ≤1) are fractional shape parameters which describe the symmetric and asymmetric broadening of the complex dielectric function, τ_{HN} is characteristic relaxation time, $\tau_{HN}=1/(2\pi f_p)=1/\omega_p$, Δε denotes the dielectric strength and ε_∞ describes the value of the real part ε´ for $\omega>>\omega_p$.

Real and imaginary parts for the HN-function are given as follows.

$$\varepsilon'(\omega)-\varepsilon_\infty = \Delta\varepsilon\, r(\omega)\cos(\gamma\Psi(\omega)) \;\; ; \;\; \varepsilon'' = \Delta\varepsilon\, r(\omega)\sin(\gamma\Psi(\omega)) \tag{42}$$

with

$$r(\omega)=[1+2(\omega\tau_{HN})^\beta\cos(\frac{\beta\pi}{2})+(\omega\tau_{HN})^{2\beta}]^{-\gamma/2} \tag{43}$$

and

$$\psi(\omega)=\arctan\left[\frac{\sin(\beta\pi/2)}{(\omega\tau_{HN})^{-\beta}+\cos(\beta\pi/2)}\right] \tag{44}$$

The maximum frequency of the dielectric loss ω_p is given by

$$\omega_P = \frac{1}{\tau_{HN}}\left[\sin\frac{\beta\pi}{2+2\gamma}\right]^{1/\beta}\left[\sin\frac{\beta\gamma\pi}{2+2\gamma}\right]^{-1/\beta} \tag{45}$$

The HN function is actually a combination of the Debye-, Cole/Cole- and the Cole/Davidson-function. The specific case β=1, γ=1 gives the Debye relaxation law (Equ. 36); the case γ=1,

β≠1 corresponds to the so-called Cole/Cole (CC) equation (Equ. 39); and the case β=1, γ≠1 corresponds to the Cole/Davidson (CD) formula (Equ. 40). Some examples of the HN-function for selected shape parameters are given in Fig. 13.

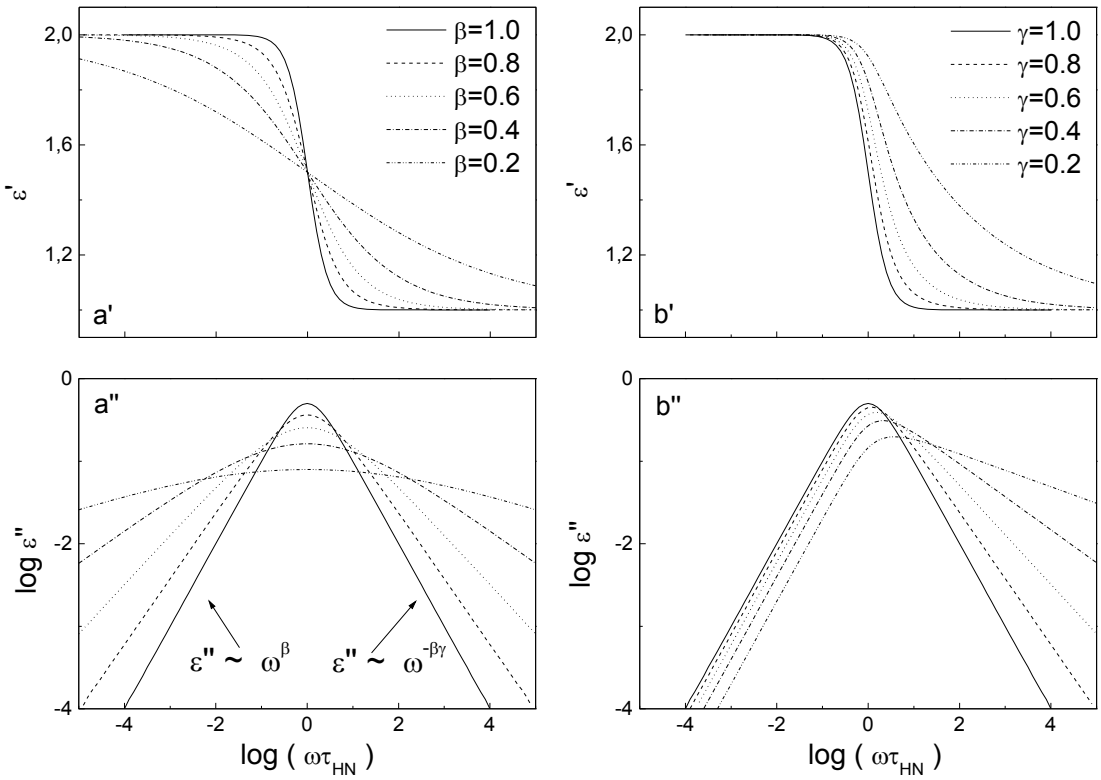

Fig. 13 *Complex dielectric permittivity for the Havriliak/Negami-function (τ_{HN}=1 s, $\Delta\varepsilon$=1, ε_∞=1). (a' & a'') with varying β values and γ=1; (b' & b'') with varying γ values and β=1. The figure was taken from Ref. 188.*

3.1.4 Fitting HN Function to the Experimental Results

Among the model functions to describe the dielectric relaxation processes, the HN-function (Equ. 41) can describe the dielectric relaxation processes best. From the fit of the HN-function to the data the relaxation rate f_p and the dielectric strength Δε are determined. If two relaxation processes are observed in the experimental frequency window, a sum of two HN-functions is fitted to the experimental data.

In practice, the dielectric spectra of a complex system do not exhibit isolated loss peaks. Instead, various relaxation processes like conduction effects contribute to the dielectric spectra. Conductive contribution is treated by adding a component $\varepsilon''_{Cond}(\omega) = \sigma_0 / [\omega^s \varepsilon_0]$ to

the dielectric loss where σ_0 is related to the specific dc conductivity of the sample. The parameter s ($0<s\leq1$) describes Ohmic (s=1) and non-Ohmic (s<1) effects in the conductivity.

Different from the broadband dielectric spectroscopy measurements on bulk samples, for the thin film geometry one has to consider that the resistance R of the Al electrodes cannot be neglected. This resistance leads to an artificial loss peak (electrode peak) on the high-frequency side of the spectra with a time constant τ_{Res}=R*C´ (C´ - sample capacity). The electrode peak shifts to lower frequencies because with decreasing film thickness the sample capacity C´ increases. The frequency dependence of the electrode peak obeys a Debye-function. For optimized sample geometries the maximum position of this electrode peak $f_{Res}\sim1/\tau_{Res}$ can be shifted outside the experimental accessible frequency window. Therefore the Debye-function can be approximated by its low frequency tail and the complete function reads as [18,133]

$$\varepsilon^*_{Fit} = \varepsilon^*_{HN}(\omega) - i\frac{\sigma_0}{\omega^s \varepsilon_0} - iB*\omega \qquad (46)$$

where B is a fitting parameter mainly related to τ_{Res}.

3.2 Specific Heat Spectroscopy

In the frame of linear response theory [180,181], the complex dielectric function can be regarded as the response of the system to a periodic external electric field. Analogous to complex dielectric function, complex specific heat capacity can represent how the temperature of the system varies when a periodic external heat is applied to it. The complex dielectric function can be measured by broadband dielectric spectroscopy. The complex specific heat capacity can be determined by specific heat spectroscopy.

3.2.1 Complex Heat Capacity

Many thermal events are related to time-dependent entropy changes such as crystallization, glass transition, etc. For a time-dependent thermal event, we can describe it with a time-dependent heat capacity C(t). If the applied disturbances applied to the system during the measurement sufficiently small, a description in the frame of linear response theory is possible [189].

The relationship between the time-dependent enthalpy and the temperature is given by

$$\partial H(t) = \int_{-\infty}^{t} \frac{dC(t-t')}{dt} \partial T(t')dt' \tag{47}$$

After Fourier transformation, Equ. 47 reads as

$$H(\omega) = C^*(\omega)T(\omega) \tag{48}$$

with a frequency-dependent complex heat capacity

$$C^*(\omega) = C'(\omega) - iC''(\omega) \tag{49}$$

The frequency dependent complex heat capacity C*(ω) can be connected to time-dependent molecular movements C (t):

$$C^*(\omega) = C_\infty + i\omega \int_0^\infty \frac{dC(t)}{dt} \exp(-i\omega t)dt \tag{50}$$

The real part of the complex heat capacity C´ describes molecular motions and the imaginary part C´´ is linked to dissipation (entropy production [190]).

3.2.2 Differential AC Chip-based Calorimetry

As common in AC calorimetry, an alternating current of frequency of ω passes through the heater, leading to a small periodic heat flow of frequency 2ω. The resulting temperature oscillation with a frequency of 2ω is measured. Although AC calorimetry has been known as a sensitive technique to measure thermophysical properties of small amount of materials, addenda heat capacity of the measuring system has to be further reduced in order to carry out measurements on thin polymer films. Differential AC chip-based calorimetry with the heater and thermometer on a submicrometer-thick membrane opens up new possibilities to investigate the thermal behaviour of thin polymer films.

The differential AC-chip calorimeter is based on a commercially available chip sensor, XEN 39390 (Xensor integrations, Nl). The heater is located in the centre of a freely standing thin silicon nitride membrane (thickness 1 μm) supported by a Si frame. Such a nanocalorimeter chip has a theoretical heated hot spot area of about 30x30 μm^2, with an integrated 6-couple thermopile and two 4-wire heaters (bias and guard heater), as shown in Fig. 14. Please note that in addition to the 30x30 μm^2 hot spot also the heater strips contribute to the heated area.

The heater and thermopile are protected by a SiO_2 layer with the thickness of 0.5-1 µm. The thin film was spin coated over the whole sensor, but only the small heated area is sensed as a point heat source.

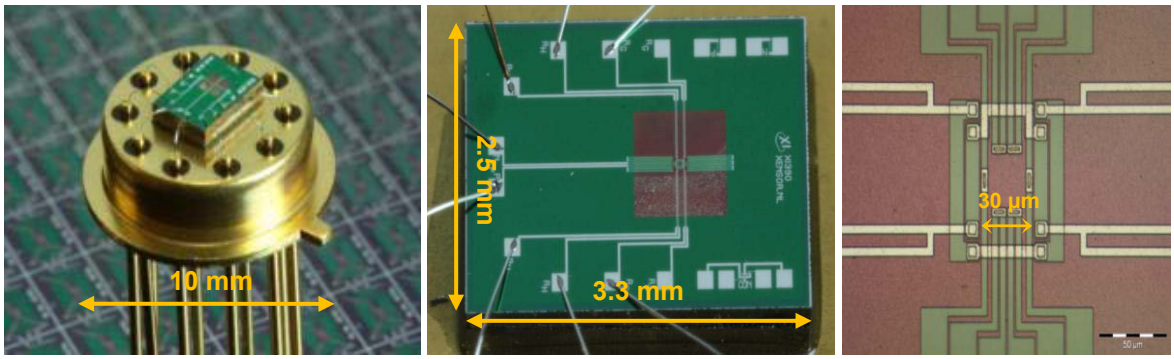

(a) (b) (c)

Fig. 14 *(a) Photograph of the nanocalorimeter chip on a TO-5 10 pin transistor housing, XEN 39390 from Xensor Integration. (b) Silicon nitride membrane fixed at 3.3×2.5 mm rectangular frame. (c) Magnified center area of the SiN membrane with the heated area of 30×30 µm and thermopile hot junctions (six white spots) placed around the heater. The arrow points to the outer of two pairs of heater strips. (a) and (b) were adapted from Ref. 191.*

The heat capacity of the empty sensor is frequency (ω) dependent, because the size of the heated area becomes smaller with increasing frequency [162]. For thin polymer films, the measured effective heat capacity of the sample approximately equals to the real part of the complex heat capacity. Considering all contributions, the apparent heat capacity of a sensor with a sample in the AC calorimeter is given by

$$C_{ap}(\omega) = [C_0(\omega) + C_s(\omega) + G/i\omega] \qquad (51)$$

where $C_0(\omega)$ and $C_s(\omega)$ are the heat capacities of the empty sensor and the sample respectively. $G/i\omega$ is the heat loss through the surrounding atmosphere. An AC calorimeter based on a single sensor is described in detail in Ref. 192 and the method was experimentally proven in Ref. 193.

The contribution of the heat capacity of the empty sensor to the measured data can be minimized by employing a differential setup. In the approximation of thin films (submicron) the heat capacity of the sample is then given by

$$C_s = i\omega\overline{C}^2(\Delta U - \Delta U_0)/SP_0 \quad (52)$$

where $\overline{C} \equiv C_0 + G/i\omega$ describes the effective heat capacity of the empty sensor, S is the sensitivity of the thermopile, P_0 is the applied heating power, ΔU is the complex differential thermopile signal for an empty and a sensor with a sample, where ΔU_0 is the complex differential voltage measured for two empty sensors. The amplitude and the phase angle of the complex differential voltage are considered as measure for the complex heat capacity.

3.3 Capacitive Scanning Dilatometry

Capacitive Scanning Dilatometry (CSD) relies on the analysis of the temperature dependence of the real part of dielectric permittivity ε'(T) or capacity C'(T) for thin films capped between two aluminum layers under the assumption that no dielectric active processes take place in the selected frequency and temperature range [17,150,194]. The real part of the permittivity can be expressed by $\varepsilon'(f,T)=\varepsilon_\infty(T)+\Delta\varepsilon(f,T)$ where ε_∞ is the real part of the permittivity in the high frequency limit and Δε is related to a dielectric dispersion due to molecular fluctuations. If the detection frequency f is set to such a value that no relaxation process is present ($\Delta\varepsilon\approx 0$), the temperature dependence of ε′ is given by $\varepsilon'(T)=\varepsilon_\infty(T)\sim\varepsilon_\infty(T_R)(1-\alpha(T)\Delta T)$ where ΔT is a temperature change with regard to a reference temperature T_R ($T=T_R+\Delta T$) and α(T) is the thermal expansion coefficient normal to the film surface. And thus the temperature coefficient of ε′ is proportional to α(T).

For a parallel plate capacitor in the Al-capped thin film geometry the temperature dependence of the geometrical capacitance is $C_0(T)=\varepsilon_0\frac{A}{d(T)}\sim\varepsilon_0\frac{A}{d(T_R)}(1-\alpha(T)\Delta T)$, d(T) is the thickness of the film in dependence of the temperature and A is the electrode area [195]. The relation between the temperature coefficient of C′ and the linear thermal expansion coefficient normal to the film surface is given by $\alpha(T)\sim -\frac{1}{C'(T_R)}\frac{dC'(T)}{dT}$ where C'(T) is the capacitance at a temperature T and T_R is a standard temperature.

Similar to other techniques, CSD can be used to determine the thermal T_g at which a kink occurs in the temperature dependence of C' or ε′due to the change of thermal expansion coefficient from the value of the glassy state to that of the liquid state. It is noteworthy to mention that CSD is very suitable to detect the volumetric change in non-polar polymers at

glass transition, while it fails to deal with polar polymers due to the contribution from dielectric dispersion.

3.4 Differential Scanning Calorimetry

Differential Scanning Calorimetry is a very useful technique to characterize the physical properties of polymers. It can be used to determine melting, crystallization, glass transition temperatures. Because of its simplicity and ease of use, DSC has been widely used in polymer science.

DSC is based on the following relation assuming time-independent sample and specific heat capacity:

$$\delta Q = C\Delta T = cm\Delta T \tag{53}$$

where δQ is the heat exchanged, ΔT is the temperature change caused by the exchanged heat, C is the heat capacity, c = C/m is the specific heat capacity, m is the sample mass.

Differential scanning calorimeter generally consists of two sample positions: one for the sample under investigation and the other for a reference sample, which is often an empty crucible. Both the sample and reference are heated by separate heaters. The temperature of the sample and reference is kept nearly equal during the experiment and the actual differential heat flow is measured as a function of temperature. When a temperature difference between the sample and reference occurs due to exothermic or endothermic thermal transitions in the sample, the power input is adjusted to remove this difference.

4 EXPERIMENTAL SECTION

4.1 Methods

4.1.1 Broadband Dielectric Spectroscopy

A high resolution ALPHA analyzer (Novocontrol) is used to measure the complex dielectric function $\varepsilon^*(f) = \varepsilon'(f) - i\varepsilon''(f)$ in the frequency range typically from 10^{-1} Hz to 10^7 Hz. The temperature was controlled by a Quatro Novocontrol cryosystem with ±0.1 K isothermal temperature stability. The temperature control system introduces evaporated nitrogen through a heater and uses this flow to control the sample temperature. The minimum stabilization time at a given temperature was 2 min. The stabilization time is reset if the temperature goes out of the ±0.1 K range. During the whole measurement the sample was kept in a pure nitrogen atmosphere to reduce moisture uptake or oxidation during the experiments. WinDETA is the standard control and evaluation software for the dielectric measurements.

4.1.2 Specific Heat Spectroscopy

In the calorimetric measurements by specific heat spectroscopy using differential AC chip-based calorimetry the temperature-scan-mode was used, which means that the frequency was kept constant while the temperature was scanned with a heating/cooling rate of 1.0 or 2.0 K/min. During the measurement the heating power for the modulation is kept constant at about 25 μW which ensures that the amplitude of the temperature modulation is less than 0.5 K [162]. The frequency is varied typically between 1 Hz and 1000 Hz. In the following discussion the amplitude and phase angle of the complex differential voltage are considered as measure for the complex heat capacity.

4.1.3 Capacitive Scanning Dilatometry

CSD measurements on nonpolar polymers like PS can be simultaneously done during the BDS measurements under identical conditions. An effective heating/cooling rate of 0.13 K/min is applied.

4.1.4 Differential Scanning Calorimetry

The glass transition temperature of the bulk materials are determined by the Differential Scanning Calorimetry (DSC). The DSC measurements were performed using a SEIKO® DSC 220C instrument equipped with a liquid nitrogen cooling accessory. The samples were heated

and cooled with a rate of 10 K/min. The experimental results were taken from the second rump of the measurement. The glass transition temperature of the sample was determined as the temperature at the inflection point of the change in heat flow in the DSC thermogram.

4.1.5 Spin-coating

Thin polymer films were prepared by spin-coating in the present study. It is an easy, fast and reproducible approach to form uniform thin polymer films with well controlled thickness. The spin-coater used in the experiment is SPIN150 (SPS-Europe), which is placed in a laminar flow hood for sample preparation to avoid contamination. Film thickness is controlled by varying the concentration of the solution and meanwhile keeping both rotation speed and time (3000 rpm, 60 s) constant.

4.1.6 Annealing

Films formed by spin-coating often contain residual stresses [196]. Before measurement the samples are usually heated up to melt state, held at the melt state for tens of hours and then cooled down to room temperature to remove the internal stress as well as any excess solvent. This process is called annealing. Suitable annealing protocol should be carried out on a thin film sample according to its thermal properties.

4.1.7 Metal Deposition

Thin polymer films are capped between two Al layers used as electrodes in the dielectric measurements. The setup used in the present study is Edwards Auto 306 Thermal Evaporator. Thin and uniform Al layers were prepared on both sides of the film with thermal evaporation under vacuum (10^{-6} mbar). The layer thickness is controlled to be around 60 nm and the width is 2 mm.

4.1.8 Atomic Force Microscopy

Atomic Force Microscopy (AFM) is a technique to measure surface properties of the materials such as topography and structure with nanometer scale depth and spatial resolution. In the present study AFM was used to ensure the high quality of the films before and after the annealing procedure which means no inhomogeneities (no sign of dewetting) at the surface of the films and a low surface roughness. Additionally AFM is used to determine the absolute film thickness. To do so we need to make scratches cross the films and the cross section view of the AFM images of those scratches will tell us the precise film thickness. AFM

measurements were performed in the tapping mode by using either Nanopics 2100 or MFP-3D (Asylum Research, Santa Barbara, CA).

4.1.9 Contact Angle Measurement

To estimate the interfacial energy between the polymer and the substrate contact angle measurements were carried out. The measurements were performed using Automated Contact angle system G2 (Krüss) employing the static sessile drop method. The probe liquids used were ethylene glycol, formamide and water for both PC/Al and PC/SiO_2 systems. Usually 8 drops with a volume of 3 μl were dropped onto the surface of the sample or the substrate. The reported contact angles were calculated from the average of at least 6 drops.

4.1.10 X-ray Photoelectron Spectroscopy

The surface composition of miscible polymer blend films was analyzed by X-ray photoelectron spectroscopy (XPS) using a SAGE 150 (Specs, Berlin, Germany) spectrometer equipped with a hemispherical analyzer (Phoibos 100 MCD-5). Non-monochromatic Mg Kα radiation with 11 kV and 220W was employed at a pressure ca. 10^{-7} Pa in the analysis chamber. The angle between the axis of X-ray source and the analyzer lenses was 54.9 °. The analyzer was mounted at 18 ° to the surface normal. XPS spectra were acquired in the constant analyzer energy (CAE) mode. The analyzed surface area was about 3×4 mm^2. The information depth of XPS measurements is between 5 and 7 nm.

4.2 Materials

Glass transition behavior of different polymers in the thin film geometry was investigated by means of complementary experimental methods. The results for thin polymer films were compared with those of bulk polymers. The materials used in the study are introduced as follows.

4.2.1 Poly(bisphenol A carbonate)

Poly(bisphenol A carbonate) (PC, Aldrich Chemical Co.) with a molecular weight of M_w= 22 kg/mol and a polydispersity index of 1.23 was used. The chemical structure is given in Fig. 15. The glass transition temperature (T_g) of the bulk material determined by DSC is 426 K, as illustrated in Fig. 16. Dichloromethane (≥99.9%) was used to dissolve it.

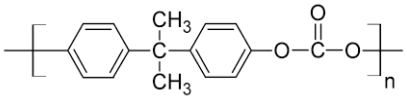

Fig. 15 *Chemical structure of poly(bisphenol A carbonate).*

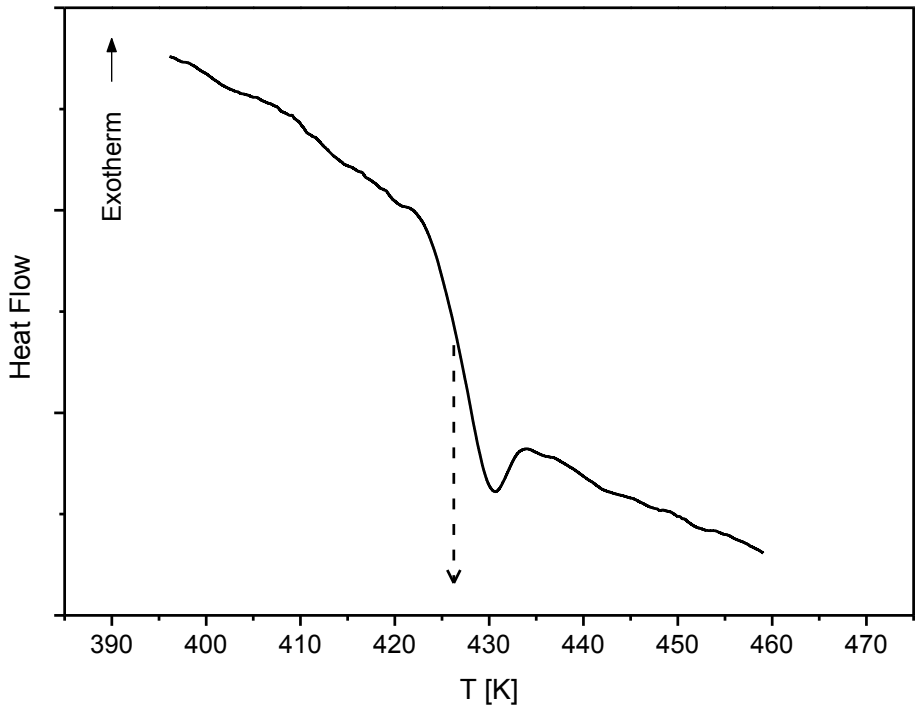

Fig. 16 *DSC curve for poly(bisphenol A carbonate). The arrow points to the T_g value, which is T_g=426 K.*

4.2.2 Polystyrene

Polystyrenes (PS) with the following molecular weights were employed: M_w=1408 kg/mol, Polymer Source, Inc.; M_w=260 kg/mol, Scientific Polymer Products, Inc. and M_w=50 kg/mol, Polysciences, Inc. The polydispersity index is between 1.1 and 1.2. The chemical structure is given in Fig. 17. According to the molecular weight of PS, the samples were named as P1408, P260 and P50 where the number in the code is related to the molecular weight. The glass transition temperatures of P50, P260 and P1408 determined by DSC are 337 K, 376 K and 377 K respectively, as illustrated in Fig. 18. Toluene (≥99.9%) was used to dissolve them.

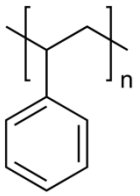

Fig. 17 *Chemical structure of polystyrene.*

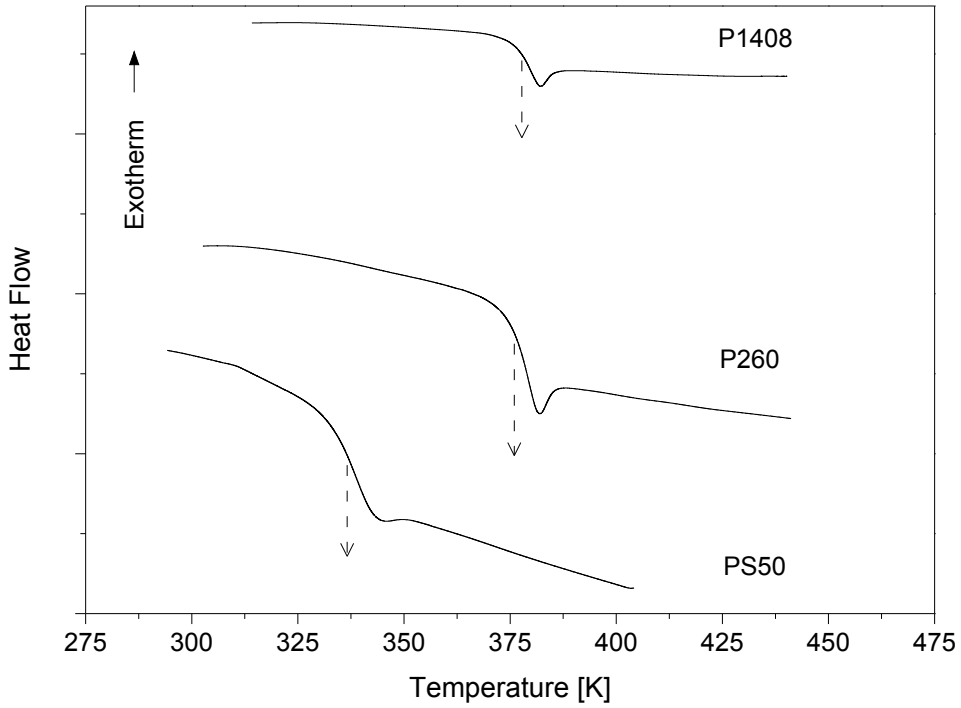

Fig. 18 *DSC curves for polystyrene with different molecular weights. The arrows point to the* T_g *values, which are* $T_{g,P50}$*=337 K,* $T_{g,P260}$*=376 K and* $T_{g,P1408}$*=377 K, respectively.*

4.2.3 Poly(vinyl methyl ether)

Poly(vinyl methyl ether) (PVME) was purchased as in aqueous solution (50 wt%) from Aldrich Chemical Company Inc. with a molecular weight of 60 kg/mol and a PI of 3. The chemical structure is given in Fig. 19. PVME was dried under vacuum at 313 K for 96 h. The glass transition temperature was estimated to be 247 K by DSC, as illustrated in Fig. 20. Toluene (≥99.9%) was used to dissolve it.

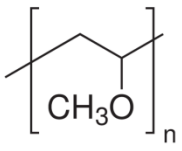

Fig. 19 *Chemical structure of Poly(vinyl methyl ether).*

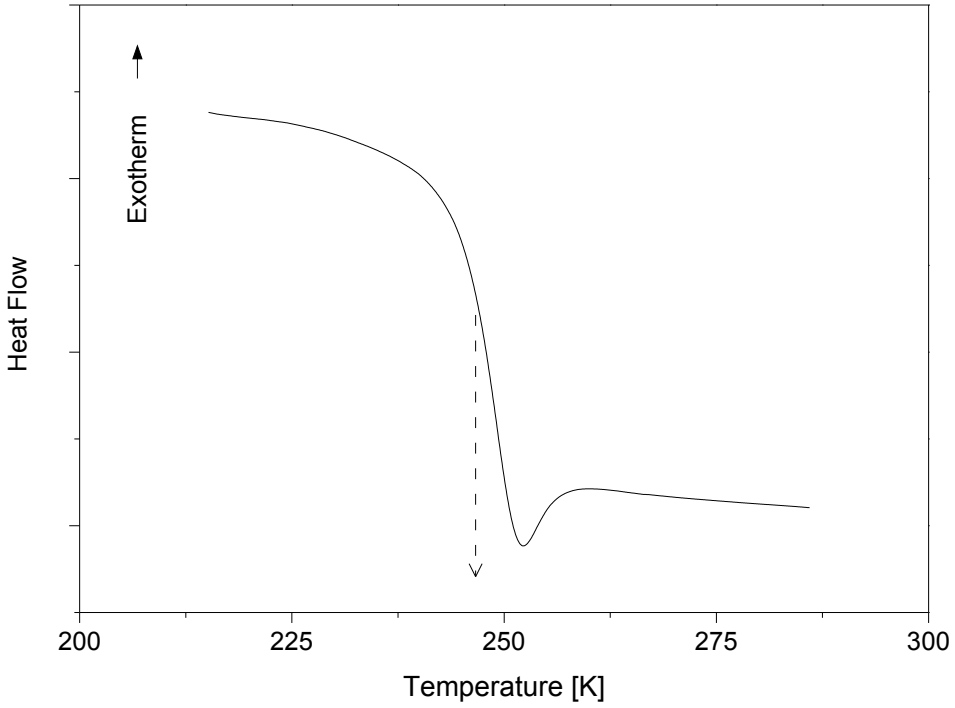

Fig. 20 *DSC curve for Poly(vinyl methyl ether). The arrow points to the T_g value, which is T_g=247 K.*

4.2.4 PS/PVME (50/50 wt%)

The above mentioned PS (M_w=260 kg/mol) and PVME (M_w=60 kg/mol) are dissolved in toluene ((≥99.9%) with the polymer weight fraction of 50/50 to prepare the polymer blend solution. The glass transition temperature of the dry polymer blend was estimated to be 278 K by DSC, as illustrated in Fig. 21.

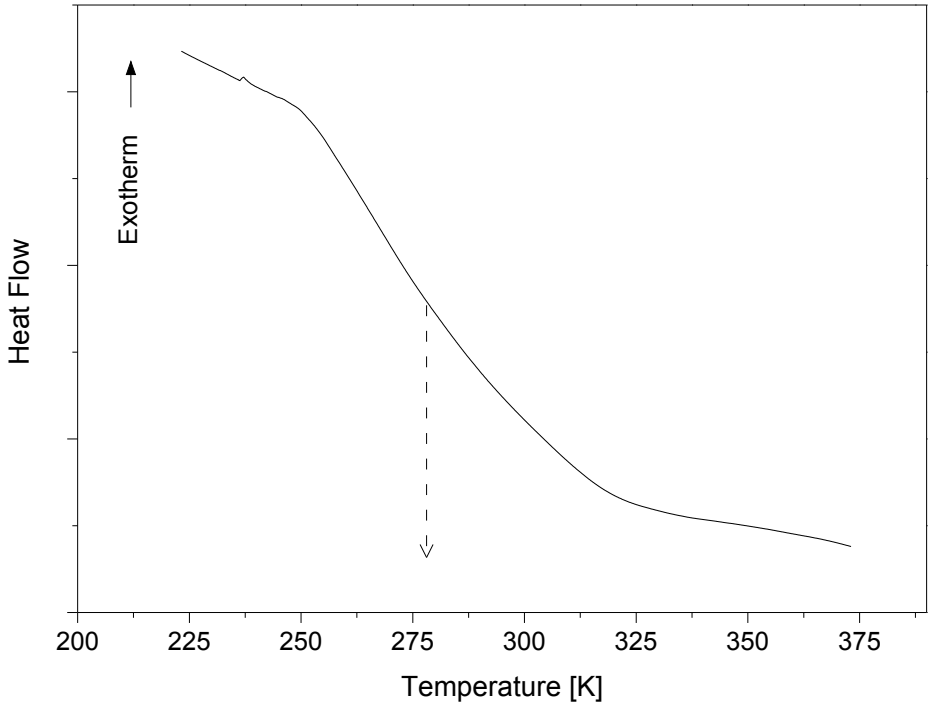

Fig. 21 *DSC curve for polymer blend PS/PVME with the weight fraction of 50/50. The arrow points to the T_g value, which is T_g=278 K.*

4.3 Sample Preparation

4.3.1 Sample Preparation for Dielectric Measurement

For the dielectric measurements the thin films were prepared between two thin aluminum electrodes where glass slides with size of 10 ×10 ×1 mm were used as substrate. The glass slides were first cleaned in an ultrasound alkaline bath at 333 K for 15 min followed by a second ultrasound bath with highly purified water (Millipore, resistivity > 18 MΩ/cm). The glass slides were further washed with purified water without ultrasound for more than 5 times. Then the glass plates were first rinsed in acetone and then in chloroform (both solvents of Uvasol quality). After that the substrates were dried in a nitrogen flow. An aluminum strip (width 2 mm, height ca. 60 nm) was deposited onto the glass substrate by thermal evaporation in an ultra-high vacuum (10^{-6} mbar). After the evaporation of this first electrode the plates were again rinsed in acetone and chloroform. Subsequently, thin films with various thicknesses were obtained by spin coating the filtered (minipore, 0.2 μm) polymer solutions of different concentration (3000 rpm, 60 s). After spin coating, all samples were annealed at a temperature well above the bulk T_g value determined by DSC in an oil-free vacuum. Detailed

information about the annealing conditions for different samples is given in Tab. 1. Atomic force microscopy (AFM) topography images before and after the annealing procedure further showed that down to 10 nm, films had low roughness and no sign of dewetting was observed. An AFM image of ultrathin PC film is shown in Fig. 22.

Tab. 1 *Annealing conditions for different thin polymer films for dielectric measurements.*

Polymer	Annealing Temperature [K]	Annealing Time [h]
PC	433	24
PS (P1408)	433	96
PS (P260a)	373	24
PS (P260b)	413	96
PS (P260c)	433	96
PS (P50)	373	24

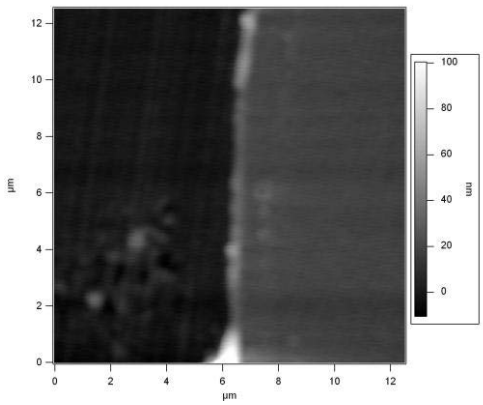

Fig. 22 *AFM image of a scratch across the PC layer (18 nm) on a silicon wafer after annealing. No sign of dewetting was found.*

The preparation of the sample was finished by the evaporation of the counter electrode on the top of the polymer film in an ultra-high vacuum (10^{-6} mbar). In general the evaporation of metals can damage the polymer surface as discussed in Ref. 197. To minimize the diffusion of metal atoms into the film and to avoid a damage of the polymer a so-called flash evaporation (>30 nm/s) was applied. It is known that under these conditions a sharp and smooth metal/polymer interface is obtained [198]. Thin polymer films are capped between two Al strips perpendicular to each other, which work as electrodes in the measurements. The effective area for the thin film geometry is assumed to be circular area with a diameter of

2.256 mm. It should be noted that a thin aluminum oxide layer (1-2 nm) might be formed at the bottom electrode [199]. This layer can influence the dielectric behavior but equivalent circuit models can be applied to estimate its influence.

The corresponding bulk sample was obtained by casting a polymer solution (10-15 wt %) on a polished glass substrate. To control the initial evaporation of the solvent from that thick film the glass plate was placed in a closed chamber. To remove the residual solvent, the bulk sample was annealed under the same conditions as for the ultrathin films. The sample thickness was about 60 μm. The bulk samples were sandwiched between two parallel round gold-covered electrodes with diameter of 20 mm for the measurement. The cross-sectional area of the samples is a little larger than that of gold electrodes. To ensure good contact between the polymer and electrode, thin gold layer was thermally deposited onto the polymer surface before measurement.

4.3.2 Sample Preparation for Calorimetric Measurement

Thin films with one free surface, were prepared directly on the surface of the sensor which is the measuring cell in this method. Firstly, the surface of the sensor was cleaned by dropping a droplet of toluene to its centre in order to remove the dust and organic contaminants on the surface by spinning. This procedure was repeated three times, followed by an annealing process under vacuum at 473 K for 2 h to cure the epoxy resin completely, which was used to glue the chip to the housing. Secondly, thin films with various thicknesses were prepared by spin coating a filtered (minipore, 0.2 μm) polymer solution (3000 rpm, 60 s) onto the central part of the sensor. The film thickness was varied by changing the concentration of the solution. After spin coating, all samples were annealed at a temperature well above their bulk T_g value in an oil-free vacuum oven in order to remove the residual solvent and the stress induced by the spin coating procedure [196]. Moreover an identical and well-defined thermal history of all samples is ensured. Annealing conditions should be optimized regarding different polymers. Detailed information about the annealing procedure is shown in Tab. 2. Because the thickness of the thin films cannot be directly measured on the sensor, a second set of films were prepared under identical conditions on a silicon wafer to estimate the film thickness by AFM. Since the silicon wafer has similar surface properties as the sensor, it can be assumed that under identical spin coating conditions the film on silicon wafer has the same thickness as that supported by the sensor. The film thickness was measured via AFM imaging over a scratch. An AFM image for a PVME film is shown as an example in Fig. 23. The

roughness in the central area of the empty sensor used in the calorimetric measurement is about 3.5 nm rms [164]. The roughness of the film spin coated onto the surface of the sensor is low and decreases with increasing film thickness. For a thickness of ca. 10 nm the roughness of the film on the sensor is comparable with that of a film prepared on a wafer [200]. AFM imaging before and after the annealing procedure showed homogeneous films with low roughness down to thicknesses of 10 nm. No sign of dewetting was observed.

Tab. 2 *Annealing conditions for different thin polymer films for calorimetric measurements.*

Polymer	Annealing Temperature [K]	Annealing Time [h]
PC	443	24
PS (P1408)	433	96
PVME	313	72
PS/PVME (P1408)	323	72

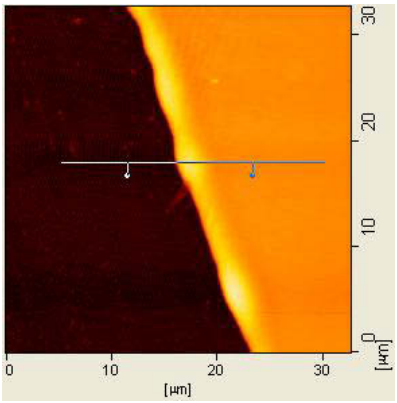

(a)

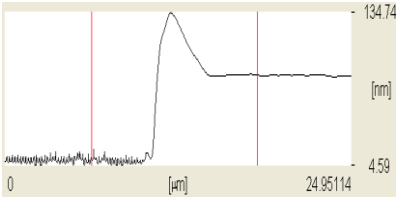

	Z1[nm]	Z2[nm]	ΔZ [nm]	Distance [µm]
■	11.28594	82.15270	70.86676	11.96288

(b)

Fig. 23 *(a) AFM image of a scratch across the PVME film (ca. 70 nm) spin coated on a silicon wafer. (b) Sectional view of the scratch along the line in the AFM image.*

5 RESULTS & DISCUSSION

5.1 Glass Transition of Ultrathin Poly(bisphenol A carbonate) Films

5.1.1 Broadband Dielectric Spectroscopy on Thin Poly(bisphenol A carbonate) Films

5.1.1.1 Broadband Dielectric Spectroscopy on Bulk Poly(bisphenol A carbonate)

Bulk PC shows at least two relaxation processes indicated by peaks in the dielectric loss ε´´ (Fig. 24), which is consistent with the results reported in the literature [201]. The β-relaxation at low temperatures is assigned to localized fluctuations [99]. In the temperature range higher than β-relaxation process, the α-relaxation (dynamic glass transition) takes place. Recently the β-relaxation in PC was investigated systematically by broadband dielectric spectroscopy and neutron scattering [202,203]. It was found that the β-relaxation consists at least of two processes [202]. This is found for the PC investigated in the present study as well (Fig. 25). In Ref. 202 a third relaxation process with a weak intensity is further discussed.

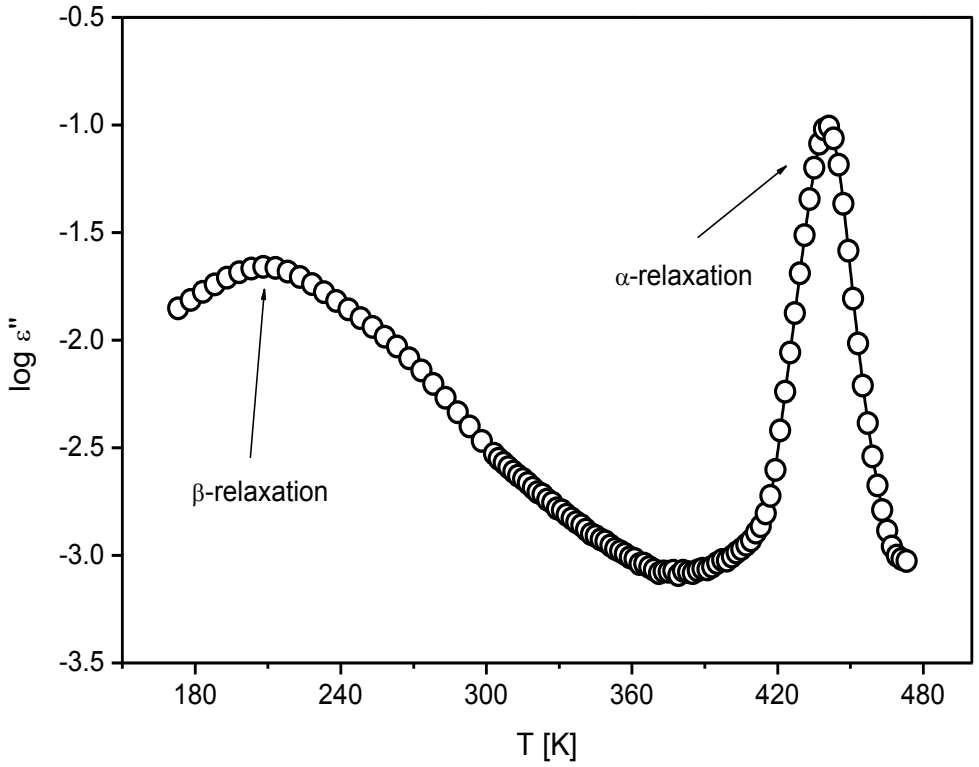

Fig. 24 *Dielectric loss vs. temperature for bulk PC at a frequency of 1 kHz. The line is a guide for the eyes.*

The carbonyl group is the only polar part in the repeat unit of PC and should be therefore involved in the β-relaxation. But there are longstanding discussions about the contributions of phenyl rings to that relaxation process [204,205]. A detailed comparison of the dielectric data with the results obtained from NMR and neutron scattering yields to the conclusion that the β-relaxation process in the low frequency region is also related to the phenylene π-flips and the 90 ° rotation of the phenylene rings becomes dominant in the high frequency flank of the loss peak part [202]. It was further concluded that both processes are strongly coupled.

The model function introduced by HN-function [206] is used to analyze the dielectric spectra quantitatively. Detailed description about the HN-function is provided in Section 3.1.3. An example of fitting the HN-function to the dielectric data is given in Fig. 25, where two HN-functions are used to fit the data of the β-relaxation of bulk PC.

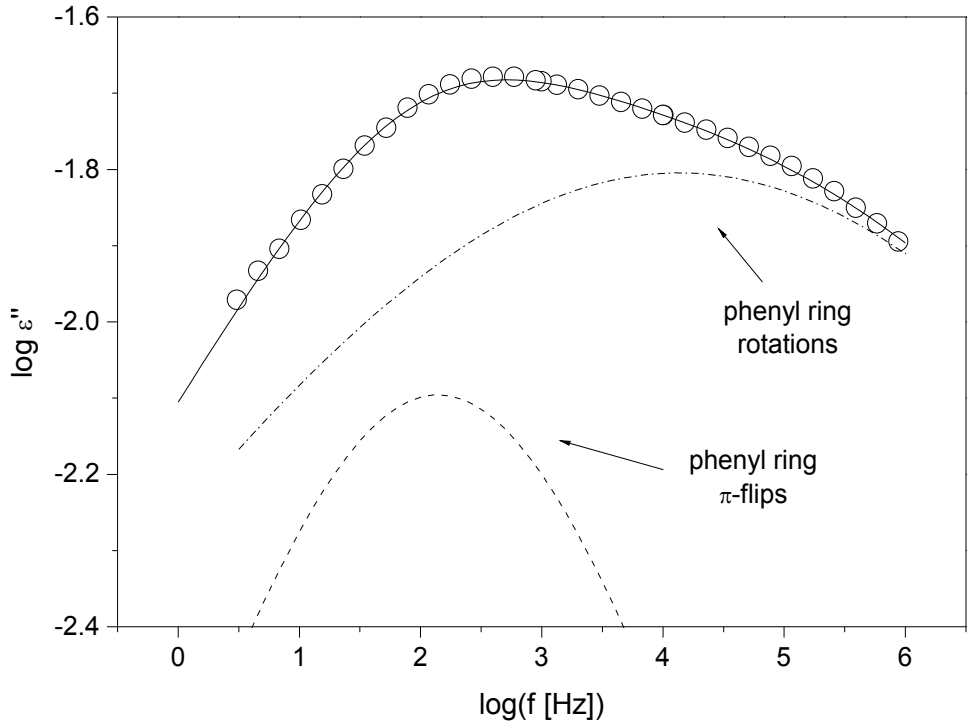

Fig. 25 *Dielectric loss versus frequency for the β-relaxation at T=198.2 K. The solid line is a fit of two HN-functions to the data. The dashed line is the contribution of the π-flips of the phenyl rings and the dotted-dashed line gives the contributions of the rotations of the phenyl rings.*

Fig. 26 gives the temperature dependence of the α-relaxation rates for bulk PC. As it is known for glassy dynamics $f_{p,\alpha}(T)$ is curved versus 1/T, which can be well described by the VFT-equation (Equ. 1) [29-31].

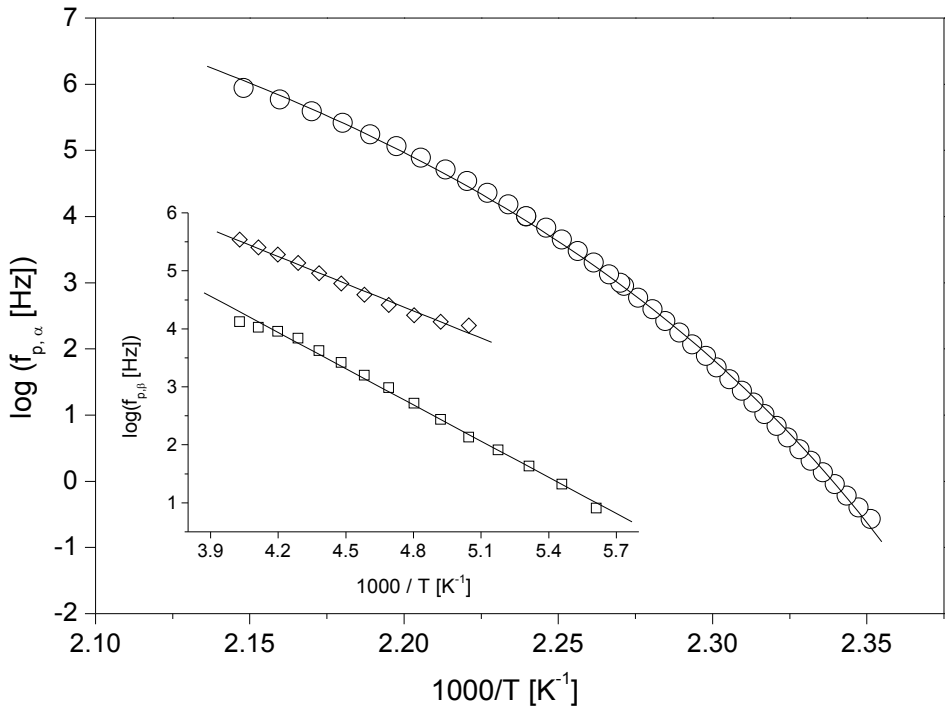

Fig. 26 *Relaxation rate $f_{p,\alpha}$ versus 1/T for the α-relaxation of bulk PC. The line is a fit of the VFT-equation to the data. The inset gives $f_{p,\beta}$ versus 1/T for the both components of the β-relaxation of bulk PC: diamonds – phenyl ring rotations; squares – phenyl ring π-flips. The lines are fits of the Arrhenius equation to the corresponding data.*

For the two components of the β-relaxation the temperature dependence of the relaxation rate obeys the Arrhenius equation (Equ. 3), as shown in inset of Fig. 26. The following activation parameters are estimated: E_A=29.9 kJ/mol and log(f_∞[Hz])=11.8 for phenyl ring rotations; E_A= 39.8 kJ/mol and log(f_∞[Hz])=12.7 for phenyl ring π-flips. These values are in agreement with data from the literature [202].

5.1.1.2 Capacitive Scanning Dilatometry on Thin Poly(bisphenol A carbonate) Films

As discussed in Section 3.3, for polymers with a relatively weak dipole moment like PC, broadband dielectric spectroscopy can be simultaneously used as capacitive scanning

dilatometry to estimate a T_g from the change in the temperature dependence of ε′ at sufficiently high frequencies, i.e. outside the appearance of the α-relaxation.

Fig. 27 gives the temperature dependence of ε′ normalized to the value at T=380 K to get rid of temperature change due to the β-relaxation for several film thicknesses. For all film thicknesses the real part of the complex permittivity decreases with increasing temperature up to a given temperature where the temperature dependence of ε′ changes. The initial deviation of the dielectric permittivity from a linear temperature dependence is used to extract the thermal glass transition temperature (Fig. 27), which is plotted versus the thickness of the layer in Fig. 28. The increase of ε′ at higher temperatures is due to the contribution of the α-relaxation.

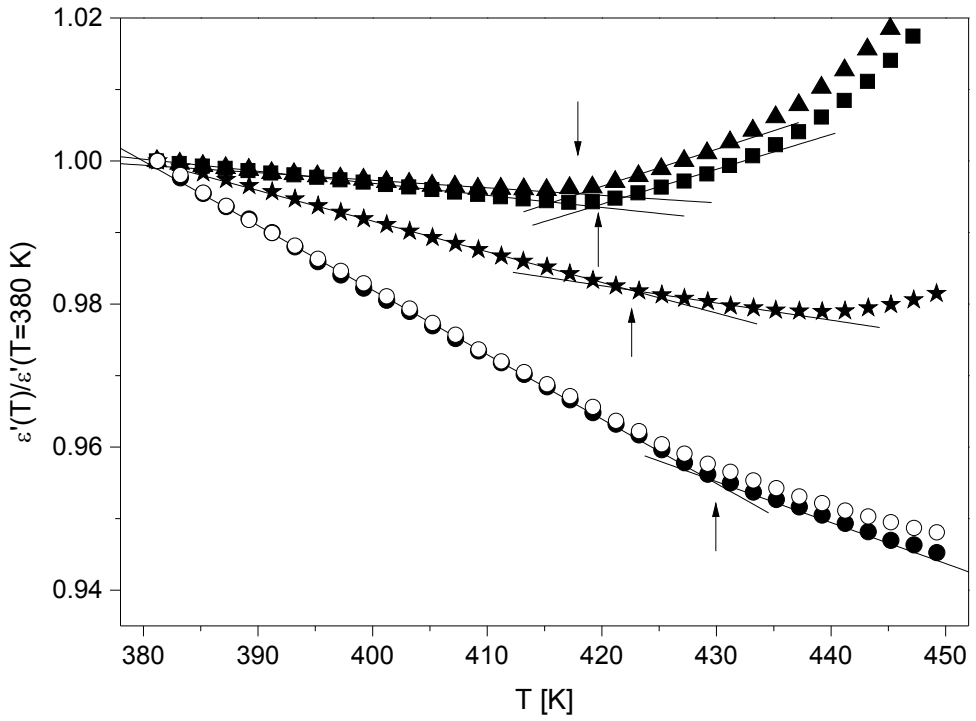

Fig. 27 *Temperature dependence of the dielectric permittivity ε′ normalized with respect to its value at T=380 K for a frequency of 10^5 Hz for different film thicknesses d: filled triangles – bulk; filled squares – 198 nm; filled stars – 47 nm; filled circles: 13 nm. The solid lines are linear fits to the data. The arrows indicate the values of T_g. The open circles are data for the 13 nm film measured for a frequency of 10^4 Hz. It is shown that the effect of the dielectric dispersion is quite weak above 10^4 Hz.*

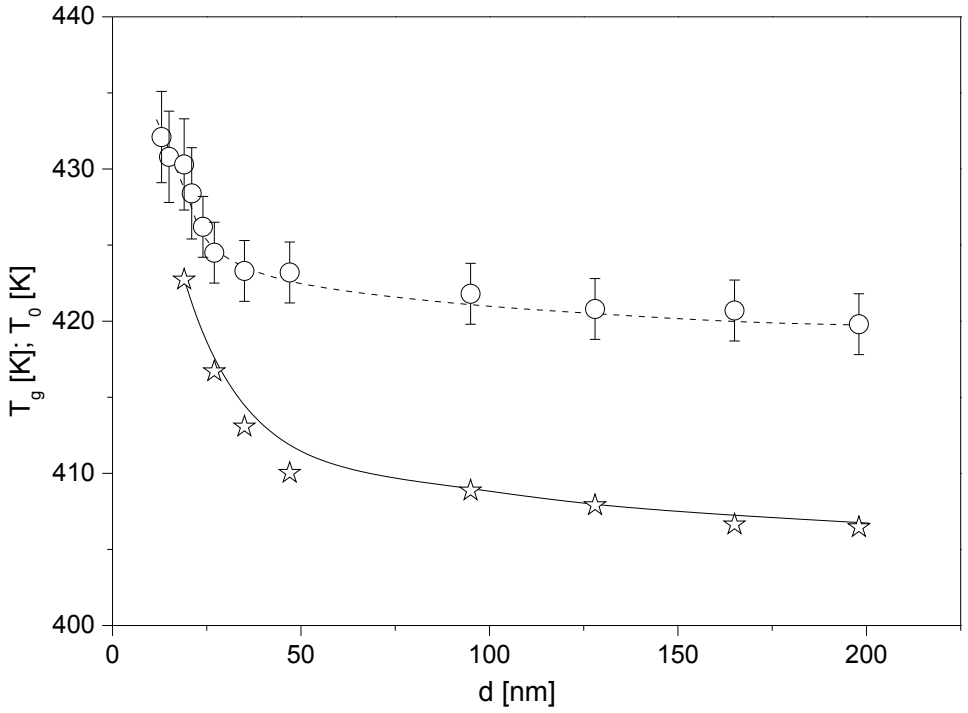

Fig. 28 *Circles – Thermal T_g as measured by capacitive scanning dilatometry versus film thickness. The dotted line is a guide for the eyes. Stars – Vogel temperature T_0 versus film thickness. The solid line is a guide for the eyes.*

Fig. 28 shows that down to a film thickness of ca. 20 nm T_g is more or less independent of the film thickness or increases slightly. For thicknesses lower than 20 nm an increase of T_g with decreasing d is observed. This behaviour is quite similar to that found for polysulfone [207] and points to a strong interaction of PC with the Al substrate which leads to the formation of an adsorbed boundary layer with a reduced mobility.

5.1.1.3 Broadband Dielectric Spectroscopy on Thin Poly(bisphenol A carbonate) Films

Fig. 29 gives an example for the analysis of the dielectric spectra of a thin PC film with a thickness of 47 nm. The thin PC films show a relatively strong conductivity contribution. Therefore the analysis of the dielectric spectra is restricted to higher frequencies and to a narrower temperature range compared to the bulk sample. The reason for the enhanced conductivity contribution might be an arrangement of the phenyl rings parallel to the electrodes which lead to the formation of pathway for conduction.

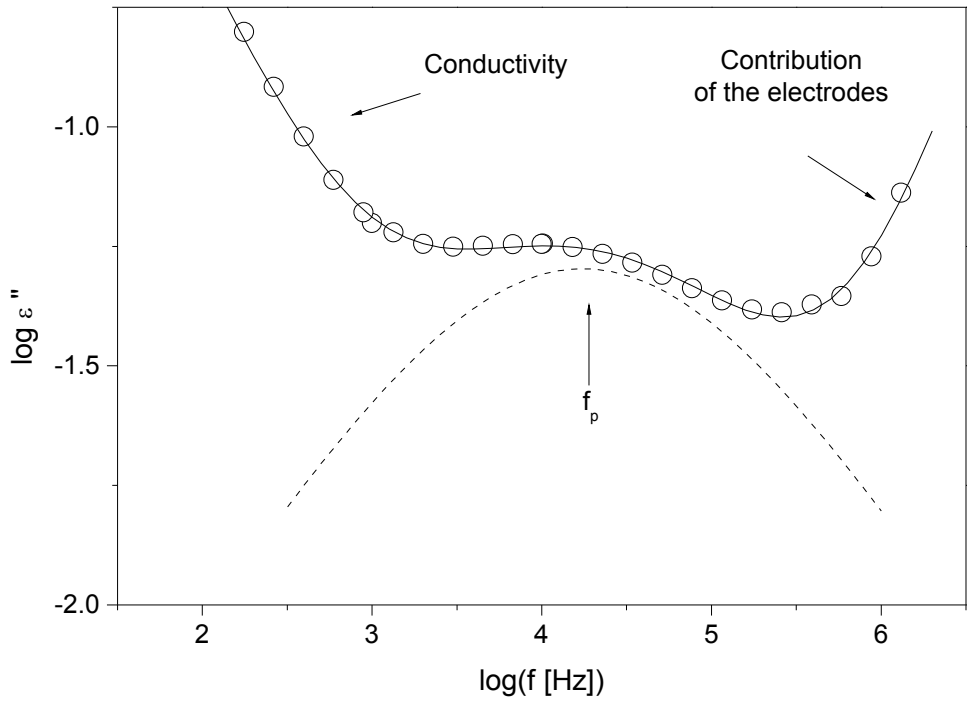

Fig. 29 *Dielectric loss versus frequency of a 47-nm-thin PC film at T= 449 K. The solid line is a fit of Equ. 46 to the data. The dashed line gives the contribution of the α-relaxation.*

In Fig. 30 the relaxation rate $f_{p,\alpha}$ is plotted versus 1/T for different film thicknesses. Besides for the lowest layer thickness all other data are collapsing into one chart. This is in agreement with the results obtained by CSD (Fig. 28). For the lowest film thickness the whole curve is shifted to higher temperatures. To analyze the temperature dependence of the relaxation rate in more detail a derivative method is used [208]. With this method the temperature dependence of $f_{p,\alpha}$ can be analysed in detail irrespective of the prefactor. For a temperature dependence according to the VFT-equation (Equ. 1)

$$\left[\frac{d\log f_p}{dT}\right]^{-1/2} = A^{-1/2}(T - T_0) \tag{54}$$

is obtained. In a plot $\left[d\log f_p / dT\right]^{-1/2}$ versus T a VFT-behavior shows up as a straight line (inset in Fig. 30). Besides the linearization of the data the number of free fit parameters is reduced which increases the significance of the estimated parameters. Since all experimental data given in the inset of Fig. 30 can be well described by straight lines, it is concluded that for all thicknesses the relaxation rates follow the VFT temperature dependence.

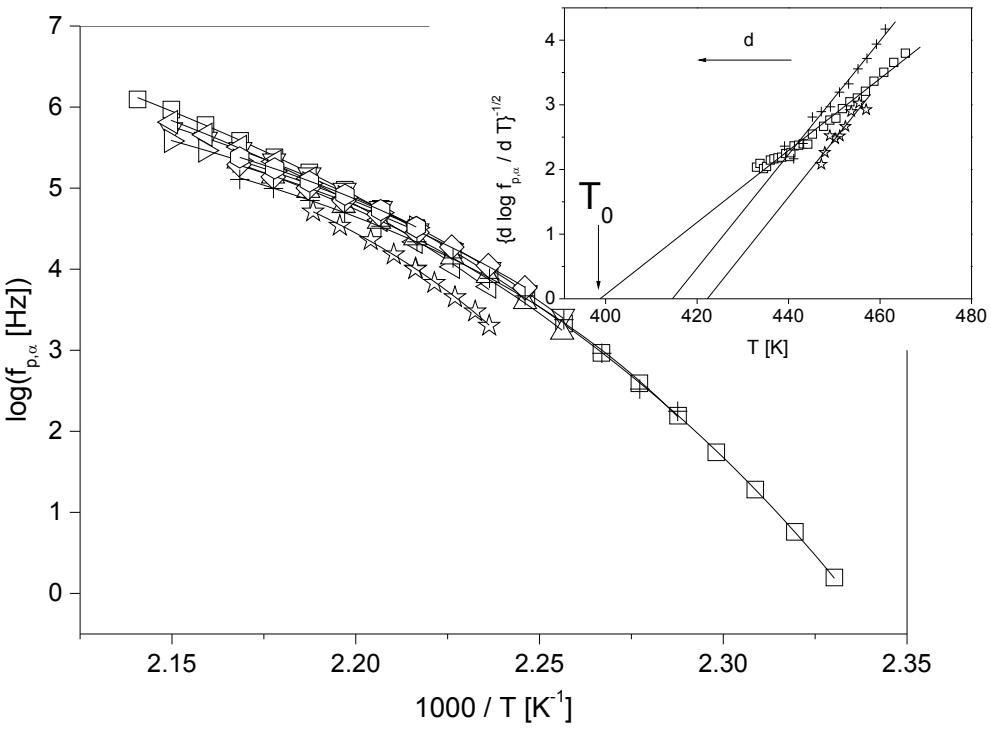

Fig. 30 *Relaxation rate $f_{p,\alpha}$ versus 1/T for the α-relaxation of PC films for the labeled film thicknesses. Bulk (squares); 198 nm (down-pointing triangles); 165 nm (left-pointing triangles); 128 nm (right-pointing triangles); 65 nm (up-pointing triangles); 47 nm (diamonds); 35 nm (crosses); 27 nm (hexagons); 19 nm (stars). Lines are fits of the VFT-equation to the corresponding data as described in the text. The inset gives* $\left(\frac{\mathrm{d}\log \mathrm{f}_{\mathrm{p},\alpha}}{\mathrm{d}\,\mathrm{T}}\right)^{-1/2}$ *vs. temperature for labelled thicknesses. Lines are linear regressions to the data.*

The following procedure was applied to estimate the parameters of the VFT-equation and the fragility strength D for a quantitative comparison. T_0 and the A parameter were taken from the derivative technique by linear regression. The prefactors were obtained by a fit of the VFT equation to the relaxation rates keeping T_0 and A fixed. The parameters are shown in Tab. 3. As discussed above for the thin films the investigated temperature range is narrower than for the bulk sample. This might complicate a direct comparison of the data for the bulk with data for the thin films. But for the thin films a similar temperature range is analysed where the thickness of the sample varies by more than one order of magnitude. Therefore the data for the thin films can be compared directly.

Tab. 3 *Estimated VFT-parameters and glass transition temperatures T_g.*

Thickness (nm)	log(f_∞ [Hz])	A (K)	T_0(K)	T_g (K)	D=A/[T_0ln(10)]
Bulk	13.22	573.4	385.0	418.5	0.646
198	9.82	242.4	406.5	419.8	0.259
165	9.68	225.3	406.6	420.7	0.240
128	8.91	190.0	407.9	420.8	0.202
95	8.95	181.9	408.8	421.8	0.193
47	8.60	169.8	410.0	423.2	0.179
35	8.24	163.8	413.1	423.3	0.172
27	8.34	131.8	416.7	424.5	0.137
19	8.20	119.4	422.7	430.3	0.122

The Vogel temperature T_0 shows a similar dependence on the film thickness as the glass transition temperature T_g estimated by CSD which indicates that both data sets analysed independently from each other are consistent (Fig. 28). Down to a film thickness of ca. 20 nm T_0 is more or less independent of the film thickness or increases slightly. For thicknesses lower than 20 nm a strong increase of T_0 with decreasing d is observed. Similar behaviour was also found for other systems [138,153,209]. The fragility strength D is calculated from the estimated VFT-parameters and plotted versus 1/d in Fig. 31. It is shown that the fragility strength decreases with deceasing film thickness and seems to reach a plateau value for low values of d.

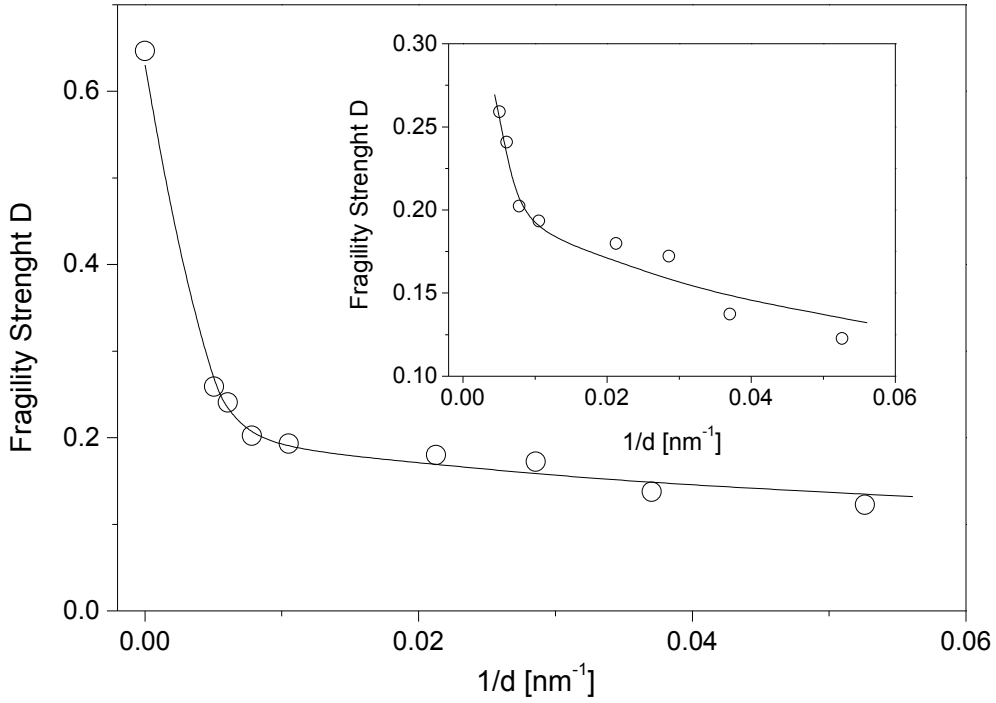

Fig. 31 *Fragility strength D vs. inverse film thickness (1/d). The inset compares the data only for the thin films. The lines are guides for the eyes.*

The dielectric strength Δε is obtained in addition to the relaxation rate from the fit of the HN-equation to the data. Kirkwood and Fröhlich [210] expressed it as a function of temperature (Equ. 31). For several layer thicknesses Δε is plotted versus temperature in Fig. 32.

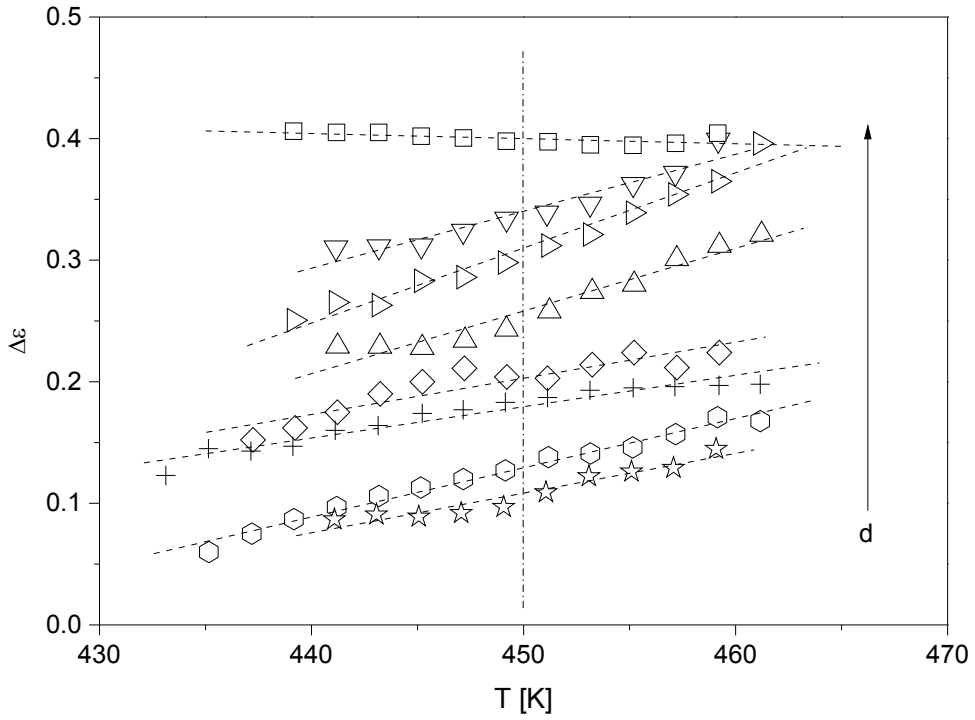

Fig. 32 *Δε versus temperature for different film thicknesses: squares – bulk, down-pointing triangles – 198 nm, right-pointing triangles – 128 nm, up-pointing triangles – 95 nm; diamonds – 47 nm, crosses – 35 nm, hexagons – 27 nm, stars – 19 nm. The dashed line is a guide for the eyes. The doted-dashed line indicates for comparison.*

In Fig. 33, Δε is plotted as a function of the inverse of the layer thickness (equivalent to the surface/volume ratio in the thin film geometry) at T= 450 K. As a general feature of the α-relaxation of thin PC films, the dielectric strength decreases with reducing film thickness. This trend was explained in terms of chain adsorption [211], as the dipole moment does depend on the film thickness. The decrease of Δε is due to a strong reduction of the number density of fluctuating dipoles in proximity of the interface, a hypothesis also proven by measurements of the local dielectric strength in multilayer experiments [212]. In the specific case of the polymer/metal system investigated, this idea is further confirmed by the high interfacial energy between polycarbonate and AlO_x (Section 5.1.3), inhibiting the motion of the segments close to the electrodes on the time and the length scale of the glass transition.

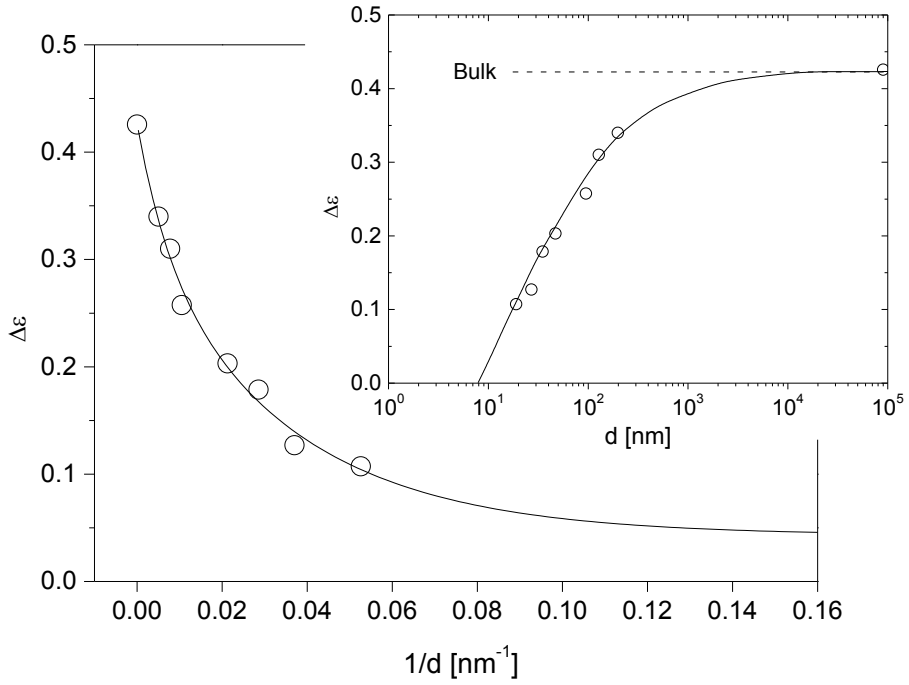

Fig. 33 *Δε vs. inverse film thickness for T=450 K. The inset gives Δε vs. d. Lines are guides for the eyes.*

The observed pronounced non-linear reduction of the dielectric strength upon increase of the surface to volume ratio suggests the presence of a strong gradient of molecular mobility along the distance from the metallic interfaces. To understand such a profile, the impact of the thickness on the temperature dependence of the dielectric strength was analyzed (Fig. 32).

Contrary to the prediction of Equ. 31 valid for the structural relaxation of bulk systems, in thin films Δε increases with increasing temperature, a behaviour was previously observed also in other polymer film of comparable thickness [152,153]. This anomalous trend is the entanglement of two different phenomena, i.e. the reduction of the mean square dipole moment in proximity of a bounding interface coupled to the impact of thermal energy on the defreezing of segmental motion [154,213]. Increasing the temperature induces a gradual release of the constraints affecting the segmental dynamics, which yields to the anomalous increase of dielectric strength upon heating.

We quantitatively determined the temperature dependence of the penetration depth of the interfacial interactions on the structural relaxation, applying an analysis recently proposed by Rotella and coworkers [211]. The profiles of mobility, based on the density number of dipoles participating to the structural relaxation, were built up mimicking the usual dependence of

density in proximity of an interface, via a function symmetric with respect to the centre of the film

$$\Delta\varepsilon(x) = \Delta\varepsilon^{BULK}[\tanh^2(3\frac{x}{\varphi}+\rho)+\tanh^2(3\frac{d-x}{\varphi}+\rho)-\tanh^2(3\frac{d}{\varphi}+\rho)] \qquad (55)$$

where *x* is the distance from the interface, φ is the length scale of the reduction of Δε and ρ is a parameter taking account the residual polarization at the interface, as $\tanh^2(\rho) = \Delta\varepsilon(0)/\Delta\varepsilon_{bulk}$.

To obtain the best fitting parameter for each data set (i.e Δε(d) in isothermal condition), the experimental data were compared to values calculated via Equ. 55. The procedure required the calculation of the total dielectric response of a film of thickness *d*, via a layer resolved approach, whose validity is supported by previous simulation work on the dielectric relaxation at the nanoscale [214].

The film is divided into *d* sub-layers, i.e. with a resolution of 1 nm; at each sub-layer, we attributed a dielectric function reproduced by the HN equation. The position and the shape of the peak of each sublayer is kept constant where the dielectric strength is varied, following a profile given by discretization of Equ. 55 in steps of 1 nm. Considering the orientation of the electric field in our experiments (perpendicular to the polymer/metal interface), the total dielectric response was obtained summing up the contributions of all the sub-layers as for capacitors in series, $C_{TOT}^{-1}(f,T) = \sum_j C_j^{-1}(f,T)$ where $C_j(f, T)$ is the capacitance of the j_{th} sub-layer. In our computation, the value of $\Delta\varepsilon_{TOT}$ was obtained directly from the real part of the dielectric function following its definition [215], as the difference between ε_S, the frequency independent value reached by the real part of the dielectric function for $\omega << \omega_0$, and ε_∞. We considered a frequency range broad enough to take into account the broadening of the structural peak, i.e. a larger separation between the frequency regions corresponding to ε_S and ε_∞, and the shift in the peak maximum upon confinement. Moreover, to limit the number of free parameters we kept the shape parameters and the position of the peak in the sub-layers constant. This is justified by our previous work [134,212] where we verified that in ultrathin films of amorphous polymers the dielectric strength depends on the interaction with the substrate and on the annealing conditions used (In the samples analyzed in our work γ_{TOTAL} was constant, and samples were prepared under the same annealing conditions). This

procedure is repeated for a matrix of couples (φ_i, ρ_i) centered around physically reasonable starting parameters, and found the best fitting values for the experimental values in Fig. 34, upon minimization of the squared deviations: $Err = \frac{1}{n_{\exp}} \sum_{i=1}^{n_{\exp}} \left(\frac{\Delta\varepsilon_i^{th} - \Delta\varepsilon_i^{\exp}}{\Delta\varepsilon_i^{\exp}} \right)^2$ where n_{exp} is the number of the experimental data points, i.e. the number of thicknesses measured at each temperature, $\Delta\varepsilon_{th}$ and $\Delta\varepsilon_{exp}$ are respectively the values of the dielectric strength obtained via the model and experimentally. The obtained values are plotted in Fig. 33. At 443 K, φ reaches 90 nm, a value which is comparable, although slightly larger, to that of PET in the same dynamic range. Compared to more flexible polymers, where φ does not exceed 40 nm, the relatively longer length scale reflects the rigidity of the chains of PC. The less flexibility combined to the previously mentioned arrangement of the phenyl rings parallel to the electrodes induces a residual polarization at the interface on the order of 20% of the bulk value, i.e $\rho \sim 0.5$, responsible for the nonzero value of $\Delta\varepsilon$ in the thinnest films. The temperature dependence of the penetration depth of the interfacial interactions increases upon cooling with an activation energy 10 folds smaller than the structural relaxation. Such a trend is in line with what is observed in ultrathin films of polystyrene labelled with polar moieties [211] and what is predicted by molecular dynamics simulations [216].

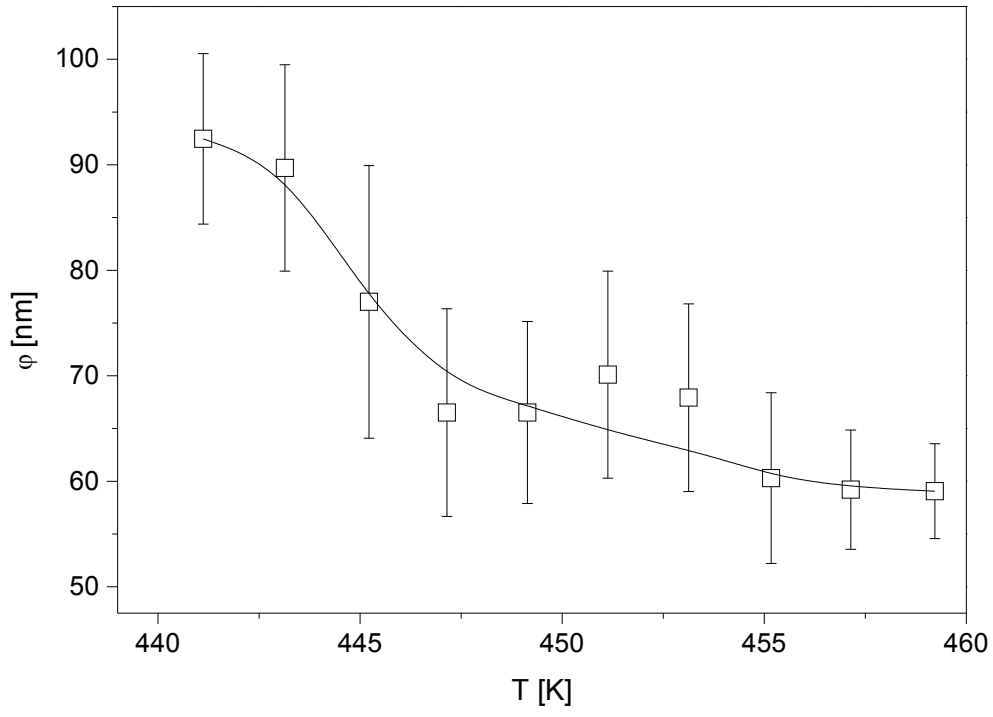

Fig. 34 *Temperature dependence of the penetration depth φ.*

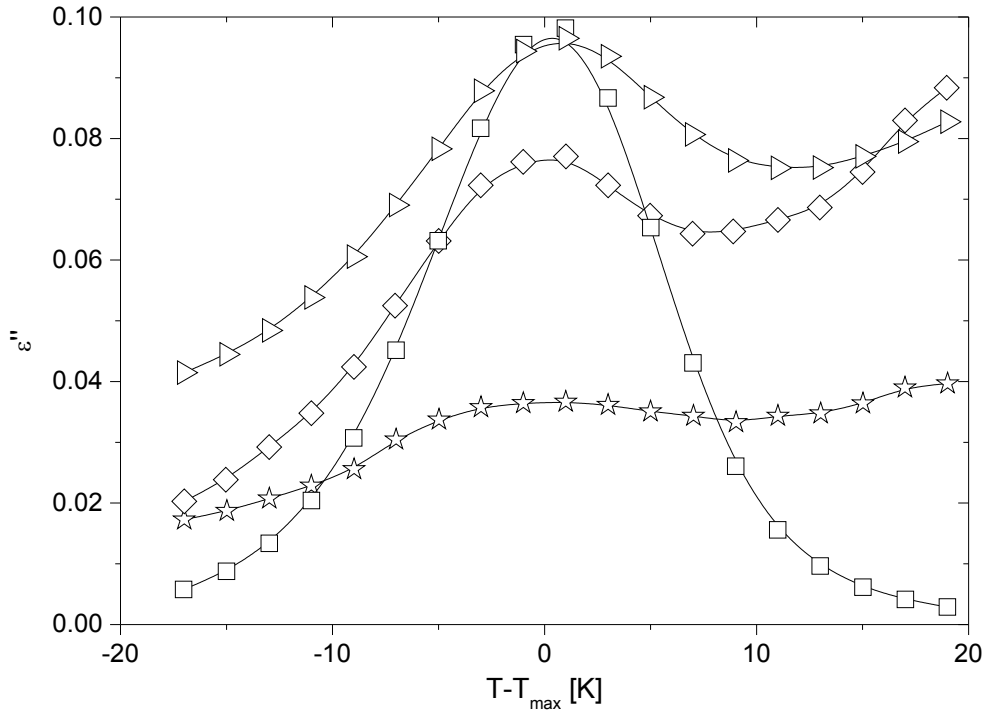

Fig. 35 *Dielectric loss versus normalized temperature at 1 kHz for different film thicknesses: squares – bulk, right-pointing triangles – 95 nm, diamonds – 47 nm, stars – 19 nm. The lines are guides for the eyes.*

The presence of a profile of mobility affecting the dynamics of the film [217,218] is reflected also in the thickness dependence of the width of the α-peak, which broadens upon reduction of the thickness (Fig. 35**)**. This broadening arises from the heterogeneity in the molecular dynamics, related to the introduction of slower modes in the distribution of relaxation times. At the polymer/metal interface, in fact, the mobility of chains is hindered down to the segmental motion, due to less available space [219] and the favorable interactions with the Al layer surface (AlO_x). The perturbations into the chain conformations responsible for such deviation from bulk dynamics vanish after a dynamic length scale λ. It is possible to estimate λ by an analysis of the thickness dependence of the broadening of the α-relaxation peak in capped films, based on the considerations of samples with symmetric interfaces [220]. In thick films, $d >> \lambda$, the volume fraction of segments relaxing like in the bulk is predominant and the width is thickness independent. Upon thickness reduction, the weight of interfacial layers on the total dielectric signal increases and because of the different timescale of the segmental relaxation at the interface [212], the α-peak broadens in the frequency domain. Such a confinement induced broadening reaches a maximum in proximity of 2λ, where the

bulk component disappears. Further reduction of the thickness corresponds to a cut off of those modes relaxing like in bulk, which leads to a reduction of the broadening. For PC, in the thickness range where it was possible to determine univocally the shape of the structural peak, i.e. down to 19 nm, only a broadening of the α-peak is observed. Consequently we can estimate that, at each interface, the interaction with the metallic substrate affect the dynamics for a length scale $\lambda \leq 9$ nm. This critical length is in line with the trends in the thickness dependence of T_g and T_0 (Fig. 28) where no confinement effect is observed for films where the separation between the two metallic layers exceeds 20 nm.

Such a dynamic length scale is much smaller than that determined via the thickness dependence of the dielectric strength, a trend in line with the behavior of almost all polymer systems investigated at the nanoscale [211]. The origin of this apparent discrepancy stays in the different averaging rules affecting the intensity ($\Delta\varepsilon$) and the shape (peak maximum, broadness, asymmetry) of a relaxation peak [154], which permit to observe a perturbation in the dynamics only at higher surface/volume ratios (thinner films) compared to those of interest to static properties like the dielectric strength.

5.1.1.4 Dielectric Loss Spectra below the Temperature Region of α-relaxation

To further discuss the dielectric data the loss part is plotted at a frequency of 1 kHz versus temperature for the bulk and thin film samples (Fig. 36). Compared to the bulk sample the dielectric loss of thin films is significantly increased for temperatures below the α-relaxation [221]. By convention a dynamic T_g can be defined by the maximum temperature of the α-relaxation which corresponds only to one point of the whole spectra. However, any finite value of the dielectric loss corresponds to certain molecular fluctuations or motions [222]. It might be that different aspects of the molecular mobility which leads to different definitions of the glass transition temperature and therefore to different thickness dependencies.

Fig. 36 additionally reveals that the intensity of the β-relaxation peak decreases with decreasing film thickness and cannot be observed for thinnest film. As discussed above the β-relaxation is assigned to different motional modes of the phenyl ring. The decrease in the intensity of the β-process means that the phenyl rings are perhaps immobilized by the polymer-substrate interaction. It is likely a planar arrangement of the phenyl rings normal to the Al layer surface. A reduction of the localized fluctuation in ultrathin PC films was also

observed by neutron scattering [223]. Moreover such a depression of the β-relaxation strength is in good agreement with previous dielectric studies of PMMA [224].

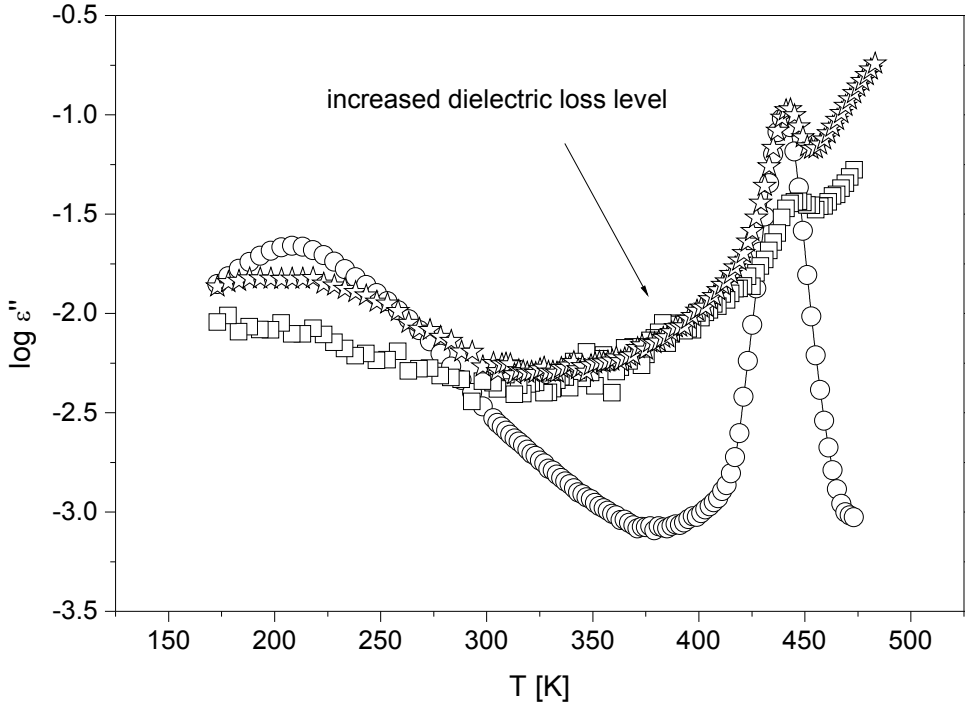

Fig. 36 *Dielectric loss versus temperature at a frequency of 1 kHz: circles - bulk polycarbonate, stars – 128 nm, squares - 19 nm.*

5.1.2 Specific Heat Spectroscopy on Thin Poly(bisphenol A carbonate) Films

The thickness dependence of dynamic T_g for thin PC films was further investigated by specific heat spectroscopy using differential AC chip-based calorimetry. In the calorimetric measurement, the amplitude U_R and the phase angle φ of the complex differential voltage are obtained as a function of temperature at a given frequency. A typical measurement at a frequency of 160 Hz for a 38-nm-thick film is shown in Fig. 37. At the dynamic glass transition the amplitude of the complex differential voltage increases step-like where the phase angle shows a peak. In the raw data of the phase angle there is an underlying step in the signal which is proportional to the amplitude signal. The phase angle is corrected by subtracting this contribution [225]. A dynamic T_g can be determined for instance as the half step temperature of U_R or by the peak temperature of the corrected phase angle. The dynamic T_g values originating from different parts of measured thermopile signals are close to each other. As shown in Fig. 37, only small differences within 1 K were found.

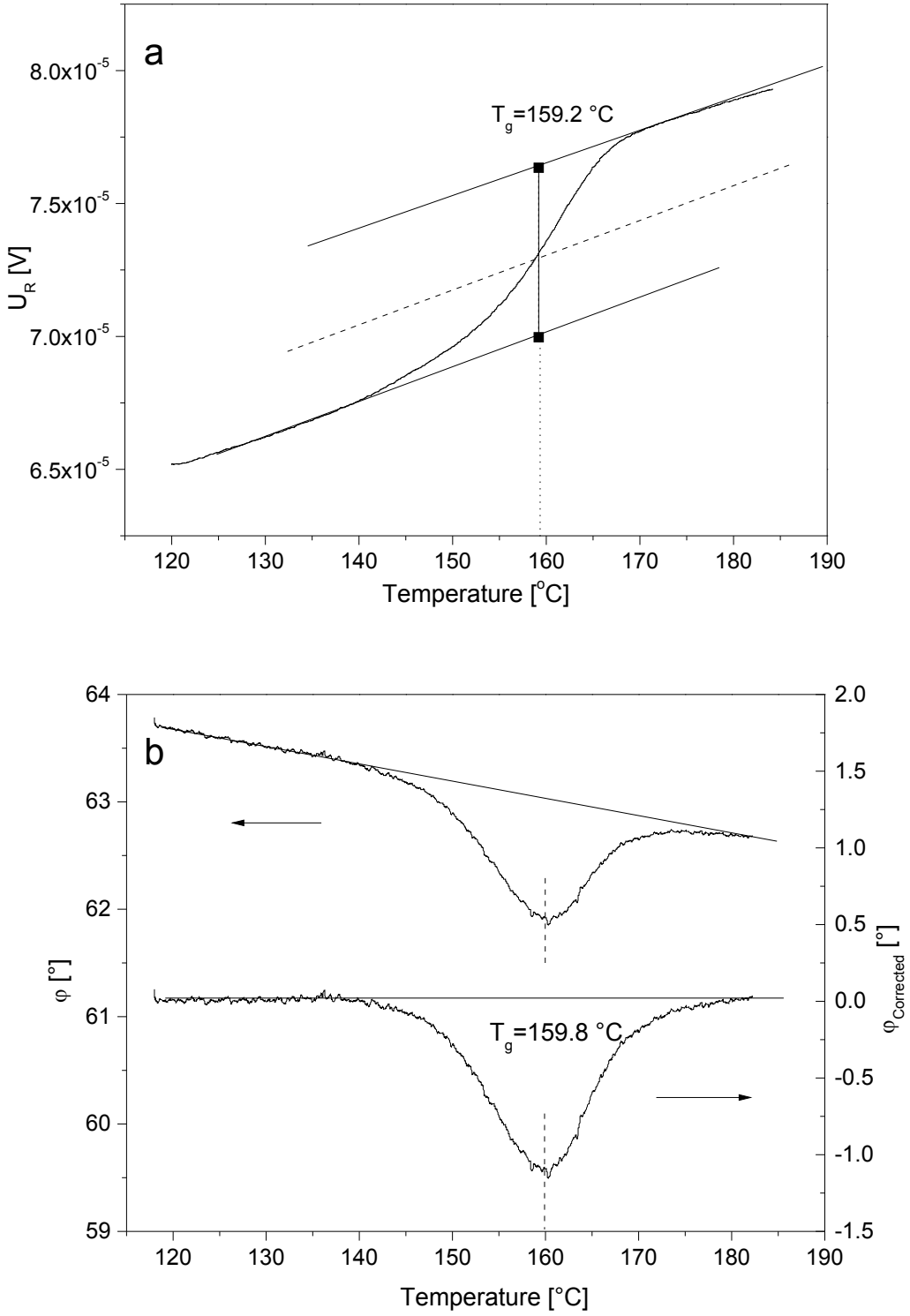

Fig. 37 *Amplitude (a) and phase angle (b) of the complex differential voltage of a thin PC film (38 nm) under a heating process at a frequency of 160 Hz. The contribution of the underlying step in heat capacity in the raw data of the phase angle (upper panel) was subtracted from the overall curve (lower panel).*

A series of measurements were carried out at the frequency of 160 Hz with an optimized sensitivity in order to determine the dynamic T_g of the thin polymer films more accurately in its dependence on the film thickness. The data were collected during continuous heating and cooling processes at a rate of 1 K/min, where the second heating run is used for analysis. To compare the results measured for different film thicknesses properly the data have to be normalized (Fig. 38). The amplitude of the complex differential voltage was normalized by its step height at the dynamic glass transition minus its value at the dynamic T_g after normalization (Fig. 38a):

$$U_R /(U_{R,T_1} - U_{R,T_2}) - U^N_{R,Tg} \qquad (56)$$

where T_1=175 °C and T_2= 140 °C are chosen. The corrected phase angle is normalized by its maximal value (Fig. 38b). For both the amplitude and the phase angle measured for the different film thicknesses the rescaled data collapse into one chart. This indicates that the temperature corresponding to half of the amplitude step as well as that corresponding to maxima of the phase angle of the complex differential voltage is independent of the film thickness down to 10 nm. In other words the dynamic T_g is independent of the film thickness down to the value of 10 nm.

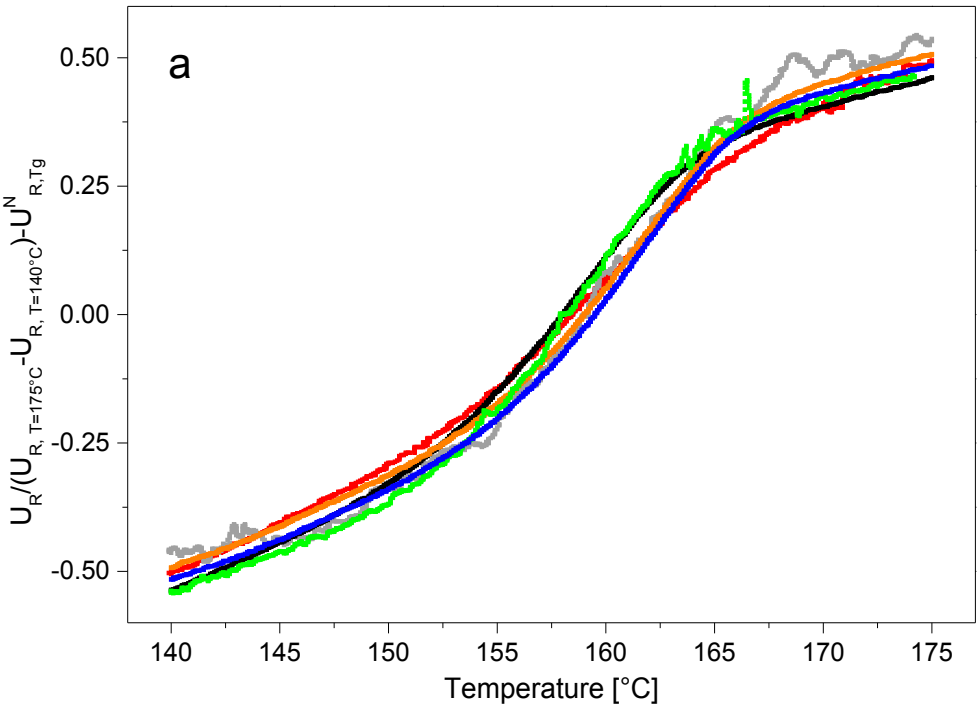

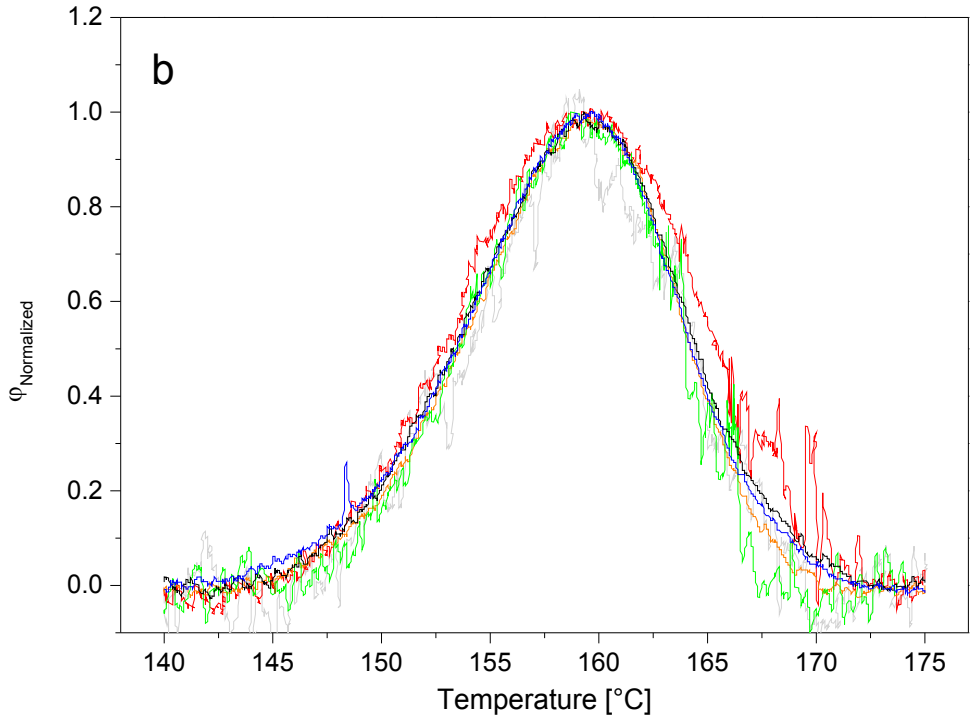

Fig. 38 *Rescaled amplitude (a) and normalized phase angle (b) of the complex differential voltage measured for thin films at a scanning rate of 1 K/min at a frequency of 160 Hz for different thicknesses: 10 nm (grey), 18 nm (green), 38 nm (black), 41 nm (orange), 55 nm (red), 120 nm (blue). Please note that for lower film thicknesses the data show a larger scatter due to the essential lower absolute values of the measured voltage.*

It is interesting to analyze the confinement effect on the cooperativity length scale ξ or the corresponding volume V_{CRR} at the dynamic glass transition for different film thicknesses, which can be calculated according to Equ. 10. Two main quantities, the specific heat capacity c_p and the mean temperature fluctuation δT should be taken into consideration for the estimation of the extent of cooperativity. The specific heat capacity of the material can be related to the measured heat capacity of the sample by

$$c_p = C_S / m = i\omega \overline{C}^2 U_R / mSP_0 = i\omega \overline{C}^2 U_R / \rho AdSP_0 \qquad (57)$$

where m is the sample mass, ρ is the density, A is the heated area of the sensor and d is the film thickness. Here ΔU_0 is assumed to be zero. In principle $\overline{C}$ and S can be estimated from the frequency dependence of the thermopile voltage of a single sensor [164]. Considering that the heated area of the sensor is rarely affected by the sample, the measured mass is

proportional to the thickness of the film. When U_R is further normalized with respect to the film thickness, the curves of U_R/d vs. T collapse together within an uncertainty of 30%, consistent with Ref. 164. This means c_p is independent of the film thickness within the experimental error. The remaining quantity to estimate the extent of cooperativity according to Equ. 10 is the mean temperature fluctuation δT. δT is the width of the glass transition and can be extracted experimentally from the temperature dependence of the specific heat capacity [42]. Recently, it became also possible to estimate δT from the phase angle estimated by specific heat spectroscopy [44-46,226]. It can be estimated by fitting Gaussians to the data of the phase angle (Fig. 39) and the standard deviation σ of the Gaussian fitting is δT= σ. δT is independent of the film thickness with a mean value of 9.7±0.7 K (Fig. 40). Since the specific heat capacity is also independent of the thickness it can be concluded that there is no thickness dependence of the CRR volume or cooperativity length scale according to Equ. 10 developed by Donth [12,41]. This means the extent of the cooperativity is smaller than the lowest film thickness (10 nm). This is in agreement with the data given in Ref. 226.

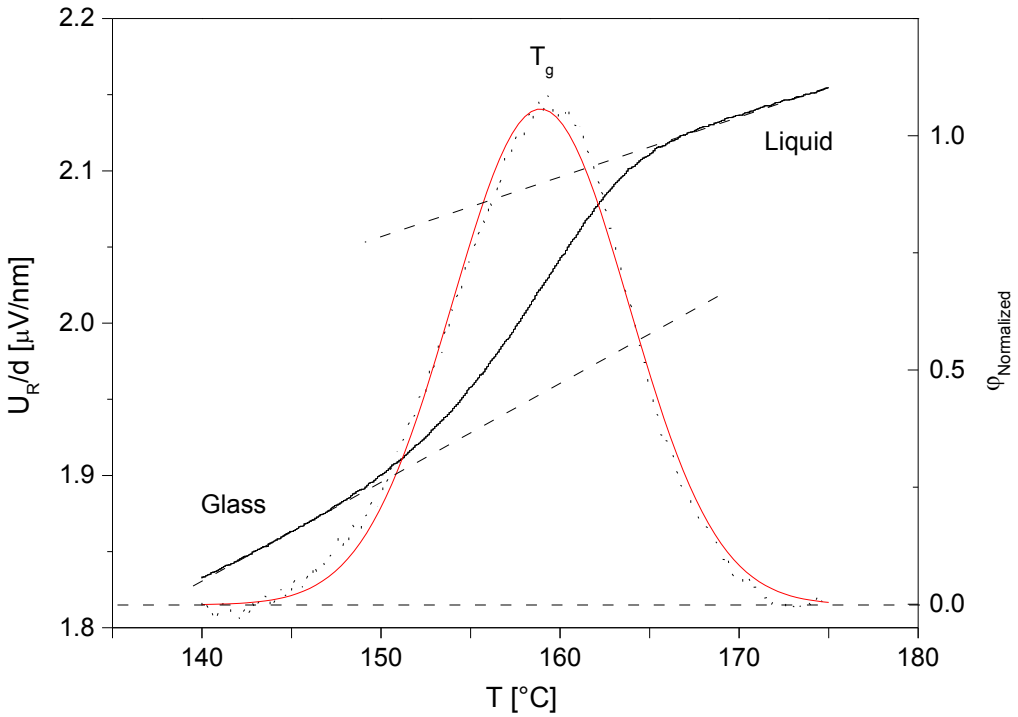

Fig. 39 *Normalized amplitude (solid line) and phase angle (dotted line) of the complex differential voltage versus temperature for a film with the thickness of 38 nm at the frequency of 160 Hz. The red solid line is a fit of a Gaussian to the data of the normalized phase angle.*

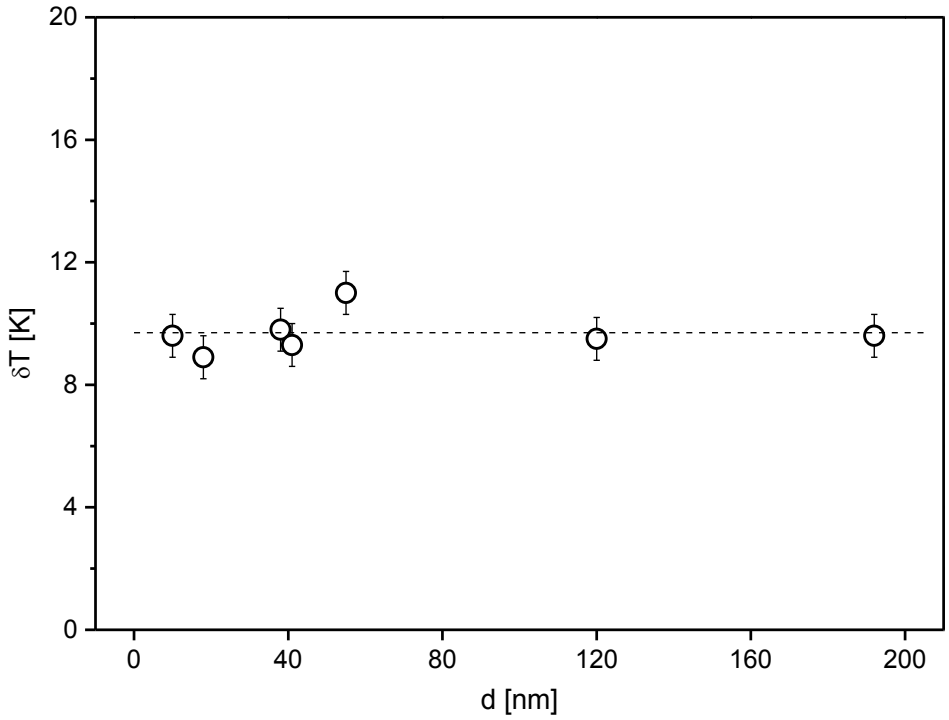

Fig. 40 *Mean temperature fluctuation δT as a function of the film thickness.*

The dynamic glass transition temperatures as obtained for different frequencies are used to construct the relaxation map (Fig. 41) with film thickness as parameter. Data for bulk polycarbonate measured with broadband dielectric spectroscopy taken from Section 5.1.1 are included as well. The calorimetric data are close to the dielectric ones. For a given frequency the data measured for different film thicknesses are located in a quite narrow temperature range. The temperature difference between the films of the various thicknesses for each frequency is within ±3 K, which is close to the uncertainty of the differential AC chip-based calorimetry measurement. This is in agreement with other polymers investigated by the same method [162-164]. The calorimetric data are curved when plotted versus 1/T and can be described by the VFT-equation [29-31].

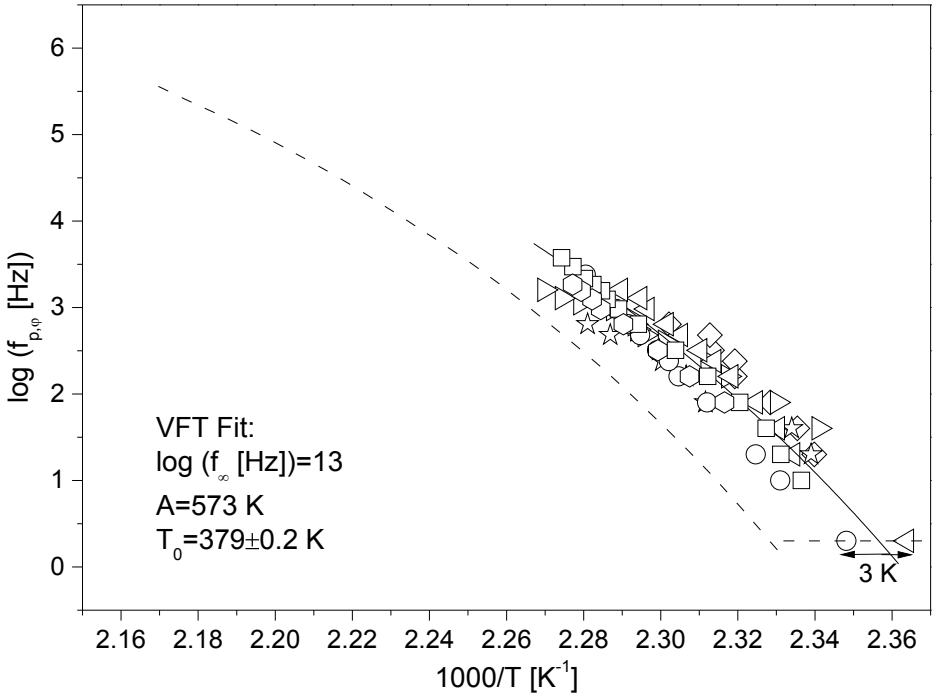

Fig. 41 *Relaxation map for the dynamic glass transition of PC films: stars-10 nm, diamonds-18 nm, left-pointing triangles-38 nm, circles-41 nm, right-pointing triangles-55 nm, squares-120 nm, hexagons-192 nm. The dashed line corresponds to dielectric data for bulk PC (60 µm). The solid curve represents the VFT fit with parameters indicated in the graph. The data are determined from the peak position of the phase angle.*

To reduce the number of free fit parameters the following procedure was applied to estimate the parameters of the VFT equation. Both A= 573 K and log(f_∞[Hz])=13 were taken from Tab. 3 for the bulk PC. T_0 was obtained by a fit of the VFT equation to the data including all thicknesses keeping A and log f_∞ constant. All VFT parameters are included in Fig. 41. The VFT-equation describes the calorimetric data quite well and the deviation of the data from the fit is in the experimental error limit even for the thinnest film thicknesses and the lowest frequencies.

In the relaxation map, a systematic shift between the relaxation rate determined from specific heat and broadband dielectric spectroscopy is observed. The trace of the calorimetric points is shifted by about one order of magnitude to higher frequencies compared to the dielectric data. This behaviour is different from that reported in Ref. 227 where the opposite arrangement of the dielectric and thermal signals is given. Also Jacobsen et al. [228] provide some evidence for two simple glass-formers that the dielectric response is faster than the calorimetric signal

although the differences of the different data sets are small. On the other hand it was also reported for two other polymers that the dielectric and calorimetric data collapse into one chart [229,230]. From this brief literature survey it is concluded that both specific heat and broadband dielectric spectroscopy detect the dynamic glass transition process, while each method provides a different window to look at the underlying phenomena. Dielectric spectroscopy is sensitive to fluctuations of dipole moments, while specific heat spectroscopy detects entropy (or enthalpy) fluctuations. Why the data for polycarbonate presented in Ref. 227 and here show a different arrangement remains unclear at the moment. Please also note that the both investigated materials are different. This is also expressed by the different sets of VFT fitting parameters estimated here and presented in Ref. 227. A detailed discussion of the dielectric and thermal response is beyond the scope of the thesis and will be presented elsewhere.

5.1.3 Discussion on the Dielectric and Calorimetric Results in Terms of Interfacial Interaction

It is known that the interaction of the polymer with the substrate has a great influence on the average T_g across the whole film. The interfacial energy between the polymer and substrate was estimated through theoretical calculation based on contact angle measurements.

The results obtained in the dielectric measurements of Al-capped PC films indicated strong interaction between PC and Al. To confirm it, contact angle measurements were carried out. The contact angle values for thin PC layer are given in Tab. 4. The contact angle values were used as input to calculate the interfacial energy between the substrate and the polymer γ_{SP} in the frame of the Fowkes-van Oss-Chaudry-Good (FOCG) model [231]. The surface tension is given by

$$\gamma^{Total} = \gamma^{LW} + \gamma^{P} = \gamma^{LW} + 2\sqrt{\gamma^{+}\gamma^{-}} \qquad (58)$$

where γ^{LW} is the dispersive and γ^{P} the polar component. The polar component is further expressed by the electron-acceptor γ^{+} and the electron donor component γ^{-} [231,232]. γ^{LW} , γ^{+} and γ^{-} were estimated by solving the system of the corresponding Young and Dupré equations [231] (system of three equations) using the contact angles θ_i measured for each test liquid i.

$$(1+\cos\theta_i)\gamma^{PC} = 2\left[\left(\gamma_{PC}^{LW}\gamma_{L,i}^{LW}\right)^{1/2} + \left(\gamma_{PC}^{+}\gamma_{L,i}^{-}\right)^{1/2} + \left(\gamma_{PC}^{-}\gamma_{L,i}^{+}\right)^{1/2}\right] \quad (59)$$

PC symbolizes polycarbonate and L the test liquids where the corresponding values for the test liquids were taken from Ref. 232 (Tab. 5). The values obtained for both AlO_x and PC layer are displayed in Tab. 6. The combining rule of Good-Girifalco-Fowkes [233] and expressions for the Lewis acid-base interactions across the interface [231] were applied to estimate γ_{SP} between PC and AlO_x

$$\gamma_{SP} = (\sqrt{\gamma_S^{LW}} - \sqrt{\gamma_P^{LW}})^2 + 2\left[(\gamma_S^{+}\gamma_S^{-})^{1/2} + (\gamma_P^{+}\gamma_P^{-})^{1/2} - (\gamma_S^{+}\gamma_P^{-})^{1/2} - (\gamma_S^{-}\gamma_P^{+})^{1/2}\right] \quad (60)$$

S und P refer to the substrate and the polymer. The data for aluminium are taken from Ref. 153. The dispersive part of the AlO_x/PC is calculated to be 0.35 mJ/m^2 and the polar one is 2.16 mJ/m^2 leading to a total energy of 2.51 mJ/m^2. This value is higher than the critical value of 2 mJ/m^2 [119], which is related to a thickness independent T_g value. The real interfacial energy could be even higher than the calculated γ_{SP} due to the formation of chemical bonds or specific interaction between AlO_x and PC. The interfacial chemical interaction between spin coated polycarbonate and thermally evaporated aluminium has been studied by X-ray photoelectron spectroscopy in detail [234]. C=O and C-O entities of polycarbonate react with Al atoms to form an Al-O-C like complex. Al-C bonding also forms due to the interaction between phenyl ring and Al atoms. Aluminium oxide (O-Al) and aluminium hydroxides (HO-A1) can be detected at the Al/PC interface. The formation of these chemical bonds contributes to the attractive PC/AlO_x interaction. Such high interfacial energy leads to an increase of T_g as observed in the dielectric experiments due to chain adsorption to the Al surface.

In the calorimetric measurements, PC is supported on the sensor. A silicon wafer with around 500-nm-thick SiO_2 layer used here is assumed to have similar surface property as the chip sensor. The contact angle values obtained for SiO_2 layer are listed in Tab. 7. The values for the energy components are shown in Tab. 8. The total energy is estimated to be 2.15 mJ/m^2, which is close to the critical value of 2 mJ/m^2 [119].

In the PC/SiO_2 system considered here with relatively lower interfacial energy, the SiO_2 layer has only a small or even no effect on the mobility of the polymer segments in proximity to it. The free surface effect cannot be compensated or overcame due to chain rearrangement near the interface, as reported in some references [223,235]. But in the present study, the dynamic

glass transition temperature is found to be independent of the film thickness. It can be reconciled in terms of the high temperature window of the measurement. Ediger' group has studied the segmental dynamics of thin PS films with an optical photobleaching technique [165]. A high-mobility layer was observed at the film surface at $T_{g,Bulk}$, while in the higher temperature range ($>T_{g,Bulk}$) the relaxation time of the fast process became close to that of the bulk process. No evidence of a fast process in the accessible temperature range ($>T_{g,Bulk}$+5 K) was detected [165]. Forrest et al. related the cooling rate of ellipsometric measurements to a relaxation time. It is shown that experiments probing relaxation times shorter than a critical value or temperature higher than a critical value of 378 K for PS thin films only show bulk behavior. In the present study no thickness dependence of the dynamic T_g for the PC films is observed down to 10 nm, which means the critical temperature, T*, for PC is lower than the temperature window of the measurement where the relaxation process can be observed.

Tab. 4 *Contact angle values of the test liquids with polycarbonate. The error bars result from the average of the measurements on 8 drops.*

	Ethylene glycol	Formamide	Water
Poly(bisphenol A carbonate)	67.63±0.47	71.77±0.7	92.97±0.35

Tab. 5 *Total surface energy γ^{Total} and its dispersive γ^{LW} and polar component γ^{P} for the test liquids according to the data given in Ref. 232.*

	Ethylene glycol	Formamide	Water
γ^{Total} [mJ/m^2]	48.0	58	72.8
γ^{LW} [mJ/m^2]	29	39	26
γ^{+} [mJ/m^2]	2.60	3.1	34.2
γ^{-} [mJ/m^2]	34.8	29.1	19

Tab. 6 *Total surface energy γ^{Total} and its dispersive γ^{LW} and polar component γ^{P} for polycarbonate and aluminum oxide. The data for aluminium were taken from Ref.153.*

	γ^{Total} [mJ/m^2]	γ^{LW} [mJ/m^2]	γ^{+} [mJ/m^2]	γ^{-} [mJ/m^2]
Poly(bisphenol A carbonate)	33.21	32.95	0.03	0.56
Aluminum	30.4	26.5	0.5	7.7

Tab. 7 *Contact angle values of the test liquids with polycarbonate and silicon wafer with SiO_2 layer. The error bars result from the average of the measurements on 6 drops.*

	Ethylene glycol	Formamide	Water
SiO_2 layer	39.0±0.6	48.2±1.0	61.0±0.4

Tab. 8 *Total surface energy γ^{Total} and its dispersive γ^{LW} and polar component γ^{P} for polycarbonate and silicon wafer with dioxide layer.*

[mJ/m^2]	γ^{Total}	γ^{LW}	γ^{+}	γ^{-}
Polycarbonate	33.21	32.95	0.03	0.56
SiO_2 layer	43.77	40.31	0.27	10.97

Comparing the results obtained here with literature data, agreement but as well contradiction can be found. Torkelson et al. investigated the thickness dependence of T_g of polycarbonate layers prepared on the surface of a silica substrate by fluorescence spectroscopy [235]. Specular X-ray reflectivity and Positron annihilation lifetime spectroscopy measurements were carried out by Soles et al. to study the dynamics in thin polycarbonate films spin coated on the Si wafers with a uniform oxide surface [223,236]. The corresponding shifts of T_g with respect to the bulk value in dependence on the film thickness are plotted in Fig. 42 where the dielectric data presented in Fig. 28 were included as well. Please note that besides the dielectric measurements where the samples are capped between two aluminium layers all other samples have one free surface.

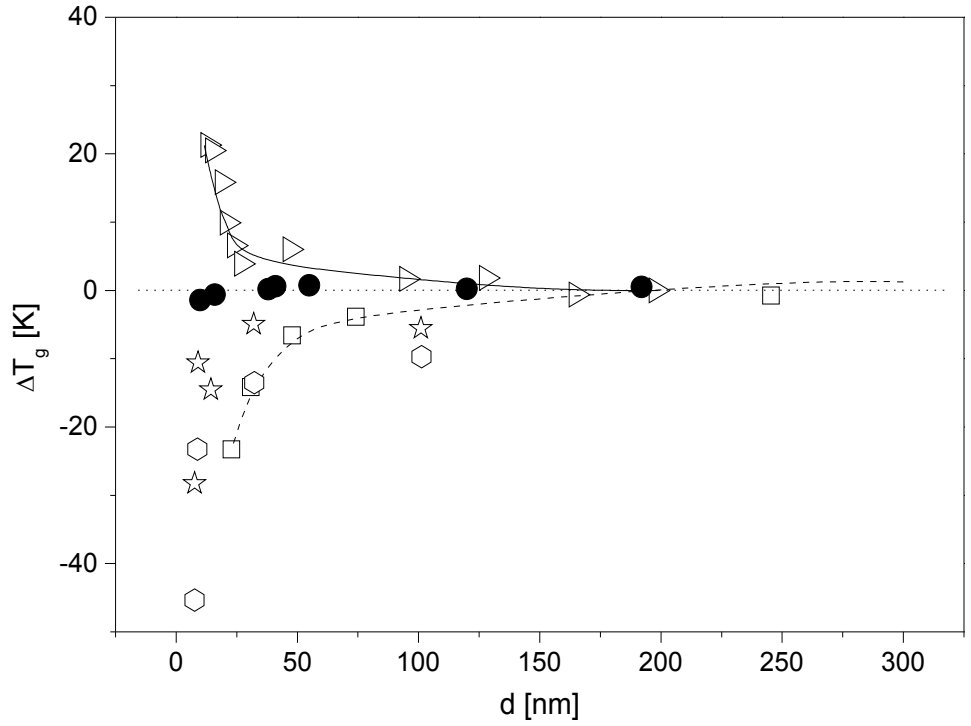

Fig. 42 *Dependence of the glass transition temperatures vs. film thickness for thin PC films: solid circles – data from AC chip-based calorimetry; squares – data obtained by fluorescence spectroscopy [235]; hexagons – Specular X-ray reflectivity [236]; stars – Positron annihilation lifetime spectroscopy [236]; right-pointing triangles – broadband dielectric spectroscopy [Fig. 28]. Lines are guides for the eyes.*

For the data measured by fluorescence spectroscopy, by specular X-ray reflectivity and by positron annihilation lifetime spectroscopy a strong reduction of the glass transition temperature with decreasing film thickness is observed, while broadband dielectric spectroscopy measurement shows an increase of the glass transition temperature. The calorimetric measurements discussed here show a constant value of the glass transition temperature down to 10 nm. The diverging results might be discussed in terms of the interplay of different aspects which have impacts on the glass transition behaviour of thin polymer films. In the case of the dielectric data, two factors are of importance, the sample geometry and the interfacial energy. Here the PC film is capped between two Al layers with no free surface. The PC/Al interfacial energy was further confirmed to be strong. This leads to the formation of reduced mobility layer in the proximity of both Al layers due to chain adsorption, which results in an increase of T_g. The remaining measurements were performed on the PC films supported by silicon wafer with dioxide layer, which lack attractive

interactions with the substrates. The free surface effect predominates. As a result, all measurements show a decrease of glass transition temperature with decreasing film thickness except that it is constant in the calorimetric measurement. In the techniques which point to a T_g depression, a thermodynamic property (or an associated quantity) is measured during a temperature scanning and an observed change in slope is interpreted as the thermal glass transition temperature. The heating/cooling rate is relatively low, which means a low frequency or large relaxation time when related to the dynamic techniques. In the case of differential AC chip-based calorimetry, the dynamic glass transition temperature in a typical frequency range from 10 to 4000 Hz is measured directly, where no thickness dependence is observed. This is consistent with the BDS measurements on thin PS films supported on silicon wafer showing no thickness dependence of segmental dynamics [156].

5.2 Glass Transition of Ultrathin Polystyrene Films

5.2.1 Glass Transition Temperature Depression and Invariant Segmental Dynamics

It was reported that sample preparation, measurement conditions and thermal history may result in pronounced changes in the segmental dynamics in thin polymer films [237]. Broadband dielectric spectroscopy provides a unique way to investigate the thermal T_g and dynamic T_g simultaneously on the same sample which is non-polar polymer. Results obtained in such a way can reduce the inaccuracy coming from the factors mentioned above and help us to know more about the intrinsic feature of the dynamics in thin polymer films.

In the following section the thermal T_g and the dynamic T_g of thin PS films are discussed in detail. The thermal T_g is determined by CSD. The dynamic one is determined by BDS, additionally with SHS. It is shown that the thermal T_g decreases with film thickness from several microns down to 15 nm, whereas the dynamic T_g of PS is independent of the film thickness both for aluminium-capped films and supported films with one free surface.

Fig. 43 shows the temperature dependence of the real part of the sample capacity normalized with respect to the value at 330 K for P1408 with different thicknesses. The selected frequency is 1.7e+05 Hz, where the α-dispersion does not influence the capacity values. As introduced in Section 3.3, the initial deviation of the capacity from a linear temperature is used to extract a thermal T_g. These T_g values decrease with the reduction of film thickness, as indicated in Fig. 43.

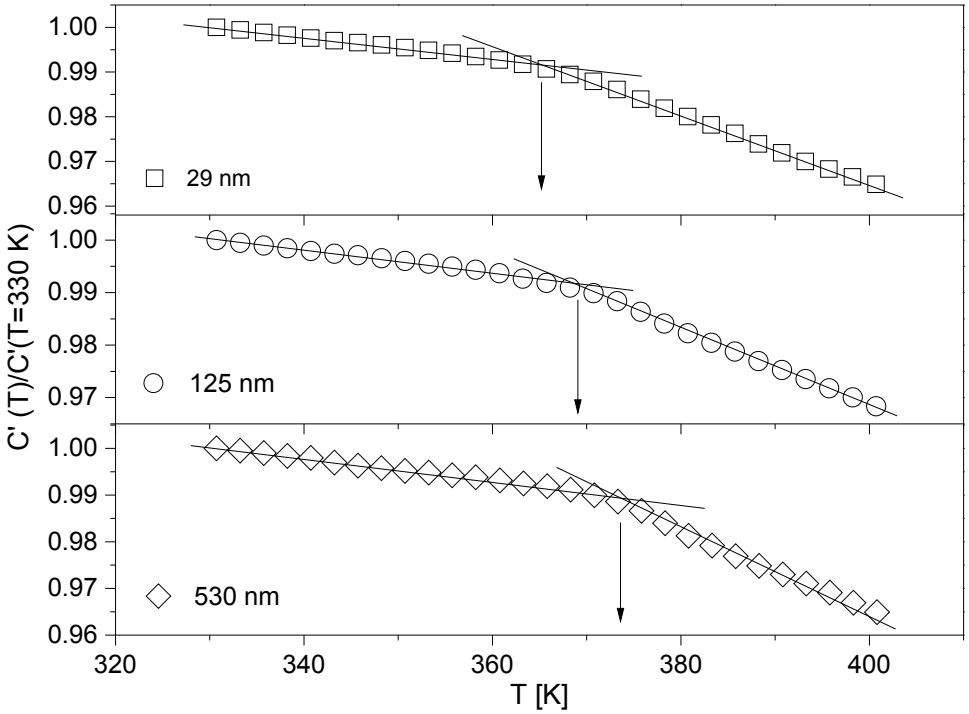

Fig. 43 *Temperature dependence of the capacitance normalized with respect to the values at 330 K at the frequency of 1.7e+05 Hz for PS films (M_w=1408 kg/mol) at the given thicknesses after annealing for 4 days at T=433 K. The solid lines are linear fits to the data in the different temperature ranges. The arrows indicate the thermal T_g.*

Fig. 44 presents the dielectric loss as a function of temperature at the frequency of 6 kHz for different film thicknesses. The contribution of the conductivity was removed from the raw spectra. To do so, for each spectrum of ε"(ω=const) plotted in the temperature domain, a polynomial function was used to fit the data obtained at relatively high and low temperatures which do not contain any contribution from the α process of PS. These contributions were subsequently taken off from the whole spectrum to obtain the neat contribution of the α-relaxation process. Fig. 44 proves that the segmental dynamics of thin PS films is independent of the film thickness. As discussed in detail in Ref. 148, this statement is true in the whole frequency window of the dielectric study, which is consistent with previous findings [238].

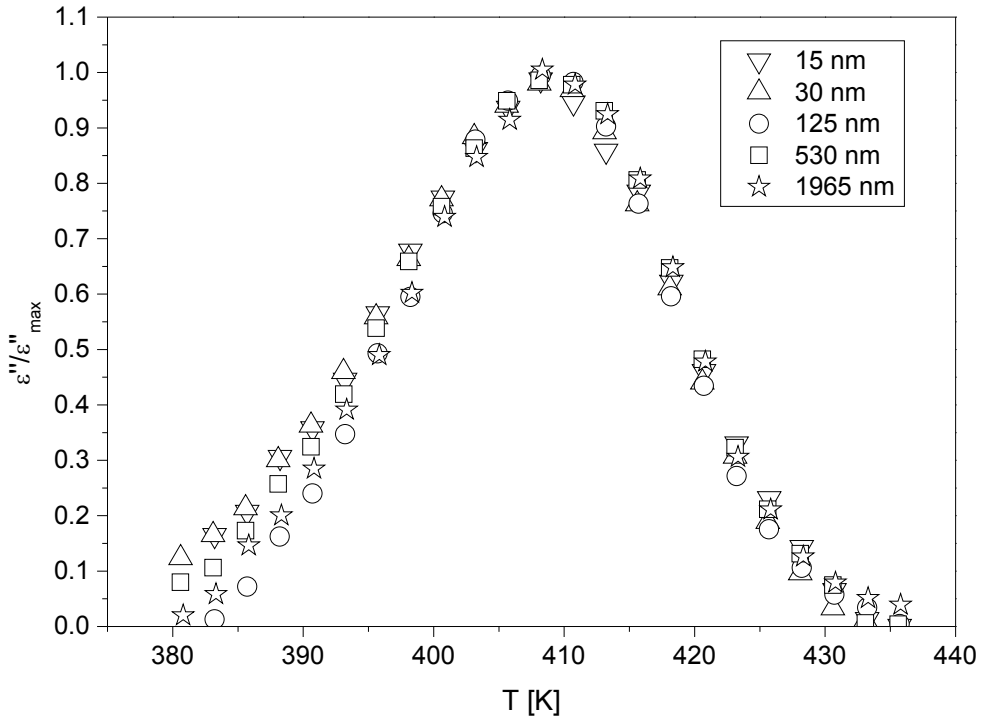

Fig. 44 *Temperature dependence of dielectric loss normalized with respect to its maximal value at the frequency of 6 kHz for the PS films (M_w=1408 kg/mol) for the labelled thicknesses after annealing for 4 days at T=433 K.*

The segmental dynamics were further investigated by means of SHS. The amplitude U_R and the phase angle φ of the complex differential voltage as measure of the complex heat capacity were obtained as a function of temperature at a given frequency. A series of measurements were carried out at the frequency of 360 Hz for various film thicknesses. The data were collected during continuous heating and cooling processes at a rate of 2 K/min, where the second heating run is used for analysis. The data obtained for different film thicknesses are normalized for comparison (Fig. 45). The amplitude of the complex differential voltage was normalized by its step height at the dynamic glass transition minus its value at the dynamic T_g after normalization $U_R/(U_{R,T=450K}-U_{R,T=360K})-U^N_{R,T_g}$ (Fig. 45a) where the corrected phase angle is normalized by its maximal value (Fig. 45b). The rescaled data for different film thicknesses collapse into one chart. This indicates that the dynamic T_g is independent of the film thickness down to 18 nm. In other words the segmental dynamics is independent of the film thickness down to the value of 18 nm at the frequency of 360 Hz. This conclusion can be extended to the frequency range from 1 Hz to 1000 Hz as shown in Ref. 148. This is in agreement with AC chip-based calorimetry studies on other polymers [163,239,240].

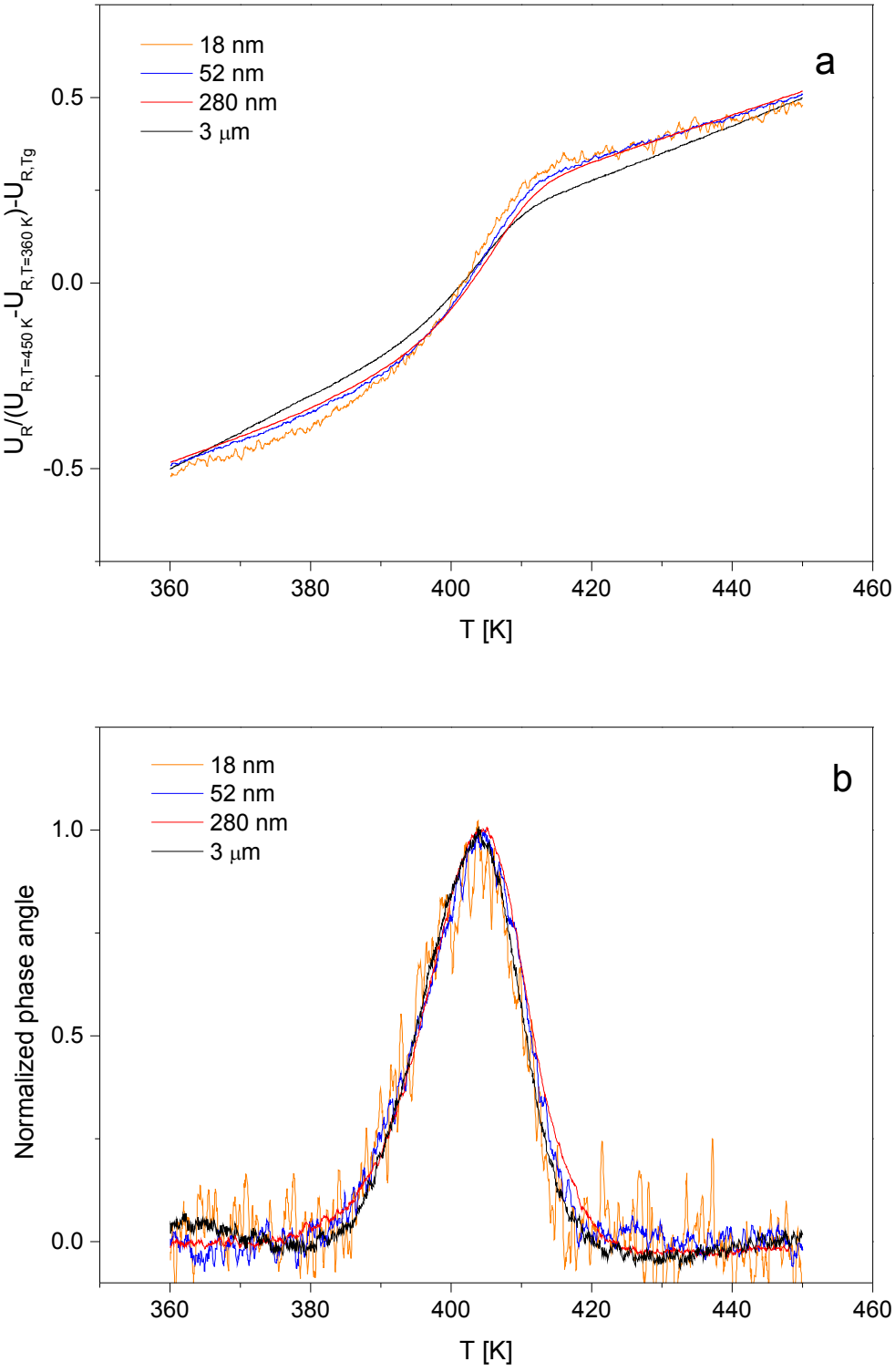

Fig. 45 *Temperature dependence of the normalized amplitude (a) and the normalized phase angle (b) of the complex differential voltage for PS films (M_w=1408 kg/mol) with the indicated thicknesses after annealing for 4 days at T=433 K at a frequency of 360 Hz as measured by differential AC chip-based calorimetry.*

To emphasize the lack of thickness dependence of the dynamic T_g, Fig. 46 displays the relaxation map obtained by both BDS and SHS for the segmental dynamics of PS thin films. The typical relaxation rate, determined as the frequency of the peak maximum is plotted versus the inverse temperature for all systems. For all thicknesses the data collapse into one chart independent of both the applied perturbation (electrical or thermal) and the sample geometry (supported film with one free surface or Al-capped film).

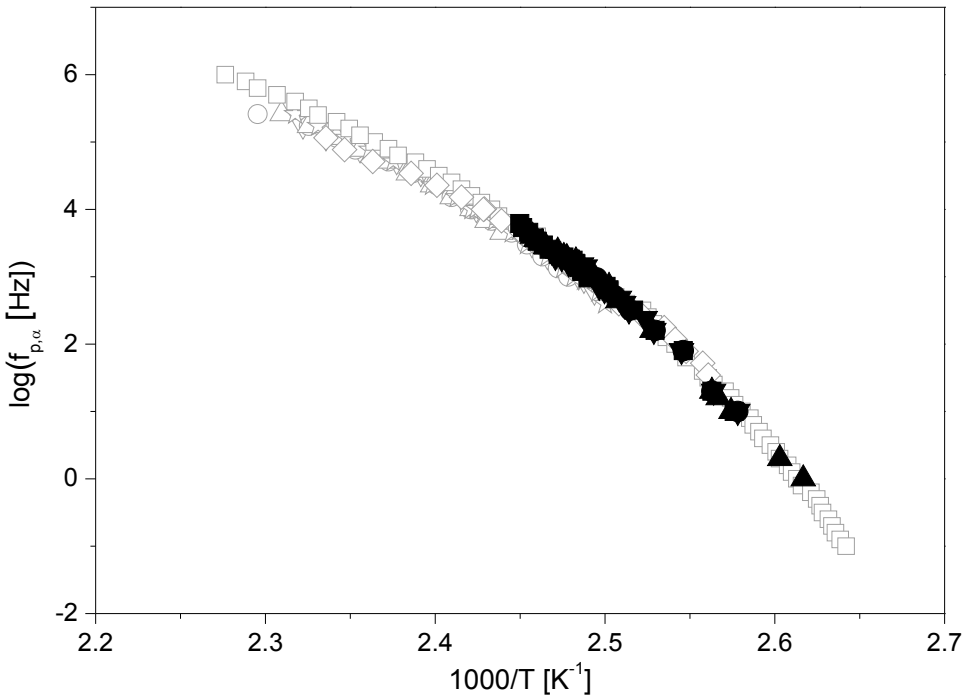

Fig. 46 *Relaxation map for the dynamic glass transition of PS films. Data shown as hollow symbols are obtained using broadband dielectric spectroscopy: bulk (squares); 1200 nm (up-pointing triangles); 500 nm (circles); 130 nm (stars); 30 nm (diamonds); 15 nm (down-pointing triangles). Data shown as solid symbols are obtained with specific heat spectroscopy: 3000 nm (down-pointing triangles); 280 nm (up-pointing triangles); 52 nm (squares); 18 nm (circles).*

The present study shows that a T_g depression and unchanged segmental dynamics are simultaneously observed for PS films with thickness from several microns down to 15 nm. It is important to emphasize that this has been found for samples prepared under identical conditions and, in the case of dielectric techniques, in a single measurement on the same sample. These findings are also independent of the type of the perturbation applied to the sample: thermal in the case of AC chip-based calorimetry and electrical for BDS. The results

can be understood in terms of the different information obtained by techniques probing the way a polymer melt leaves equilibrium when cooling down and those providing direct characterization of the spontaneous fluctuations occurring in the supercooled state. Thus the most obvious consequence is that the equilibrium to out-of-equilibrium transition occurring at T_g is not uniquely related to the intrinsic molecular mobility, with geometric factors [241], the nature of the interface [15,138] and the heating/cooling rate [16,159,242] also important in thin films.

5.2.2 Role of Molecular Weight and Annealing Protocol

As discussed in Section 5.2.1 Al-capped thin PS films show T_g depression, while an increase of T_g was observed for Al-capped thin PC films as presented in Section 5.1.1. But the interfacial energy of PS/Al is estimated to be 5.6 mJm^{-2} [134], which is much higher than that of PC/Al with the value of 2.5 mJm^{-2}. This is not surprising, because many studies showed that the interfacial energy alone is not the only relevant parameter to describe T_g (d) of thin polymer films. Grohens et al. reported that PMMA stereoregularity had great effect on its T_g in the vicinity of an attractive substrate. The chain rearrangements and the density changes occurred at interfaces are different for i-PMMA and s-PMMA [135]. Glynos et al. demonstrated the important role of the chain structure of the macromolecule on the thickness dependence of T_g by comparing the behaviour of linear chains with star-shaped macromolecules [136]. The change of the local density due to the chain adsorption is assumed to be a further important parameter to describe the thickness dependence of T_g, which propagated from the adsorbed layer to the interior part of the film.

In this work, we have investigated the effects of the annealing protocol and the molecular weight on the glass transition and segmental dynamics in thin PS films in a wide range of molecular weight. Since the adsorption kinetics should slow down for higher molecular weights, it is expected that the increase of the local density in the adsorption layer due to segment rearrangement is more pronounced for PS films with lower molecular weight under the same sample preparation conditions, and hence the T_g depression may be more suppressed compared to PS films with a higher molecular weight.

Fig. 47 shows the temperature dependence of the real part of the complex capacity normalized to the value at T=329 K for PS films (P260) with different thicknesses, which are annealed under the same conditions as films prepared from P1408 (433 K, 4 days). The data are taken at the frequency of 6.4e+04 Hz to get rid of the dispersion effects. T_g is identified as the

crossover temperature of the linear fits of the capacity in the glassy and melt state. Similarly, there is a systematic T_g decrease with decreasing film thickness. The loss part of the dielectric permittivity normalized with respect to its maximal value at the frequency of 60 kHz for the PS films (P260) is plotted in Fig. 48 as a function of temperature. The dynamic glass transition temperatures, indicated as the α-relaxation peaks for the PS films do not change with the film thickness in the frequency window of the dielectric measurement.

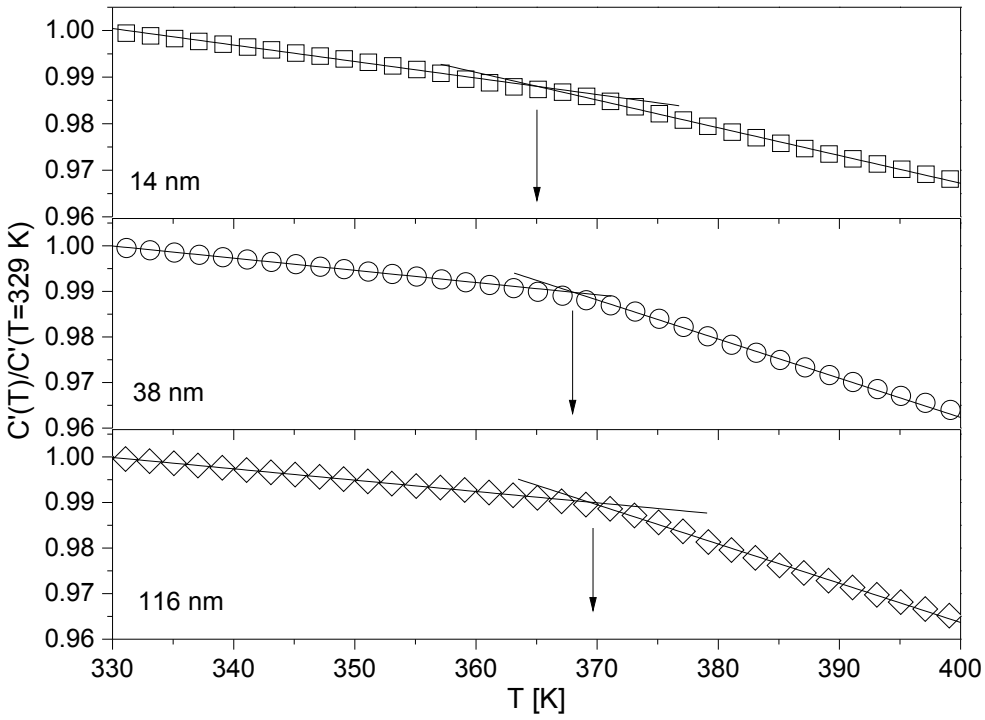

Fig. 47 *Temperature dependence of the capacitance normalized with respect to the values at 329 K at the frequency of 64 kHz for the PS films (M_w=260 kg/mol) with the indicated thicknesses after annealing for 4 days at T= 433 K. The solid lines are linear fits of the data, and the arrows indicate the thermal T_g.*

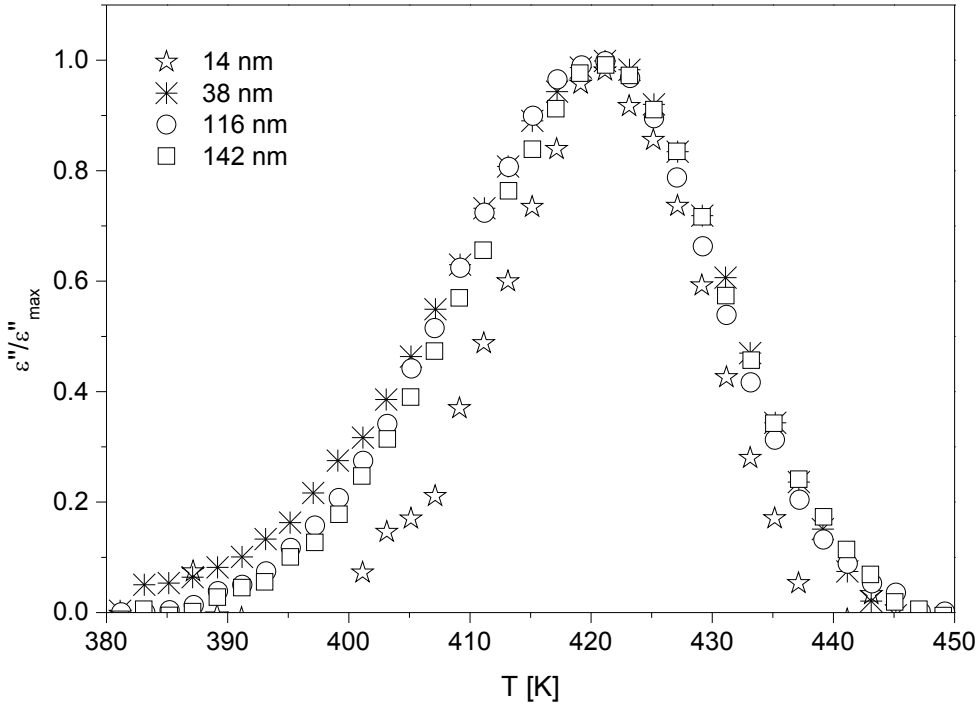

Fig. 48 *Temperature dependence of dielectric loss normalized with respect to its maximal value at the frequency of 60 kHz for the PS films (M_w=260 kg/mol) with the indicated thicknesses after annealing for 4 days at the temperature of 433 K.*

It was reported that the residue solvent in the thin films induced a shift of the α-relaxation peak and through annealing can exclude the plasticizer effect [237]. In the present study different annealing protocols have been carried out on the same sample with the film thickness of 142 nm. A shift in the position of the alpha relaxation peak after 1 day annealing at the temperature of 373 K by about 2 K from its value after further strong annealing processes was observed (Fig. 49). This is consistent with the experimental findings in Ref. 243. It means that the investigated sample is still in a metastable state after the first annealing step and after the second and third annealing process the polymer thin film is considered as stable, showing reproducible experimental results.

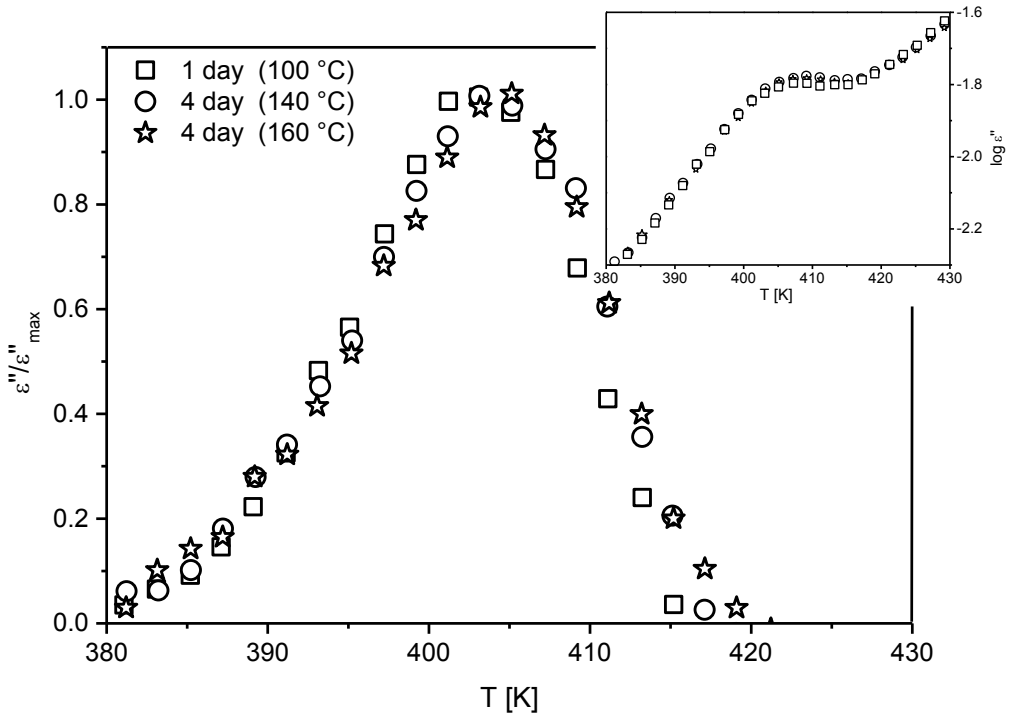

Fig. 49 *Temperature dependence of dielectric loss normalized with respect to its maximal value at the frequency of 1 kHz for a 142-nm-thick PS film (M_w=260 kg/mol) after annealing for 1 day at the temperature of 373 K, 4 days at the temperature of 413 K and further 4 days at the temperature of 433 K. The inset shows the original data with the contribution of conductivity.*

Fig. 50 shows the temperature dependence of capacity normalized to the value at T=321 K for films prepared from P50 with different thicknesses, which are annealed for 4 days at the temperature of 373 K. The data are taken at the frequency of 3.5e+05 Hz. It is interesting that there is an increase of T_g for the 11-nm-film compared to the 65-nm-thick film. This is consistent with the experimental findings in Ref. 154. The loss part of the dielectric permittivity normalized with respect to its maximal value at the frequency of 16 kHz for the PS films (P50) is plotted in Fig. 51 as a function of temperature. The dynamic glass transition temperatures, indicated as the α-relaxation peaks for the PS films do not change with the film thickness in the frequency window of the present study.

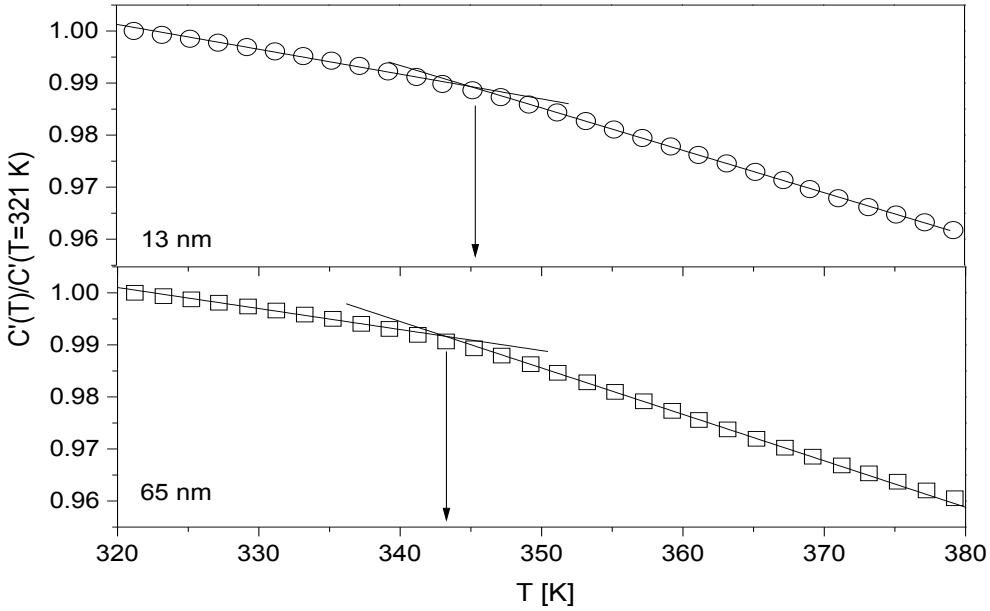

Fig. 50 *Temperature dependence of the capacitance normalized with respect to the values at 321 K at the frequency of 350 kHz for P50 films for the indicated thicknesses after annealing for 4 days at T=373 K. The solid lines are linear fits of the data, and the arrows indicate* T_g.

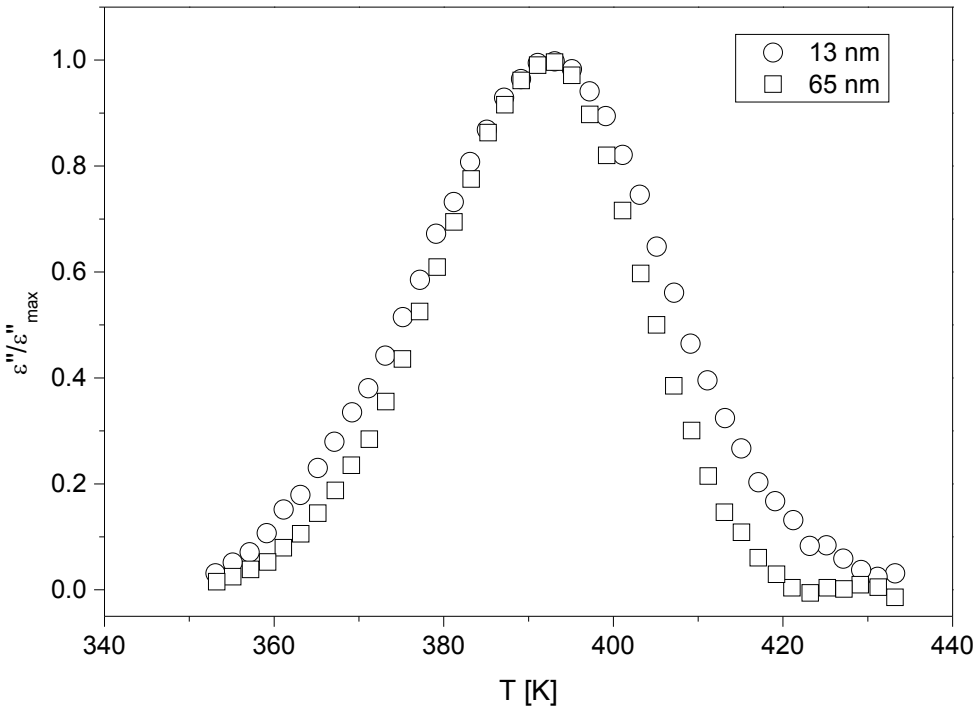

Fig. 51 *Temperature dependence of dielectric loss normalized with respect to its maximal value at the frequency of 16 kHz for P50 films for the indicated thicknesses after annealing for 4 days at T= 373 K.*

Finally the thickness dependence of the thermal T_g for the different PS films is presented in a compilation plot in Fig. 52. It is shown that T_g decreases with film thickness from several hundreds of nm to 15 nm for the PS films (M_w=1408 kg/mol) and from several tens of nm for the PS films (M_w=260 kg/mol). Additionally for the PS films (M_w=260 kg/mol), there is no obvious annealing effects on the thickness dependence of T_g values under investigation. For freestanding PS films, much larger T_g reductions than for supported films of similar thickness are observed [148,244]. T_g depression observed in the present study is in agreement with some reports [5,197,244-246]. From these results it might be clear that the free surface effect is important in determining the T_g in thin PS films, and thermal evaporation of a metal coating on top of the film may not remove its effect for $M_w \geq 260$ kg/mol. For the P50 film with the thickness of 11 nm, a slight increase of T_g was observed. This can be explained in terms of the strong effect of an irreversibly adsorbed layer onto the Al substrate from the PS melt by annealing at a temperature much higher than $T_{g,bulk}$ [129,154,247], which overcomes the free surface effect. It is noteworthy to mention that no effects of the adsorbed layer on the segmental dynamics of the films down to 13 nm were observed. The underlying reason for it is not clear. A tentative explanation could be the impact of thermal energy on the defreezing of segmental motion, which weakens the adsorption layer effects on the segmental dynamics, as discussed in Section 5.1.1. This behaviour was previously observed in other polymer films with comparable thicknesses [133,154]. The whole discussions made above were about the specific case of thin polystyrene films capped between two Al layers. To extend the conclusions to other thin film geometries, more factors like the chemical structure of the polymer and interfacial interaction between the polymer and the substrate need to be considered.

From Fig. 52, it can be further concluded that the molecular weight of the PS films has a strong impact on the T_g deviation from their bulk value. For PS films with similar annealing processes the change of the interfacial conformation state from the bulk depends on molecular weight. Chain arrangement at the interface results in a local densification of chain segments which reduce the free surface effect. It is noteworthy that after long time annealing at high temperature, the films are considered to correspond to conformational equilibrium on a laboratory timescale. This is confirmed by the annealing experiments performed on the PS films of P260, which shows that further annealing protocols have no effect on the segmental mobility. For higher molecular weights, the adsorption kinetics slows down because of the less efficient chain transport to the interface. For the lower molecular weight (M_w=260

kg/mol), the effect of free surface is weaker than that for the higher molecular weight (M_w=1408 kg/mol). In the case of the samples with the lowest molecular weight P50 (M_w=50 kg/mol), the effect of the free surface is totally suppressed, and therefore an increase of T_g is observed for the film of 11 nm compared to the thicker film of 65 nm. It is noteworthy to mention that the demonstration of the thickness dependence of T_g with respect to M_w in supported PS films is in difference with some early studies where no molecular weight dependence of T_g depression was observed [118,149,150]. For the measurements presented here one effect must be considered: the strength of the local density perturbation compared to the bulk value due to an irreversibly adsorbed layer. As previously reported [134] it is strongly related to the thickness of the irreversibly adsorbed layer, which is governed by high annealing temperature and long annealing time. In our study, the PS films were annealed at temperature much higher than $T_{g,bulk}$ for a long time before the measurements, allowing the adsorbed layer to equilibrate at the polymer/aluminium interface. In the above mentioned literatures, the annealing temperature is lower than $T_{g,bulk}$ and the annealing time is relatively short. It can be therefore expected that the resulting structure of the adsorbed layer and its effect on T_g deviation is quite different from that in our study. To clarify this issue more, further experimental data and analysis are needed.

To analyze the results obtained here in detail a model firstly proposed by Tsui et al. was modified and used [117]. The T_g deviation of a film with the thickness of d compared to the bulk value can be described by $\Delta T_g = T_g - T_g^{bulk} = (\delta T_g / \delta\rho)(2d_0 / d)(\rho_i - \rho)$, where ρ_i is the density of the polymer over a distance d_0 from the Al substrate and the remaining film with the thickness of $d - 2d_0$ having the bulk density ρ. Please note that ρ_i is not directly measured in the experiment. $\delta T_g / \delta\rho$ is the variation of T_g due to a change in the mass density ρ. $\delta T_g / \delta\rho$ for PS is taken as 1.35×10^3 cm^3K/g from Ref. 117. For the thin PS film (M_w=1408 kg/mol) with the thickness of 15 nm, a 13 K reduction in T_g is observed which means the value of $2d_0(\rho_i - \rho)$ is about 1.67×10^{-8} g/cm^2. If $d_0 = 3$ nm (several Kuhn lengths) is taken for the calculation, it results in $\rho_i - \rho = -0.028$. This means around a 3% decrease of the density at both Al interfaces is obtained. In the case of 14-nm-thin film (M_w=260 kg/mol), a 5 K decrease in T_g requires around 1% reduction of the density. When $\rho_i - \rho$=0, the T_g of a film will be independent of the film thickness. When is positive, it results in an increase in T_g. This model describes the combined effects on the T_g deviation

of thin polymer films. It provides a quantitative measure for the perturbations on the overall segment density. Quite recently, Boucher et al. proposed the model of free volumes holes diffusion [244,248], which is able to describe simultaneously T_g depression, acceleration of physical aging, and invariant segmental dynamics. In the frame of this model, a polymer can maintain equilibrium when cooling down by diffusing free volume holes out of the available interfaces of the system. Thus the efficiency of maintaining equilibrium is determined by the rapidity of free holes volume diffusion, which is restricted to the molecular mobility of the polymer and the amount of interface, scaling with the reciprocal of the film thickness. The latter effect would explain why Al-capped PS films display a weaker T_g depression compared to freestanding ones and their molecular weight dependence of T_g deviation. It is well-established that PS chains adsorb onto Al substrates during annealing, thus reducing the amount of interface available for free volume diffusion. Meanwhile, the adsorption kinetics is dependent on the molecular weight.

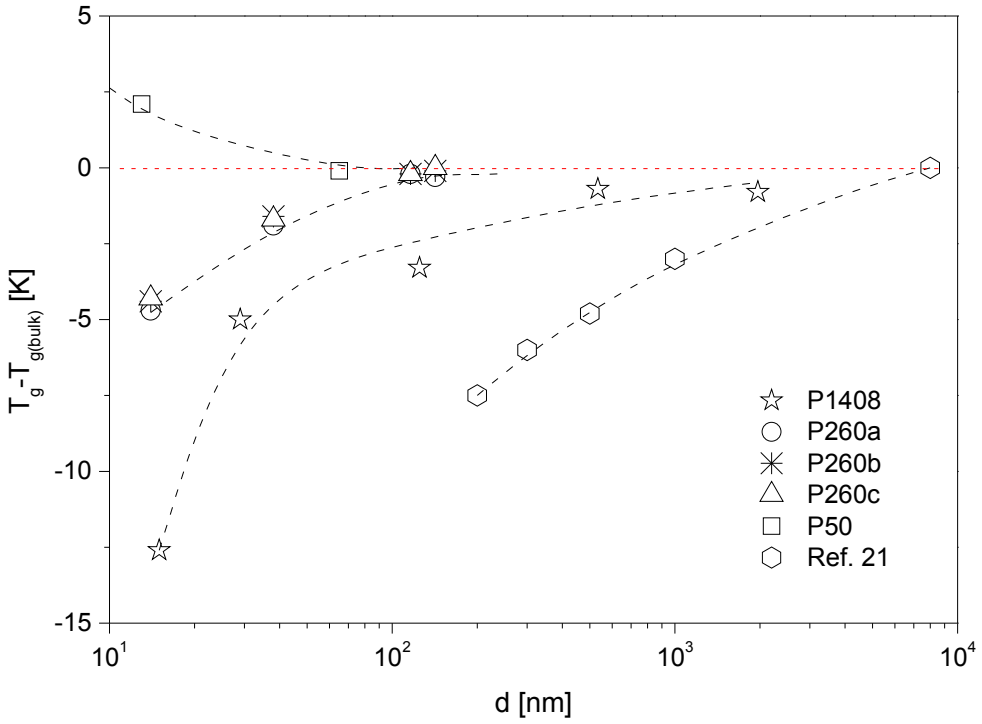

Fig. 52 *Thermal T_g determined by means of CSD for PS thin films with different molecular weight prepared under different annealing protocols is plotted as a function of film thickness. The data denoted by hexagons are repotted from Ref. 241, which are freestanding films with M_w=1408 kg/mol.*

In summary, the segmental dynamics is found to be independent of the film thickness with respect to M_w, whereas a T_g depression for PS films with a high molecular weight and an increase of T_g for low molecular weight PS films are observed. These experimental facts provide evidence that a mobile surface layer is important for the dependence of T_g on the film thickness for thin PS films and, by increasing the adsorption layer effect (extremely long time annealing, higher annealing temperature, reduction of molecular weight of the applied polymer, or improvement of polymer-substrate interaction), it is possible to compensate the surface mobile layer effect and recover bulk like behaviour of thin polymer films. Interfacial energy affects the T_g of thin polymer films, but it is not the only parameter to determine the T_g deviation. Local changes in the density of the interfacial layer/adsorption layer at the nanoscale level are proposed.

5.3 Glass Transition of Ultrathin Poly(vinyl methyl ether) Films

The film thickness dependence of the dynamic T_g of thin PVME films was studied by SHS using differential AC chip-based calorimetry. A series of measurements were carried out at the frequency of 640 Hz. The data were collected during continuous heating and cooling at a rate of 2 K/min. The data for different film thicknesses are normalized for comparison (Fig. 53). The amplitude of the complex differential voltage was scaled by its step height at the dynamic glass transition minus its value at the dynamic T_g after normalization, $U_R / (U_{R,T=210K} - U_{R,T=330K}) - U^N_{R,T_g}$ (Fig. 53a), where the corrected phase angle is normalized according to its maximum value (Fig. 53b). All rescaled data for different thicknesses collapse into one chart for both the amplitude and the phase angle. This indicates that the dynamic T_g is independent of the film thickness down to 12 nm.

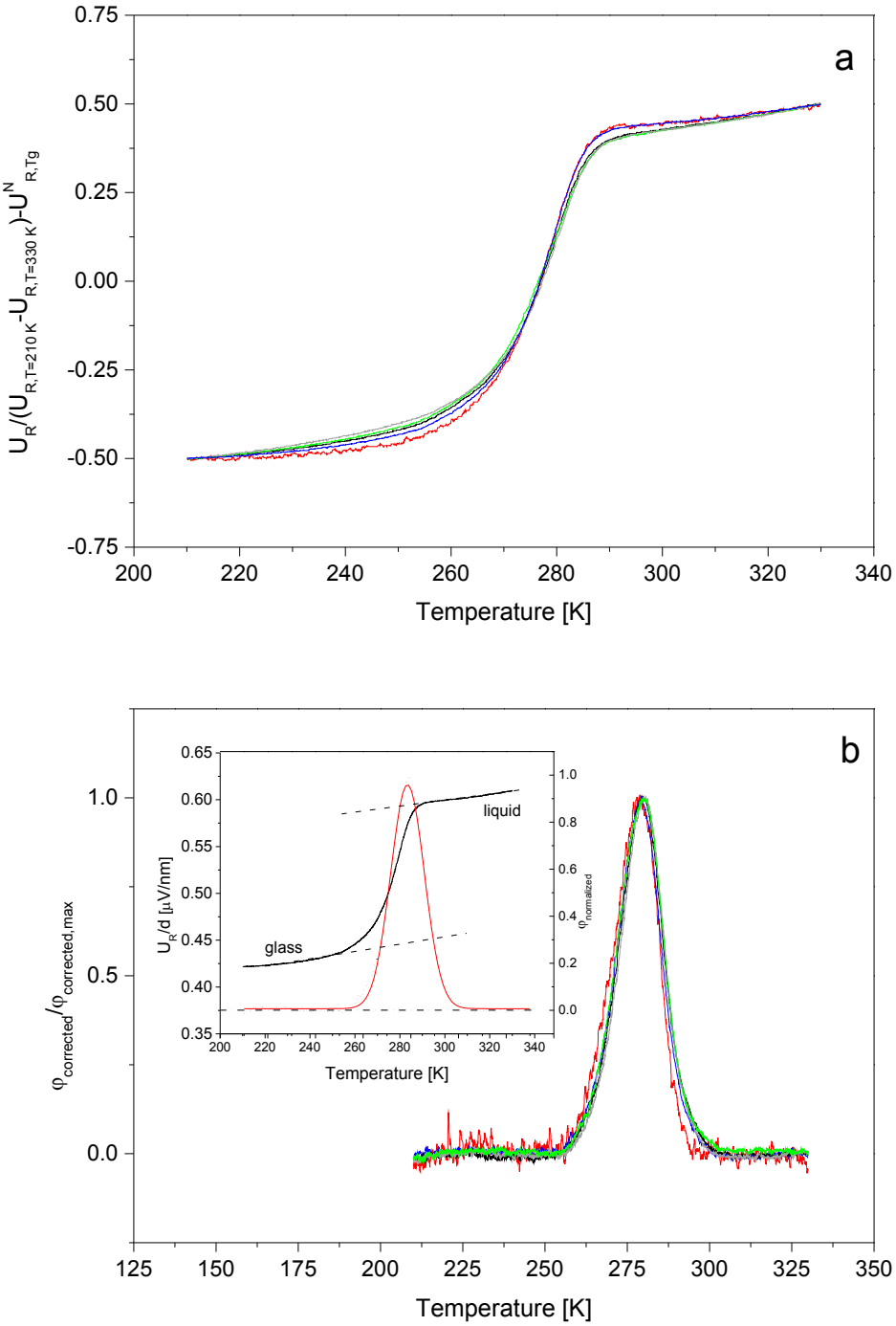

Fig. 53 *Rescaled amplitude (a) and normalized phase angle (b) of the complex differential voltage measured for thin films at a scanning rate of 2 K/min at a frequency of 640 Hz for different thicknesses: 12 nm (red), 58 nm (blue), 168 nm (black), 192 nm (green), and 218 nm (grey). Inset: normalized amplitude (solid line) and phase angle (dotted line) of the complex differential voltage as a function of temperature for a film with the thickness of 58 nm at a frequency of 640 Hz. The red solid line is a fit of a Gaussian to the data of the normalized phase angle.*

In the thesis specific heat capacity is found to be independent of the film thickness within the experimental error limit. More detailed information can be found in Section 5.1.2. The mean temperature fluctuation δT can be estimated by fitting Gaussians to the data of the phase angle (inset in Fig. 53b). δT estimated as standard deviation σ of the Gaussian is found to be independent of the film thickness with a mean value of 7.0±0.1 K. So it can be concluded that there is no thickness dependence of the CRR volume or cooperativity length scale. This means that the extent of the cooperativity is smaller than the lowest film thickness (12 nm). This is in agreement with results obtained for polycarbonate given in Ref. 226.

The dynamic T_g values obtained for different frequencies are used to construct the relaxation map with the film thickness as parameter (Fig. 54). Data for bulk PVME measured by means of BDS are included as well. The calorimetric data are close to the dielectric ones. For a given frequency the data measured for different film thicknesses are located in a quite narrow temperature range. The temperature difference between the films of various thicknesses for each frequency is within ±2 K, which is close to the uncertainty of the AC calorimeter measurement. This is in agreement with AC chip-based calorimetry studies on other polymers [162-164,239]. The calorimetric data are plotted versus 1/T. The resulting data points for the various film thicknesses can be described by the VFT-equation [29-31]. The data for all thicknesses were included in a common fit. The VFT fitting parameters for both calorimetric and dielectric data are included in Fig. 54. The VFT-equation describes the calorimetric data quite well and the deviation of the data from the fit is within the experimental error limit (±2 K) even for the thinnest film thicknesses and the lowest frequencies.

A systematic shift between the relaxation rate determined from specific heat spectroscopy and dielectric spectroscopy is observed. The trace of the calorimetric points is shifted by about one order of magnitude to lower frequencies compared to the dielectric data. This difference is much larger than the experimental errors and consistent with the behavior reported in Ref. 227 where the same arrangement of the dielectric and thermal signals is observed. The reason for this shift is not yet understood. A tentative explanation is that for PVME thin films the response to the temperature perturbation (specific heat spectroscopy) weights slower modes of the molecular mobility more than the response to the applied perturbation of the electric field (broadband dielectric spectroscopy). A more detailed discussion needs more experimental data on a larger set of materials and theoretical input and is beyond the scope of the thesis.

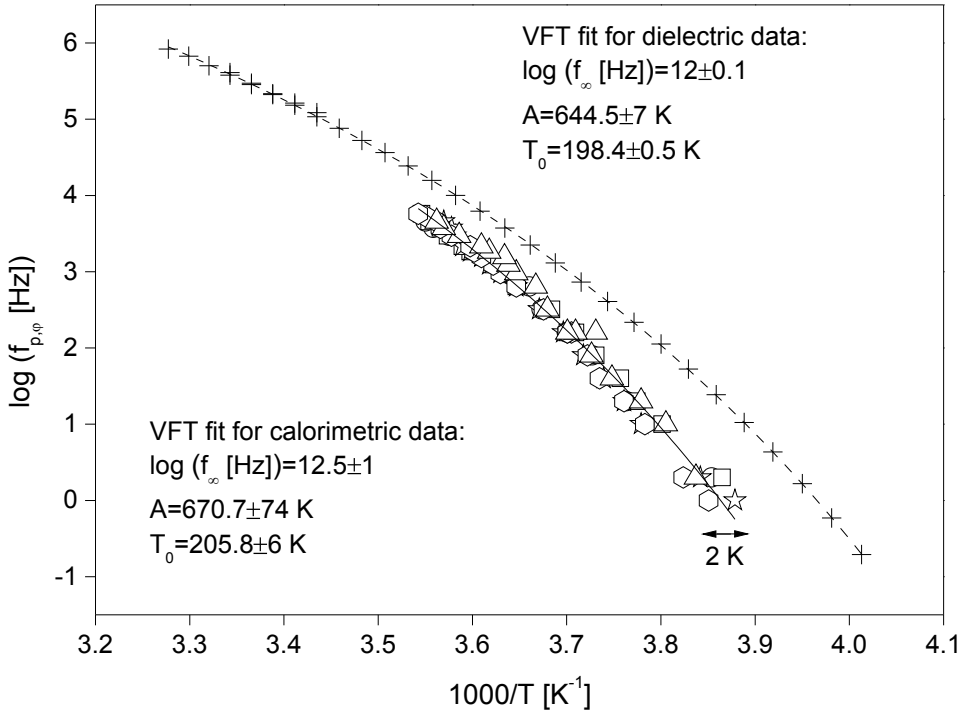

Fig. 54 *Relaxation map for the dynamic glass transition of PVME films: triangles-12 nm, hexagons-58 nm, stars-168 nm, squares-192 nm, circles-218 nm. The crosses correspond to dielectric data for bulk PVME (60 μm). The dashed curve represents the VFT fit to the dielectric data. The solid curve represents the VFT fit to the calorimetric data. All parameters are indicated in the graph. The calorimetric data are determined from the peak position of the phase angle.*

5.4 Glass Transition of Ultrathin Films of A Miscible Polymer Blend

The vast majority of studies on the glass transition of thin polymer films were carried out on homopolymers, whereas only very limited work has been done on the chain dynamics of polymer blend thin films. It would be interesting to investigate the glass transition of polymer blend thin films. We have applied specific heat spectroscopy using differential AC chip-based calorimetry to study the segmental dynamics of miscible polymer blend thin films, which is PS/PVME with a weight fraction of 50/50.

Fig. 55 shows a single T_g in each of the DSC thermograms for the solution-cast films, which confirms the miscibility of the polymer blend film. Broadening effect can be typically observed in many polymer blend systems which can be explained in terms of the dynamic heterogeneity. It is also found for PVME/PS (50/50 wt%) as presented in Fig. 55.

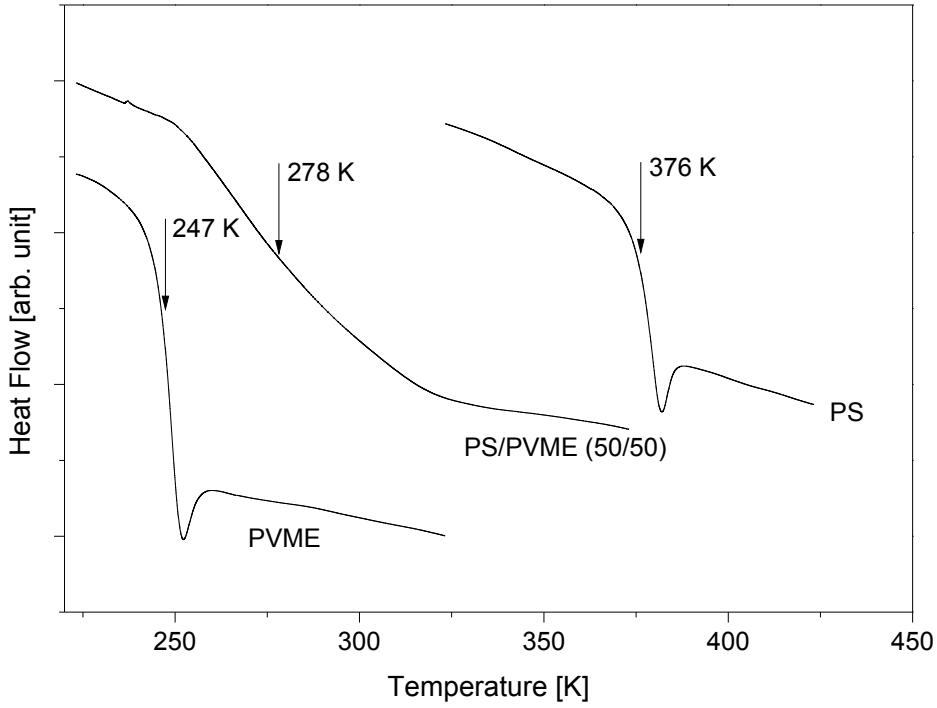

Fig. 55 *DSC curves for solution-cast films of PVME, PS and PVME/PS (50/50 wt%), arrows point to the T_g values.*

Specific heat spectroscopy by means of differential AC chip-based calorimetry also detects a single T_g (Fig. 56), which confirms the miscibility of the blend system in the temperature range under investigation. Additionally, the broadening effect can be also observed like in traditional DSC. Fig. 57 shows the normalized phase angle of the complex differential voltage, which can be simultaneously obtained with amplitude signal of the complex differential voltage during the AC calorimetry measurement, further prove the broadening effect. It is worth mentioning that the measured calorimetric T_g values are higher in the thin films, which were carried out by means of differential AC chip-based calorimetry. It is due to the higher temperature modulation frequency of AC calorimetry (480 Hz) in comparison with the effective frequency of the DSC measurements (e.g. 0.01 Hz). This is in agreement with Ref. 249. The influence of the measurement frequency on the position of the glass transition temperature of a polymer is well described by the empirical VFT-equation [29-31].

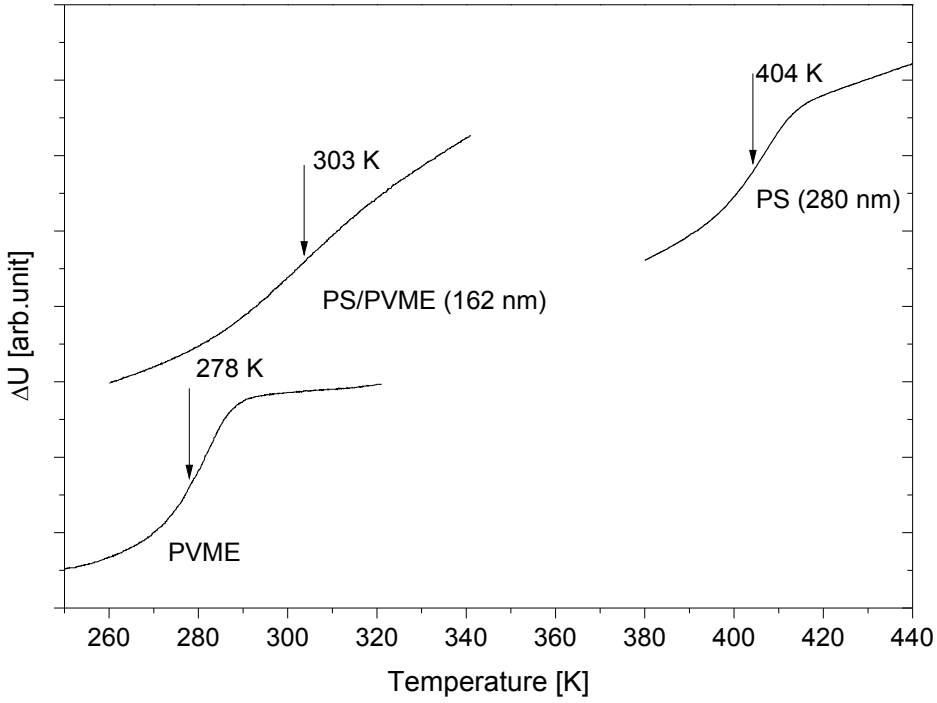

Fig. 56 *Amplitude of the complex differential voltage collected under a heating rate of 2 K/min at a frequency of 480 Hz for PVME, PS and PVME/PS (50/50 wt%) films.*

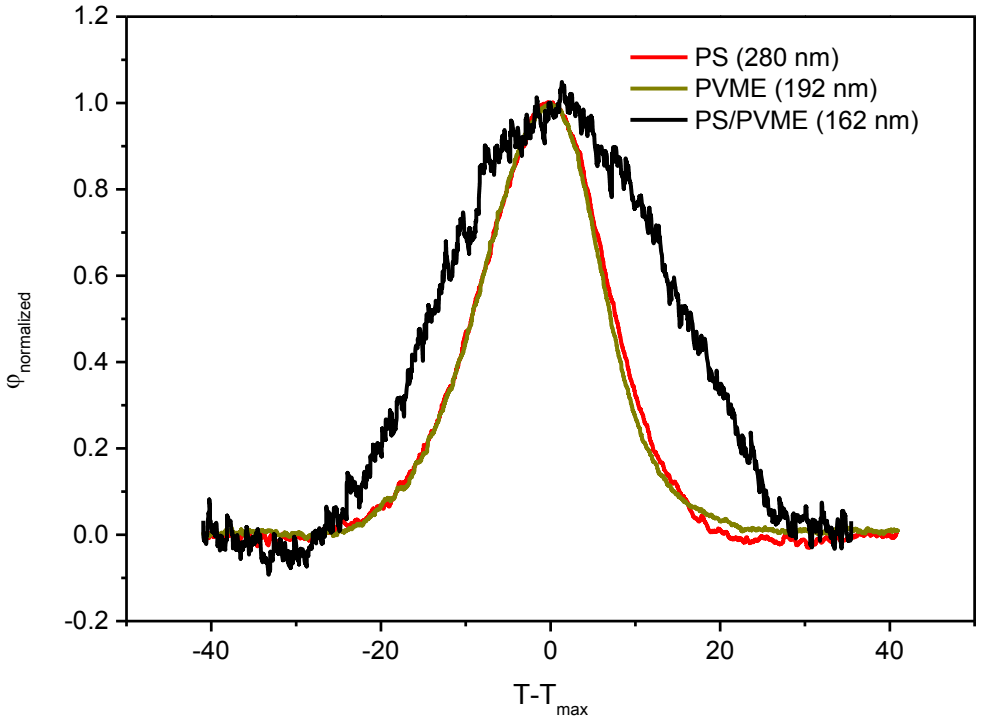

Fig. 57 *Normalized phase angle of the complex differential voltage measured for PVME, PS and PVME/PS (50/50 wt%) films at a scanning rate of 2 K/min at a frequency of 480 Hz.*

Fig. 58 shows the phase angle signal of the complex differential voltage for a series of PS/PVME blend films with the thickness between 11 and 340 nm at a frequency of 320 Hz. It can be concluded that the dynamic glass transition temperature is decreasing with the reduction of film thickness. Dynamic glass transition temperature is plotted as a function of film thickness in Fig. 59. When the thickness is lower than 60 nm, there is a slight increase of dynamic glass transition temperature with increasing the film thickness. When the film thickness approaches 80 nm, the dynamic glass transition temperature jumps to a higher value and seems to reach a plateau for even thicker films.

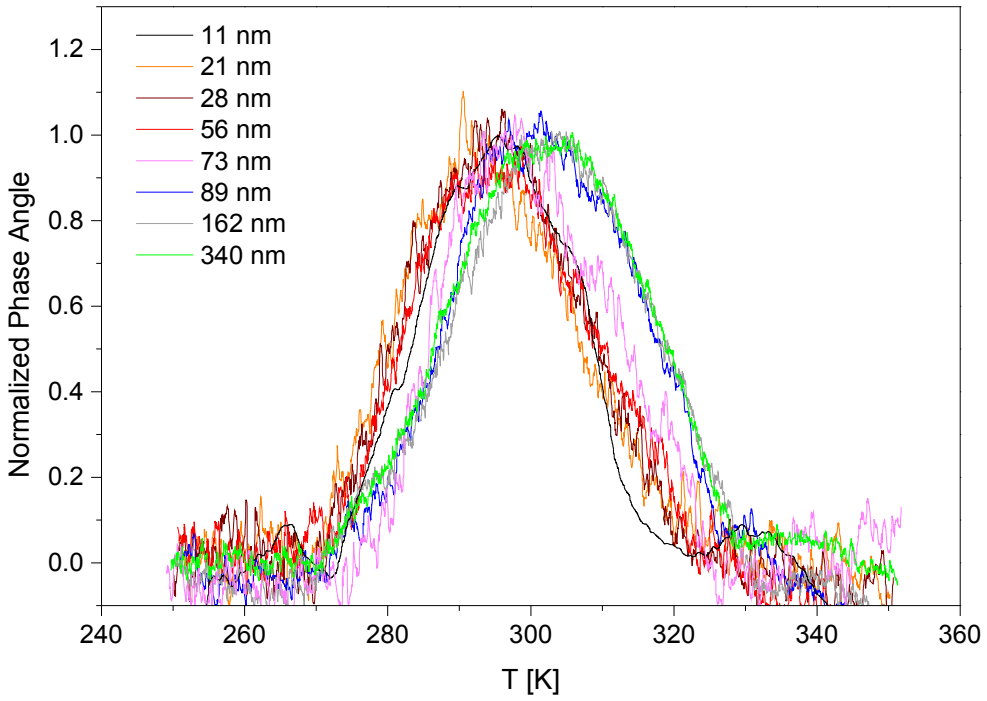

Fig. 58 *Normalized phase angle of the complex differential voltage measured for the polymer blend thin films (PS/PVME 50/50 wt%) with different film thicknesses at the frequency of 320 Hz. The T_g values can be estimated by the peak value from the phase angle. Please note that for the lowest film thickness the curve is obtained after smoothing with adjacent points averaging methods (Origin 8.0, 400 points) to reduce the data scatter due to the essential lower absolute values of the measured voltage.*

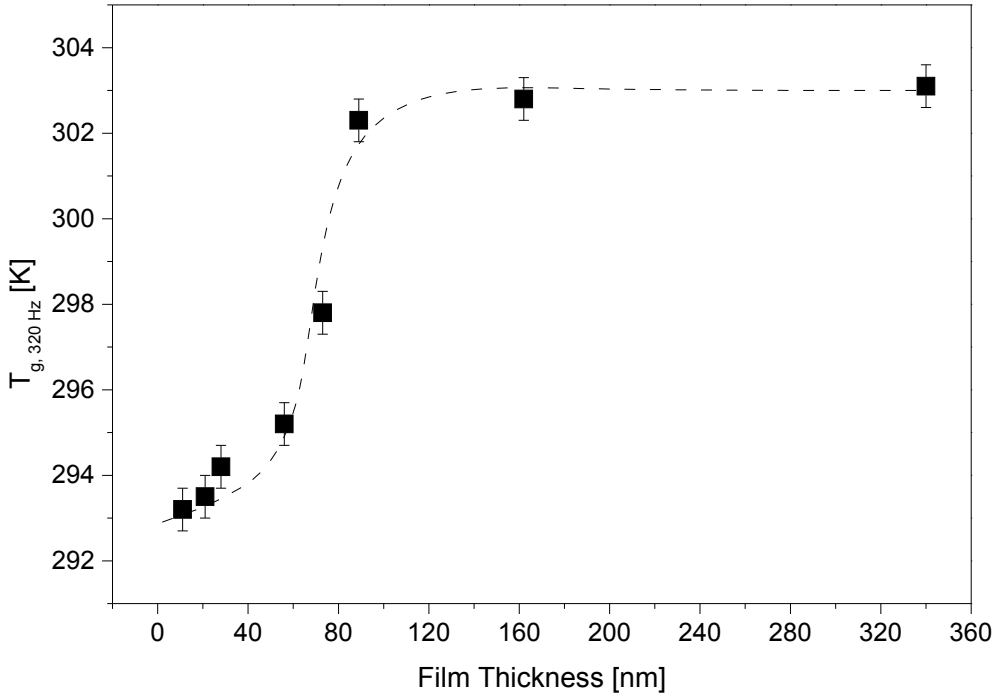

Fig. 59 *Dynamic T_g is plotted as a function of film thickness for thin PS/PVME blend films.*

To analyze the dynamic glass transition temperature for polymer blend thin films with different thicknesses in a wide frequency range, the relaxation map with the film thickness as a parameter is constructed, as shown in Fig. 60. Data for bulk PS/PVME (50/50 wt%) blend measured by means of broadband dielectric spectroscopy are include as well. It can be concluded that the above mentioned relation between dynamic T_g and film thickness holds in the whole frequency range under investigation. The calorimetric data are plotted versus 1/T. The resulting curves can be described by the VFT- equation [29-31].

The VFT-equation describes the calorimetric data quite well even for the thinnest film thicknesses and the lowest frequencies. Moreover, a systematic shift between the relaxation rate determined from specific heat spectroscopy and dielectric spectroscopy is observed as well. It is further observed that the calorimetric data for the thinner films are more close to the dielectric ones. This is consistent with the surface enrichment effect. For thinner films the top surface layer is more mobile than the interior part due to the surface enrichment of PVME component, which is manifested calorimetrically as a shift in the relaxation map.

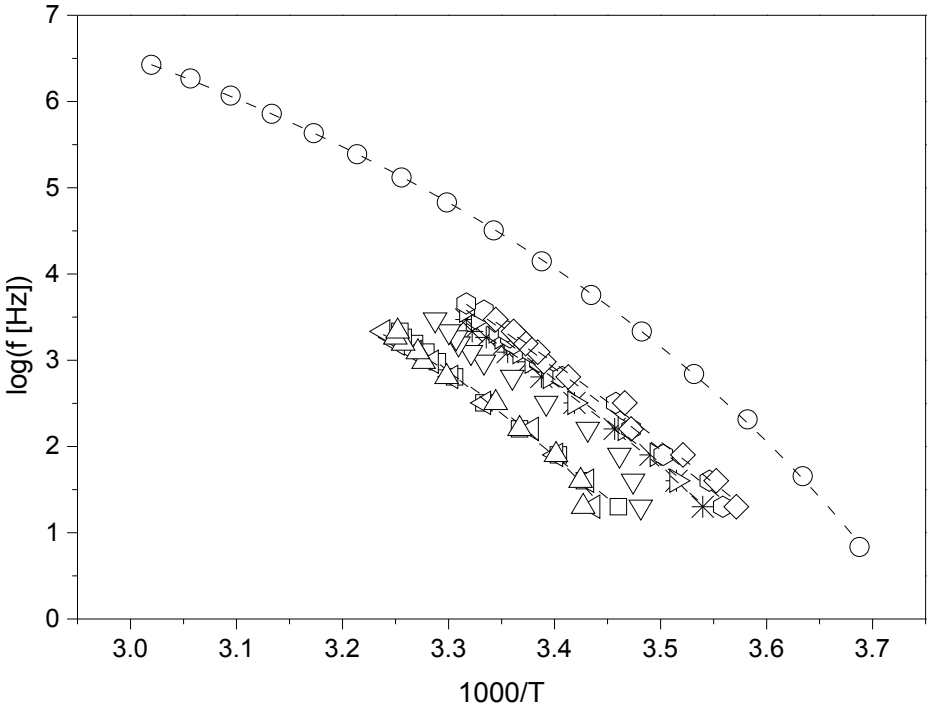

Fig. 60 *Relaxation map for the dynamic glass transition of PS/PVME (50/50 wt%) blend films with different thicknesses: up-pointing triangles-340 nm; left-pointing triangles-162 nm; squares-89 nm; up-pointing triangles-73 nm; stars-56 nm; right-pointing triangles-28 nm; hexagons-21 nm and diamonds-11 nm. The data are determined from the peak position of the phase angle. The circles correspond to the dielectric data for bulk samples. The dashed lines represent the VFT fittings to the data.*

The surface enrichment of polymer blend thin film with the lower surface energy component is widely observed in polymer blend systems. In the present study of PVME/PS system, PVME has a lower surface energy than PS [250]. The free surface enrichment is induced by PVME rather than PS. X-ray photoelectron spectroscopy (XPS) was used to probe the surface composition in order to examine such surface enrichment phenomena. The C1s spectrum for PS/PVME blend film with the thickness around 200 nm is shown in Fig. 61. The spectrum is constituted by the two characteristic spectra of the pure homopolymers. The C1s spectra for pure PVME is a doublet containing contributions from carbon-oxygen (at 286.6 eV) and carbon-hydrogen bonds (at 285 eV) [251]. The C1s spectrum for PS shows only a singlet carbon-hydrogen peak and a small satellite peak at 291.6 eV due to a $\pi \rightarrow \pi *$ shake-up transition [252]. The surface composition can be extracted from the spectrum by resolving the two contributions and calculating the integrated area under each peak. According to

$$\frac{I_{C\text{-}O}}{I_{C\text{-}H}} = \frac{2w/M_V}{8(1-w)/M_S + 3w/M_V}, \qquad (61)$$

the weight fraction of PVME, *w*, can be deduced by calculating the ratio of the peak area corresponding to carbon-oxygen to the total carbon-hydrogen peak area. $I_{C\text{-}O}$ is the integrated intensity of carbon-oxygen peak and $I_{C\text{-}H}$ is the integrated intensity of total carbon-hydrogen. M_V and M_S are the molecular weights of the styrene and vinyl methyl ether monomeric units, respectively. The calculated surface composition of PVME is 84%, which is 34% higher than the bulk value. Since blend composition and molecular weight of the constituents have effects on the degree of surface enrichment, the present result was consistent with many earlier studies which also showed the air/surface enrichment of PVME [250,251,253]. Tanaka et al. further point out that for PS/PVME blend films prepared on hydrophilic SiO substrates the PVME weight fraction at the air-facing surface began to decrease with decreasing film thickness for thickness less than ca. 30 nm. Above 30 nm, the surface enrichment effect is more or less independent of the film thickness.

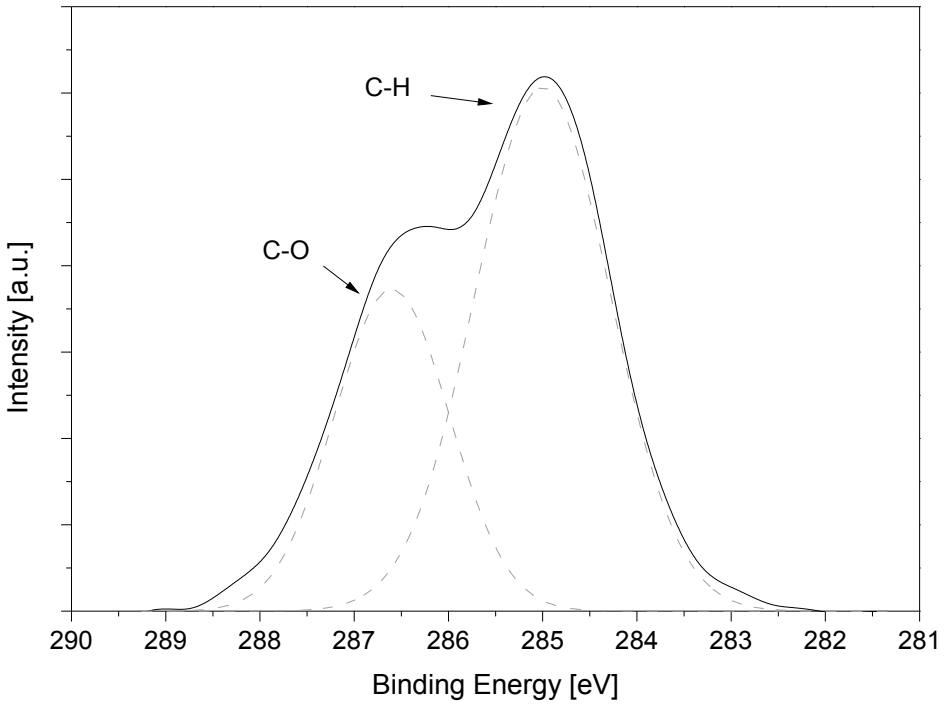

Fig. 61 *XPS C1s core-level spectra for PS/PVME (50/50 wt%) blend film with the thickness of 200 nm.*

6 CONCLUSIONS

It is widely known when polymers are confined to the nanoscale, deviations from bulk properties in terms of the glass transition temperature, physical aging, viscosity and many other aspects are observed. From a technological point of view, the glass transition temperature and the related relaxation behavior of ultrathin polymer films is of great interest in a broad variety of fields like coatings, membranes, organic electronic devices, etc. From the scientific point of view, ultrathin polymer film provides an ideal sample geometry for studying the confinement effects on the glass transition behavior because the confining dimension (film thickness) can be easily tuned by spin coating. To achieve a more complete understanding of the confinement effects on polymer properties is of scientific and technological importance. In this dissertation, the glass transition temperature and the segmental dynamics in homopolymers and miscible polymer blend confined in thin films have been thoroughly studied.

BDS, CSD and SHS were employed to examine the glass transition temperature and segmental dynamics of ultrathin PC films. For ultrathin PC films capped between two aluminium layers an increase of Vogel temperature as well as the glass transition temperature with decreasing film thickness was observed when the thickness is less than 20 nm. Moreover, the segmental relaxation time at a fixed temperature was found to increase for ultrathin PC films (<20 nm) in the dielectric measurements. The dielectric results are discussed in terms of the formation of a interfacial layer of PC segments adsorbed onto the Al electrode due to the strong interaction between the Al and PC layers (2.51 mJ/m^2). The interfacial lay has a reduced molecular mobility with regard to bulk PC behavior. As the dielectric strength is proportional to the number of segments fluctuating on the time and length scale of the dynamic glass transition, it is used as a unique probe of the deviations from bulk behavior. The temperature dependence of the penetration depth of the interfacial interactions on the structural relaxation is further quantitatively determined. The dynamic length scale of the perturbations into the chain conformations responsible for the deviation from bulk behavior is estimated to be smaller than 9 nm. In the calorimetric measurements, no thickness dependency of the segmental dynamics was detected within the experimental error limit for the supported PC films (10-192 nm). The interfacial energy between the PC and the SiO_2 substrate (2.15 mJ/m^2) points to a slightly attractive interaction with limited effect on the reduction of PC segmental mobility near the interface, consistent with the observations.

Furthermore, the width of the glass transition is found to be independent of the film thickness which indicates that the extent of the cooperativity is essentially smaller than 10 nm.

We have used BDS, SHS and CSD to study the glass transition temperature and segmental dynamics as a function of film thickness for Al-supported polystyrene (PS) thin films with three different M_w values (M_w=50 kg/mol, M_w=260 kg/mol, M_w=1408 kg/mol). On the one hand, the segmental dynamics is independent of the film thickness for each M_w in the temperature window of the dielectric measurement. On the other hand, the thermal glass transition temperature decreases with film thickness from several hundreds of nm to 15 nm for the PS films (M_w=1408 kg/mol) and from several tens of nm to 14 nm for the PS films (M_w=260 kg/mol). For the PS film (M_w=50 kg/mol) with the thickness of 11 nm, a slight increase of thermal T_g was observed. These experimental findings indicate that the equilibrium to out-of-equilibrium transition occurring at thermal T_g is not uniquely related to the intrinsic segmental mobility. Additionally, with geometric impact, the nature of the interface, the heating/cooling rate and other factors may also play important roles in the glass transition of thin polymer films. The observations are explained in terms of the formation of irreversibly adsorbed layer onto the Al substrate due to chain adsorption. The influence of M_w and annealing protocol on the T_g deviation in thin films from the bulk value is investigated in detail.

SHS using differential AC chip-based calorimetry in the frequency range typically from 1 Hz to 1 kHz with a sensitivity of pJ/K was employed to study the dynamic glass transition behavior of ultrathin poly(vinyl methyl ether) (PVME) films with thicknesses ranging from 218 nm down to 12 nm. The amplitude and the phase angle of the complex differential voltage as a measure of the complex heat capacity were obtained as a function of temperature at a given frequency simultaneously. Both spectra are used to determine the dynamic glass transition temperature as a function of both the frequency and the film thickness. As the main result no thickness dependence of the dynamic glass transition temperature was observed down to a film thickness of 12 nm within the experimental uncertainty of ±2 K. Further the width of the glass transition is independent of the film thickness which indicates that the extent of the cooperativity is essentially smaller than 12 nm.

SHS was further applied to study the segmental dynamics of miscible polymer blend thin films, which is PS/PVME with a weight fraction of 50/50. The broadening of the glass transition due to blending is observed in a wide frequency range. Film thickness dependence

of the dynamic glass transition temperature is observed, in contrast to the behaviour of homopolymer thin films. In a polymer blend system where the entropic effects are negligible, the surface enrichment of a component with lower surface energy is widely observed. PVME has a lower surface energy compared to PS. PVME preferentially resides at the film surface to decrease the overall free energy of the system. It is well known that the glass transition temperature of bulk miscible polymer blends varies with composition. The resulting surface layer of the film with a PVME-rich environment has higher molecular mobility compared to the bulk-like interior. The faster dynamics of the surface layer exert a dominate influence on the average glass transition temperature of the polymer film with the thickness lower than 80 nm. Differential AC chip-based calorimetry is proved to be a unique and powerful technique to quantitatively determine the surface layer effect on the dynamics of the whole film.

REFERENCES

[1] Walheim, S.; Schäffer, E.; Mlynek, J.; Steiner, U. *Science* **1999,** 283, 520-522.
[2] Lu, G.; Blakesley, J.; Himmelberger, S.; Pingel, P.; Frisch, J.; Lieberwirth, I.; Salzmann, I.; Oehzelt, M.; Di Pietro, R.; Salleo, A.; Koch, N.; Neher, D. *Nature Communications* **2013,** 4, 1588.
[3] Frank, C. W.; Rao, V.; Despotopoulou, M. M.; Pease, R. F. W.; Hinsberg, W. D.; Miller, R. D.; Rabolt, J. F. *Science* **1996,** 273, 912-915.
[4] Reiter, G. *Europhysics Letters* **1993,** 23, 579.
[5] Forrest, J. A.; Dalnoki-Veress, K. *Advances in Colloid and Interface Science* **2001,** 94, 167-195.
[6] Kawana, S.; Jones, R. A. L. *Physical Review E* **2001,** 63, 021501.
[7] Priestley, R. D.; Ellison, C. J.; Broadbelt, L. J.; Torkelson, J. M. *Science* **2005,** 309, 456-459.
[8] O'Connell, P. A.; McKenna, G. B. *The European Physical Journal E* **2006,** 20, 143-150.
[9] Hall, D. B.; Miller, R. D.; Torkelson, J. M. *Journal of Polymer Science Part B: Polymer Physics* **1997,** 35, 2795-2802.
[10] Anderson, P. W. *Science* **1995,** 267, 1615-1616.
[11] Debenedetti, P. G.; Stillinger, F. H. *Nature* **2001,** 410, 259-267.
[12] Donth, E.-J., *The glass transition: relaxation dynamics in liquids and disordered materials*. Springer: Berlin, 2001.
[13] Wang, X.; Zhou, W. *Macromolecules* **2002,** 35, 6747-6750.
[14] Koh, Y. P.; Simon, S. L. *Journal of Polymer Science Part B: Polymer Physics* **2008,** 46, 2741-2753.
[15] Keddie, J. L.; Jones, R. A. L.; Cory, R. A. *Europhysics Letters* **1994,** 27, 59.
[16] Fakhraai, Z.; Forrest, J. A. *Physical Review Letters* **2005,** 95, 025701.
[17] Lupaşcu, V.; Picken, S. J.; Wübbenhorst, M. *Journal of Non-Crystalline Solids* **2006,** 352, 5594-5600.
[18] Priestley, R. D.; Broadbelt, L. J.; Torkelson, J. M.; Fukao, K. *Physical Review E* **2007,** 75, 061806.
[19] Ellison, C. J.; Torkelson, J. M. *Nature Materials* **2003,** 2, 695-700.
[20] Schönhals, A., Molecular Dynamics in Polymer Model Systems in *Broadband Dielectric Spectroscopy*. Kremer, F.; Schönhals, A., eds., Springer: Berlin, 2002, p. 226.
[21] Mijović, J.; Lee, H.; Kenny, J.; Mays, J. *Macromolecules* **2006,** 39, 2172-2182.
[22] Fitz, B. D.; Mijovic, J. *Macromolecules* **1999,** 32, 4134-4140.
[23] Frick, B.; Richter, D. *Science* **1995,** 267, 1939-1945.
[24] Papon, A.; Montes, H.; Hanafi, M.; Lequeux, F.; Guy, L.; Saalwächter, K. *Physical Review Letters* **2012,** 108, 065702.
[25] Birge, N. O.; Nagel, S. R. *Physical Review Letters* **1985,** 54, 2674-2677.
[26] Kremer, F.; Sch nha ls, A., *Broadband dielectric spectroscopy*. Springer: Berlin, 2002.
[27] Schönhals, A., Molecular Dynamics in Polymer Model Systems in *Broadband Dielectric Spectroscopy*. Kremer, F.; Schönhals, A., eds., Springer: Berlin, 2002, p. 102.
[28] Schönhals, A.; Kremer, F., Amorphous Polymers in *Polymer Science: A Comprehensive Reference*, Volume 1. Matyjaszewski, K.; Möller, M., eds., Elsevier, 2012, p. 201-226.
[29] Vogel, H. *Physikalische Zeitschrift* **1921,** 22, 645-646.
[30] Fulcher, G. S. *Journal of the American Ceramic Society* **1925,** 8, 339-355.
[31] Tammann, G.; Hesse, W. *Zeitschrift für anorganische und allgemeine Chemie* **1926,** 156, 245-257.

[32] Angell, C. A. *Journal of Non-Crystalline Solids* **1991,** 131–133, Part 1, 13-31.
[33] Angell, C. A. *Journal of Research of the National Institute of Standards and Technology* **1997,** 102, 171-185.
[34] Williams, M. L.; Landel, R. F.; Ferry, J. D. *Journal of the American Chemical Society* **1955,** 77, 3701-3707.
[35] Ferry, J. D., *Viscoelastic properties of polymers*. 3d ed.; Wiley: New York, 1980.
[36] Bower, D. I., *An introduction to polymer physics*. Cambridge University Press: Cambridge; New York, 2002.
[37] Doolittle, A. K. *Journal of Applied Physics* **1951,** 22, 1471-1475.
[38] Cohen, M. H.; Turnbull, D. *The Journal of Chemical Physics* **1959,** 31, 1164-1169.
[39] Cohen, M. H.; Grest, G. S. *Physical Review B* **1979,** 20, 1077-1098.
[40] Adam, G.; Gibbs, J. H. *The Journal of Chemical Physics* **1965,** 43, 139-146.
[41] Donth, E.-J., *Relaxation and thermodynamics in polymers: glass transition*. 1st ed.; Akademie Verlag: Berlin, 1992.
[42] Donth, E. *Journal of Non-Crystalline Solids* **1982,** 53, 325-330.
[43] Schneider, K.; Schönhals, A.; Donth, E. *Acta Polymerica* **1981,** 32, 471-475.
[44] Donth, E.; Hempel, E.; Schick, C. *Journal of Physics: Condensed Matter* **2000,** 12, L281.
[45] Donth, E.; Huth, H.; Beiner, M. *Journal of Physics-Condensed Matter* **2001,** 13, L451-L462.
[46] Hempel, E.; Hempel, G.; Hensel, A.; Schick, C.; Donth, E. *The Journal of Physical Chemistry B* **2000,** 104, 2460-2466.
[47] Beiner, M.; Kahle, S.; Schröter, K.; Donth, E. *Macromolecules* **1998,** 31, 8973-8980.
[48] Kahle, S.; Korus, J.; Hempel, E.; Unger, R.; Höring, S.; Schröter, K.; Donth, E. *Macromolecules* **1997,** 30, 7214-7223.
[49] Sillescu, H. *Journal of Non-Crystalline Solids* **1999,** 243, 81-108.
[50] Ediger, M. D. *Annual Review of Physical Chemistry* **2000,** 51, 99-128.
[51] Ranko, R. *Journal of Physics: Condensed Matter* **2002,** 14, R703.
[52] Debye, P. J. W., *Polar molecules*. The Chemical Catalog Company, inc.: New York, 1929.
[53] Kohlrausch, R. *Annalen der Physik* **1854,** 167, 179-214.
[54] Williams, G.; Watts, D. C. *Transactions of the Faraday Society* **1970,** 66, 80-85.
[55] Vidal Russell, E.; Israeloff, N. E. *Nature* **2000,** 408, 695-698.
[56] Sinnathamby, K. S.; Oukris, H.; Israeloff, N. E. *Physical Review Letters* **2005,** 95, 067205.
[57] Tracht, U.; Wilhelm, M.; Heuer, A.; Feng, H.; Schmidt-Rohr, K.; Spiess, H. W. *Physical Review Letters* **1998,** 81, 2727-2730.
[58] Jerome, B.; Commandeur, J. *Nature* **1997,** 386, 589-592.
[59] Hall, D. B.; Dhinojwala, A.; Torkelson, J. M. *Physical Review Letters* **1997,** 79, 103-106.
[60] Donth, E. *Journal of Polymer Science Part B: Polymer Physics* **1996,** 34, 2881-2892.
[61] Korus, J.; Hempel, E.; Beiner, M.; Kahle, S.; Donth, E. *Acta Polymerica* **1997,** 48, 369-378.
[62] Wang, C.-Y.; Ediger, M. D. *The Journal of Chemical Physics* **2000,** 112, 6933-6937.
[63] Chang, I.; Fujara, F.; Geil, B.; Heuberger, G.; Mangel, T.; Sillescu, H. *Journal of Non-Crystalline Solids* **1994,** 172–174, Part 1, 248-255.
[64] Donati, C.; Douglas, J. F.; Kob, W.; Plimpton, S. J.; Poole, P. H.; Glotzer, S. C. *Physical Review Letters* **1998,** 80, 2338-2341.

[65] Smith, G. D.; Bedrov, D.; Borodin, O. *Physical Review Letters* **2003,** 90, 226103.
[66] Flory, P. J., *Principles of polymer chemistry*. Cornell University Press: Ithaca, 1953.
[67] Fox, T. G. *Bulletin of the American Physical Society* **1956,** 1, 123.
[68] Gordon, M.; Taylor, J. S. *Journal of Applied Chemistry* **1952,** 2, 493-500.
[69] Sperling, L. H., *Introduction to physical polymer science*. 4th ed.; Wiley: Hoboken, N.J., 2006.
[70] Strobl, G. R., *The physics of polymers : concepts for understanding their structures and behavior*. 3rd ed.; Springer: Berlin ; New York, 2007.
[71] Runt, J. P.; Zhang, X.; Miley, D. M.; Gallagher, K. P.; Zhang, A. *Macromolecules* **1992,** 25, 3902-3905.
[72] Rellick, G. S.; Runt, J. *Journal of Polymer Science Part B: Polymer Physics* **1988,** 26, 1425-1438.
[73] Alexandrovich, P. S.; Karasz, F. E.; Macknight, W. J. *Journal of Macromolecular Science, Part B* **1980,** 17, 501-516.
[74] Cavaille, J. Y.; Etienne, S.; Perez, J.; Monnerie, L.; Johari, G. P. *Polymer* **1986,** 27, 549-562.
[75] Fried, J. R.; Karasz, F. E.; MacKnight, W. J. *Macromolecules* **1978,** 11, 150-158.
[76] Wetton, R. E.; MacKnight, W. J.; Fried, J. R.; Karasz, F. E. *Macromolecules* **1978,** 11, 158-165.
[77] O'Reilly, J. M.; Sedita, J. S. *Journal of Non-Crystalline Solids* **1991,** 131–133, Part 2, 1140-1144.
[78] Mansour, A. A.; Madbouly, S. A. *Polymer International* **1995,** 37, 267-276.
[79] Katana, G.; Kremer, F.; Fischer, E. W.; Plaetschke, R. *Macromolecules* **1993,** 26, 3075-3080.
[80] Mansour, A. A.; Madbouly, S. A. *Polymer International* **1995,** 36, 269-277.
[81] Arbe, A.; Alegría, A.; Colmenero, J.; Hoffmann, S.; Willner, L.; Richter, D. *Macromolecules* **1999,** 32, 7572-7581.
[82] Urakawa, O.; Fuse, Y.; Hori, H.; Tran-Cong, Q.; Yano, O. *Polymer* **2001,** 42, 765-773.
[83] Miller, J. B.; McGrath, K. J.; Roland, C. M.; Trask, C. A.; Garroway, A. N. *Macromolecules* **1990,** 23, 4543-4547.
[84] Roland, C. M.; Ngai, K. L. *Macromolecules* **1991,** 24, 2261-2265.
[85] Alegria, A.; Colmenero, J.; Ngai, K. L.; Roland, C. M. *Macromolecules* **1994,** 27, 4486-4492.
[86] Min, B.; Qiu, X.; Ediger, M. D.; Pitsikalis, M.; Hadjichristidis, N. *Macromolecules* **2001,** 34, 4466-4475.
[87] Hirose, Y.; Urakawa, O.; Adachi, K. *Macromolecules* **2003,** 36, 3699-3708.
[88] Lutz, T. R.; He, Y.; Ediger, M. D.; Cao, H.; Lin, G.; Jones, A. A. *Macromolecules* **2003,** 36, 1724-1730.
[89] Dionísio, M.; Fernandes, A. C.; Mano, J. F.; Correia, N. T.; Sousa, R. C. *Macromolecules* **2000,** 33, 1002-1011.
[90] Schantz, S. *Macromolecules* **1997,** 30, 1419-1425.
[91] Pathak, J. A.; Colby, R. H.; Floudas, G.; Jérôme, R. *Macromolecules* **1999,** 32, 2553-2561.
[92] Schmidt-Rohr, K.; Clauss, J.; Spiess, H. W. *Macromolecules* **1992,** 25, 3273-3277.
[93] Roland, C. M.; Ngai, K. L. *Macromolecules* **1992,** 25, 363-367.
[94] Anastasiadis, S. H.; Fytas, G.; Vogt, S.; Gerharz, B.; Fischer, E. W. *Europhysics Letters* **1993,** 22, 619.

[95] Chin, Y. H.; Inglefield, P. T.; Jones, A. A. *Macromolecules* **1993,** 26, 5372-5378.
[96] Schönhals, A., Molecular Dynamics in Polymer Model Systems in *Broadband Dielectric Spectroscopy*. Kremer, F.; Schönhals, A., eds., Springer: Berlin, 2002, p. 274.
[97] Yin, H.; Schönhals, A., Dielectric Properties of Polymer Blends in *Polymer Blend Handbook*. Wilkie, Charles A.; Utracki, L. A., eds., Springer, 2014.
[98] Colmenero, J.; Arbe, A. *Soft Matter* **2007,** 3, 1474-1485.
[99] Schartel, B.; Wendorff, J. H. *Polymer* **1995,** 36, 899-904.
[100] Katana, G.; Zetsche, A.; Kremer, F.; Fischer, E. W. *ACS Polymer Preprints* **1992,** 33, 122-123.
[101] Zetsche, A.; Fischer, E. W. *Acta Polymerica* **1994,** 45, 168-175.
[102] Meier, G.; Vlassopoulos, D.; Fytas, G. *Europhysics Letters* **1995,** 30, 325.
[103] Schönhals, A., Molecular Dynamics in Polymer Model Systems in *Broadband Dielectric Spectroscopy*. Kremer, F.; Schönhals, A., eds., Springer: Berlin, 2002.
[104] Cendoya, I.; Alegría, A.; Alberdi, J. M.; Colmenero, J.; Grimm, H.; Richter, D.; Frick, B. *Macromolecules* **1999,** 32, 4065-4078.
[105] Jones, R. A. L.; Kramer, E. J. *Polymer* **1993,** 34, 115-118.
[106] Katana, G.; Fischer, E. W.; Hack, T.; Abetz, V.; Kremer, F. *Macromolecules* **1995,** 28, 2714-2722.
[107] Kumar, S. K.; Colby, R. H.; Anastasiadis, S. H.; Fytas, G. *The Journal of Chemical Physics* **1996,** 105, 3777-3788.
[108] Kamath, S.; Colby, R. H.; Kumar, S. K.; Karatasos, K.; Floudas, G.; Fytas, G.; Roovers, J. E. L. *The Journal of Chemical Physics* **1999,** 111, 6121-6128.
[109] Salaniwal, S.; Kant, R.; Colby, R. H.; Kumar, S. K. *Macromolecules* **2002,** 35, 9211-9218.
[110] Lodge, T. P.; McLeish, T. C. B. *Macromolecules* **2000,** 33, 5278-5284.
[111] Chung, G. C.; Kornfield, J. A.; Smith, S. D. *Macromolecules* **1994,** 27, 964-973.
[112] Chung, G. C.; Kornfield, J. A.; Smith, S. D. *Macromolecules* **1994,** 27, 5729-5741.
[113] Keddie, J. L.; Jones, R. A. L.; Cory, R. A. *Faraday Discussions* **1994,** 98, 219-230.
[114] DeMaggio, G. B.; Frieze, W. E.; Gidley, D. W.; Zhu, M.; Hristov, H. A.; Yee, A. F. *Physical Review Letters* **1997,** 78, 1524-1527.
[115] Forrest, J. A.; Dalnoki-Veress, K.; Dutcher, J. R. *Physical Review E* **1997,** 56, 5705-5716.
[116] Prucker, O.; Christian, S.; Bock, H.; Rühe, J.; Frank, C. W.; Knoll, W. *Macromolecular Chemistry and Physics* **1998,** 199, 1435-1444.
[117] Tsui, O. K. C.; Russell, T. P.; Hawker, C. J. *Macromolecules* **2001,** 34, 5535-5539.
[118] Ellison, C. J.; Mundra, M. K.; Torkelson, J. M. *Macromolecules* **2005,** 38, 1767-1778.
[119] Fryer, D. S.; Peters, R. D.; Kim, E. J.; Tomaszewski, J. E.; de Pablo, J. J.; Nealey, P. F.; White, C. C.; Wu, W.-l. *Macromolecules* **2001,** 34, 5627-5634.
[120] Grohens, Y.; Hamon, L.; Reiter, G.; Soldera, A.; Holl, Y. *European Physical Journal E* **2002,** 8, 217-224.
[121] Yamamoto, S.; Tsujii, Y.; Fukuda, T. *Macromolecules* **2002,** 35, 6077-6079.
[122] Sharp, J. S.; Forrest, J. A. *Physical Review E* **2003,** 67, 031805.
[123] Kim, J. H.; Jang, J.; Zin, W.-C. *Langmuir* **2000,** 16, 4064-4067.
[124] Kim, J. H.; Jang, J.; Zin, W.-C. *Langmuir* **2001,** 17, 2703-2710.
[125] Soles, C. L.; Douglas, J. F.; Wu, W.-l.; Peng, H.; Gidley, D. W. *Macromolecules* **2004,** 37, 2890-2900.
[126] Fryer, D. S.; Nealey, P. F.; de Pablo, J. J. *Macromolecules* **2000,** 33, 6439-6447.

[127] Priestley, R. D.; Broadbelt, L. J.; Torkelson, J. M. *Macromolecules* **2005,** 38, 654-657.
[128] Mundra, M. K.; Donthu, S. K.; Dravid, V. P.; Torkelson, J. M. *Nano Letters* **2007,** 7, 713-718.
[129] van Zanten, J. H.; Wallace, W. E.; Wu, W.-l. *Physical Review E* **1996,** 53, R2053-R2056.
[130] Park, C. H.; Kim, J. H.; Ree, M.; Sohn, B.-H.; Jung, J. C.; Zin, W.-C. *Polymer* **2004,** 45, 4507-4513.
[131] Roth, C. B.; McNerny, K. L.; Jager, W. F.; Torkelson, J. M. *Macromolecules* **2007,** 40, 2568-2574.
[132] Yin, H.; Cangialosi, D.; Schönhals, A. *Thermochimica Acta* **2013,** 566, 186-192.
[133] Yin, H.; Napolitano, S.; Schönhals, A. *Macromolecules* **2012,** 45, 1652-1662.
[134] Napolitano, S.; Wubbenhorst, M. *Nature Communications* **2011,** 2, 260.
[135] Grohens, Y.; Brogly, M.; Labbe, C.; David, M.-O.; Schultz, J. *Langmuir* **1998,** 14, 2929-2932.
[136] Glynos, E.; Frieberg, B.; Oh, H.; Liu, M.; Gidley, D. W.; Green, P. F. *Physical Review Letters* **2011,** 106, 128301.
[137] Forrest, J. A.; Dalnoki-Veress, K.; Dutcher, J. R. *Physical Review E* **1998,** 58, 6109-6114.
[138] Forrest, J. A.; Dalnoki-Veress, K.; Stevens, J. R.; Dutcher, J. R. *Physical Review Letters* **1996,** 77, 2002-2005.
[139] Dalnoki-Veress, K.; Forrest, J., A.; de Gennes, P., G.; Dutcher, J., R. *J. Phys. IV France* **2000,** 10, 221-226.
[140] Dalnoki-Veress, K.; Forrest, J. A.; Murray, C.; Gigault, C.; Dutcher, J. R. *Physical Review E* **2001,** 63, 031801.
[141] Roth, C. B.; Dutcher, J. R. *European Physical Journal E* **2003,** 12, S103-S107.
[142] Roth, C. B.; Pound, A.; Kamp, S. W.; Murray, C. A.; Dutcher, J. R. *European Physical Journal E* **2006,** 20, 441-448.
[143] Mattsson, J.; Forrest, J. A.; Börjesson, L. *Physical Review E* **2000,** 62, 5187-5200.
[144] Peter, S.; Meyer, H.; Baschnagel, J.; Seemann, R. *Journal of Physics: Condensed Matter* **2007,** 19, 205119.
[145] O'Connell, P. A.; McKenna, G. B. *Science* **2005,** 307, 1760-1763.
[146] Svanberg, C. *Macromolecules* **2007,** 40, 312-315.
[147] Miyazaki, T.; Inoue, R.; Nishida, K.; Kanaya, T. *European Physical Journal-Special Topics* **2007,** 141, 203-206.
[148] Boucher, V. M.; Cangialosi, D.; Yin, H.; Schonhals, A.; Alegria, A.; Colmenero, J. *Soft Matter* **2012,** 8, 5119-5122.
[149] Fukao, K.; Miyamoto, Y. *Europhysics Letters* **1999,** 46, 649-654.
[150] Fukao, K.; Miyamoto, Y. *Physical Review E* **2000,** 61, 1743-1754.
[151] Hartmann, L.; Gorbatschow, W.; Hauwede, J.; Kremer, F. *Eur. Phys. J. E* **2002,** 8, 145-154.
[152] Serghei, A.; Tress, M.; Kremer, F. *Macromolecules* **2006,** 39, 9385-9387.
[153] Napolitano, S.; Prevosto, D.; Lucchesi, M.; Pingue, P.; D'Acunto, M.; Rolla, P. *Langmuir* **2007,** 23, 2103-2109.
[154] Napolitano, S.; Wübbenhorst, M. *The Journal of Physical Chemistry B* **2007,** 111, 9197-9199.
[155] Serghei, A.; Kremer, F. *Review of Scientific Instruments* **2008,** 79, 026101.
[156] Serghei, A.; Huth, H.; Schick, C.; Kremer, F. *Macromolecules* **2008,** 41, 3636-3639.

[157] Tress, M.; Erber, M.; Mapesa, E. U.; Huth, H.; Müller, J.; Serghei, A.; Schick, C.; Eichhorn, K.-J.; Voit, B.; Kremer, F. *Macromolecules* **2010,** 43, 9937-9944.
[158] Allen, L. H.; Ramanath, G.; Lai, S. L.; Ma, Z.; Lee, S.; Allman, D. D. J.; Fuchs, K. P. *Applied Physics Letters* **1994,** 64, 417-419.
[159] Efremov, M. Y.; Olson, E. A.; Zhang, M.; Zhang, Z.; Allen, L. H. *Physical Review Letters* **2003,** 91, 085703.
[160] Efremov, M. Y.; Warren, J. T.; Olson, E. A.; Zhang, M.; Kwan, A. T.; Allen, L. H. *Macromolecules* **2002,** 35, 1481-1483.
[161] Efremov, M. Y.; Olson, E. A.; Zhang, M.; Zhang, Z.; Allen, L. H. *Macromolecules* **2004,** 37, 4607-4616.
[162] Huth, H.; Minakov, A. A.; Schick, C. *Journal of Polymer Science Part B: Polymer Physics* **2006,** 44, 2996-3005.
[163] Huth, H.; Minakov, A. A.; Serghei, A.; Kremer, F.; Schick, C. *The European Physical Journal Special Topics* **2007,** 141, 153-160.
[164] Zhou, D.; Huth, H.; Gao, Y.; Xue, G.; Schick, C. *Macromolecules* **2008,** 41, 7662-7666.
[165] Paeng, K.; Swallen, S. F.; Ediger, M. D. *Journal of the American Chemical Society* **2011,** 133, 8444-8447.
[166] Pham, J. Q.; Green, P. F. *The Journal of Chemical Physics* **2002,** 116, 5801-5806.
[167] Besancon, B. M.; Soles, C. L.; Green, P. F. *Physical Review Letters* **2006,** 97, 057801.
[168] Frieberg, B.; Kim, J.; Narayanan, S.; Green, P. F. *ACS Macro Letters* **2013,** 2, 388-392.
[169] Kim, J. H.; Jang, J.; Lee, D.-Y.; Zin, W.-C. *Macromolecules* **2002,** 35, 311-313.
[170] Hamon, L.; Grohens, Y.; Holl, Y. *Langmuir* **2003,** 19, 10399-10402.
[171] Ao, Z. M.; Jiang, Q. *Langmuir* **2006,** 22, 1241-1246.
[172] Kremer, F.; Schönhals, A., Broadband Dielectric Measurement Techniques in *Broadband Dielectric Spectroscopy*. Kremer, F.; Schönhals, A., eds., Springer: Berlin, 2002, p. 35-57.
[173] Kremer, F.; Schönhals, A., Theory of Dielectric Relaxation in *Broadband Dielectric Spectroscopy*. Kremer, F.; Schönhals, A., eds., Springer: Berlin, 2002, p. 1.
[174] Kremer, F.; Schönhals, A., Theory of Dielectric Relaxation in *Broadband Dielectric Spectroscopy*. Kremer, F.; Schönhals, A., eds., Springer: Berlin, 2002, p. 6.
[175] Onsager, L. *Journal of the American Chemical Society* **1936,** 58, 1486-1493.
[176] Kirkwood, J. G. *The Journal of Chemical Physics* **1939,** 7, 911-919.
[177] Kirkwood, J. G. *Annals of the New York Academy of Sciences* **1940,** 40, 315-320.
[178] Kirkwood, J. G. *Transactions of the Faraday Society* **1946,** 42, A007-A012.
[179] Fröhlich, H., *Theory of dielectrics: dielectric constant and dielectric loss*. 2d ed.; Clarendon Press: Oxford, 1958.
[180] Landau, L. D,; Lifschitz, E. M., *Course of Theoretical Physics, vol. 5. Statistical Physics*. Akademie-Verlag: Berlin, 1979.
[181] Kubo, R. *Reports on Progress in Physics* **1966,** 29, 255.
[182] Kremer, F.; Schönhals, A., Theory of Dielectric Relaxation in *Broadband Dielectric Spectroscopy*. Kremer, F.; Schönhals, A., eds., Springer: Berlin, 2002.
[183] Kremer, F.; Schönhals, A., Theory of Dielectric Relaxation in *Broadband Dielectric Spectroscopy*. Kremer, F.; Schönhals, A., eds., Springer: Berlin, 2002, p. 12.
[184] Kremer, F.; Schönhals, A., Analysis of Dielectric Spectra in *Broadband Dielectric Spectroscopy*. Kremer, F.; Schönhals, A., eds., Springer: Berlin, 2002, p. 61.
[185] Cole, K. S.; Cole, R. H. *The Journal of Chemical Physics* **1941,** 9, 341-351.
[186] Davidson, D. W.; Cole, R. H. *The Journal of Chemical Physics* **1950,** 18, 1417-1417.

[187] Davidson, D. W.; Cole, R. H. *The Journal of Chemical Physics* **1951,** 19, 1484-1490.
[188] Kremer, F.; Schönhals, A., Analysis of Dielectric Spectra in *Broadband Dielectric Spectroscopy*. Kremer, F.; Schönhals, A., eds., Springer: Berlin, 2002, p. 64.
[189] Schawe, J. E. K. *Thermochimica Acta* **1995,** 260, 1-16.
[190] Haase, R., *Thermodynamics of irreversible processes*. Dover: New York, 1990.
[191] S. V. Herwaarden, application note for Xensor's nanocalorimeter chips of XEN-39390 series http://www.xensor.nl/pdffiles/sheets/nanogas3939.pdf
[192] Minakov, A. A.; Roy, S. B.; Bugoslavsky, Y. V.; Cohen, L. F. *Review of Scientific Instruments* **2005,** 76, 043906.
[193] Minakov, A.; Morikawa, J.; Hashimoto, T.; Huth, H.; Schick, C. *Measurement Science and Technology* **2006,** 17, 199-207.
[194] Bauer, C.; Böhmer, R.; Moreno-Flores, S.; Richert, R.; Sillescu, H.; Neher, D. *Physical Review E* **2000,** 61, 1755-1764.
[195] Hartmann, L.; Fukao, K.; Kremer, F., Molecular Dynamics in Thin Polymer Films in *Broadband Dielectric Spectroscopy*. Kremer, F.; Schönhals, A., eds., Springer: Berlin, 2002, p. 433.
[196] Reiter, G.; Hamieh, M.; Damman, P.; Sclavons, S.; Gabriele, S.; Vilmin, T.; Raphael, E. *Nature Materials* **2005,** 4, 754-758.
[197] Sharp, J. S.; Forrest, J. A. *Physical Review Letters* **2003,** 91, 235701.
[198] Strunskus, T.; Zaporojtchenko, V.; Behnke, K.; v. Bechtolsheim, C.; Faupel, F. *Advanced Engineering Materials* **2000,** 2, 489-492.
[199] Mathieu, H. J.; Datta, M.; Landolt, D. *Journal of Vacuum Science & Technology A* **1985,** 3, 331-335.
[200] Huth, H, Schick C. Personal Communication, 2013.
[201] Hao, N.; Böhning, M.; Goering, H.; Schönhals, A. *Macromolecules* **2007,** 40, 2955-2964.
[202] Alegría, A.; Mitxelena, O.; Colmenero, J. *Macromolecules* **2006,** 39, 2691-2699.
[203] Arrese-Igor, S.; Mitxelena, O.; Arbe, A.; Alegría, A.; Colmenero, J.; Frick, B. *Physical Review E* **2008,** 78, 021801.
[204] Schaefer, J.; Stejskal, E. O.; Buchdahl, R. *Macromolecules* **1977,** 10, 384-405.
[205] Floudas, G.; Higgins, J. S.; Kremer, F.; Fischer, E. W. *Macromolecules* **1992,** 25, 4955-4961.
[206] Havriliak, S.; Negami, S. *Journal of Polymer Science Part C: Polymer Symposia* **1966,** 14, 99-117.
[207] Labahn, D.; Mix, R.; Schönhals, A. *Physical Review E* **2009,** 79, 011801.
[208] Kremer, F.; Schönhals, A., The Scaling of the Dynamics of Glasses and Supercooled Liquids Spectra in *Broadband Dielectric Spectroscopy*. Kremer, F.; Schönhals, A., eds., Springer: Berlin, 2002.
[209] Napolitano, S.; Lupascu, V.; Wubbenhorst, M. *Macromolecules* **2008,** 41, 1061-1063.
[210] Schönhals, A.; Kremer, F., Theory of Dielectric Relaxation in *Broadband Dielectric Spectroscopy*. Kremer, F.; Schönhals, A., eds., Springer: Berlin, 2002, p. 10.
[211] Rotella, C.; Wubbenhorst, M.; Napolitano, S. *Soft Matter* **2011,** 7, 5260-5266.
[212] otella, .; Napolitano, S.; De remer, L.; Koeckelberghs, .; Wübbenhorst, M. *Macromolecules* **2010,** 43, 8686-8691.
[213] Napolitano, S.; Pilleri, A.; Rolla, P.; Wübbenhorst, M. *ACS Nano* **2010,** 4, 841-848.
[214] Peter, S.; Napolitano, S.; Meyer, H.; Wübbenhorst, M.; Baschnagel, J. *Macromolecules* **2008,** 41, 7729-7743.

[215] Kremer, F.; Schönhals, A., The Scaling of the Dynamics of Glasses and Supercooled Liquids Spectra in *Broadband Dielectric Spectroscopy*. Kremer, F.; Schönhals, A., eds., Springer: Berlin, 2002.
[216] Baschnagel, J.; Binder, K. *Macromolecules* **1995,** 28, 6808-6818.
[217] Lipson, J. E. G.; Milner, S. T. *Eur. Phys. J. B* **2009,** 72, 133-137.
[218] Milner, S. T.; Lipson, J. E. G. *Macromolecules* **2010,** 43, 9865-9873.
[219] Napolitano, S.; Rotella, C.; Wübbenhorst, M. *Macromolecular Rapid Communications* **2011,** 32, 844-848.
[220] Napolitano, S.; Wübbenhorst, M. *Polymer* **2010,** 51, 5309-5312.
[221] An alternative explanation to the trend in Fig. 36 is the effect of the nonzero dielectric dissipation of the thin oxide layer present on the surface of the metallic electrodes. The sum of the contribution of the inorganic layer, dielectric constant >9 and almost constant loss ~ 10^{-3}, to the capacitance of the polymer is more relevant in the frequency region where no molecular relaxation is active. However, considering the large value of the residual dielectric strength, the related increase in dielectric loss in between the structural relaxation and the secondary process, should be observed at thicknesses one order of magnitude smaller.
[222] Donth, E.-J., *The glass transition: relaxation dynamics in liquids and disordered materials*. Springer: Berlin, 2001.
[223] Soles, C. L.; Douglas, J. F.; Wu, W. l.; Dimeo, R. M. *Physical Review Letters* **2002,** 88, 037401.
[224] Wubbenhorst, M.; Murray, C. A.; Forrest, J. A.; Dutcher, J. R. In *Dielectric relaxations in ultra-thin films of PMMA: assessing the length scale of cooperativity in the dynamic glass transition*, Proceedings. 11th International Symposium on Electrets, 2002, pp 401-406.
[225] Weyer, S.; Hensel, A.; Schick, C. *Thermochimica Acta* **1997,** 304–305, 267-275.
[226] Saiter, A.; Delbreilh, L.; Couderc, H.; Arabeche, K.; Schönhals, A.; Saiter, J. M. *Physical Review E* **2010,** 81, 041805.
[227] Weyer, S.; Huth, H.; Schick, C. *Polymer* **2005,** 46, 12240-12246.
[228] Jakobsen, B.; Hecksher, T.; Christensen, T.; Olsen, N. B.; Dyre, J. C.; Niss, K. *The Journal of Chemical Physics* **2012,** 136, 081102.
[229] Weyer, S.; Hensel, A.; Korus, J.; Donth, E.; Schick, C. *Thermochimica Acta* **1997,** 304–305, 251-255.
[230] Schönhals, A.; Schick, C.; Huth, H.; Frick, B.; Mayorova, M.; Zorn, R. *Journal of Non-Crystalline Solids* **2007,** 353, 3853-3861.
[231] Van Oss, C. J.; Chaudhury, M. K.; Good, R. J. *Chemical Reviews* **1988,** 88, 927-941.
[232] Lee, L.-H. *Langmuir* **1996,** 12, 1681-1687.
[233] Good, R. J.; Girifalco, L. A. *The Journal of Physical Chemistry* **1960,** 64, 561-565.
[234] Massoro, C.; Le, Q. T.; Pireaux, J. J. *Surface and Interface Analysis* **1994,** 21, 425-429.
[235] Torkelson, J. M.; Priestley, R. D.; Rittigstein, P.; Mundra, M. K.; Roth, C. B. *AIP Conference Proceedings* **2008,** 982, 192-195.
[236] Soles, C. L.; Douglas, J. F.; Wu, W.-l.; Dimeo, R. M. *Macromolecules* **2003,** 36, 373-379.
[237] Serghei, A.; Kremer, F. *Macromolecular Chemistry and Physics* **2008,** 209, 810-817.
[238] Lupaşcu, V.; Huth, H.; Schick, .; W übbenhorst, M. *Thermochimica Acta* **2005,** 432, 222-228.
[239] Yin, H.; Schonhals, A. *Soft Matter* **2012,** 8, 9132-9139.
[240] Yin, H.; Schönhals, A. *Polymer* **2013,** 54, 2067-2070.

[241] oucher, V. M.; angialosi, D.; le gr a, A.; Colmenero, J. *Macromolecules* **2010,** 43, 7594-7603.
[242] Hudzinskyy, D.; Lyulin, A. V.; Baljon, A. R. C.; Balabaev, N. K.; Michels, M. A. J. *Macromolecules* **2011,** 44, 2299-2310.
[243] Perlich, J.; K r stgens, V.; Metwalli, E.; Schulz, L.; e orgii, .; Müller-Buschbaum, P. *Macromolecules* **2009,** 42, 337-344.
[244] Boucher, V. M.; Cangialosi, D.; Alegría, A.; Colmenero, J. *Macromolecules* **2012,** 45, 5296-5306.
[245] Fukao, K.; Uno, S.; Miyamoto, Y.; Hoshino, A.; Miyaji, H. *Physical Review E* **2001,** 64, 051807.
[246] Tsui, O. K. C.; Zhang, H. F. *Macromolecules* **2001,** 34, 9139-9142.
[247] Rotella, C.; Napolitano, S.; Vandendriessche, S.; Valev, V. K.; Verbiest, T.; Larkowska, M.; Kucharski, S.; Wübbenhorst, M. *Langmuir* **2011,** 27, 13533-13538.
[248] Boucher, V. M.; Cangialosi, D.; Alegria, A.; Colmenero, J.; Pastoriza-Santos, I.; Liz-Marzan, L. M. *Soft Matter* **2011,** 7, 3607-3620.
[249] Gotzen, N.-A.; Van Assche, G.; Van Mele, B. *Polymer* **2011,** 52, 4277-4283.
[250] Tanaka, K.; Yoon, J.-S.; Takahara, A.; Kajiyama, T. *Macromolecules* **1995,** 28, 934-938.
[251] Bhatia, Q. S.; Pan, D. H.; Koberstein, J. T. *Macromolecules* **1988,** 21, 2166-2175.
[252] Clark, D. T.; Dilks, A. *Journal of Polymer Science: Polymer Chemistry Edition* **1976,** 14, 533-542.
[253] Pan, D. H. K.; Prest, W. M. *Journal of Applied Physics* **1985,** 58, 2861-2870.

LIST OF ABBREVIATIONS, SYMBOLS AND CONSTANTS

List of Abbreviations

DSC	Differential scanning calorimetry
CSD	Capacitive scanning dilatometry
BDS	Broadband dielectric spectroscopy
SHS	Specific heat spectroscopy
XPS	X-ray photoelectron spectroscopy
AFM	Atomic force microscopy
VFT	Vogel-Fulcher-Tammann-equation
WLF	Williams-Landel-Ferry-equation
KWW	Kohlrausch-Williams-Watts-equation
CC	Cole-Cole function
CD	Cole-Davidson function
HN	Havriliak-Negami function
CRR	Cooperatively rearranging region
TCF	Temperature driven concentration fluctuations
SC	Self-concentration
PC	Poly(bisphenol A carbonate)/Polycarbonate
PS	Polystyrene
PVME	Poly(vinyl methyl ether)
PMMA	Poly(methyl methacrylate)
PPO	Poly(2,6-dimethyl-1,5-phenylene oxide)
M_w	Molecular weight
M_c	Critical molecular weight for entanglements
Al	Aluminum
SiO_2	Silicon dioxide
SiN	Silicon nitride

List of Symbols

T_g	Glass transition temperature
T_0	Vogel temperature
η	Viscosity
τ	Relaxation time

$f_{p,\alpha}$; $f_{p,\beta}$	α-relaxation rate; β-relaxation rate
E_A	Activation energy
c_p	Specific heat capacity
ρ	Density
ξ	Cooperative length of CRR
V_f	Free volume
V	Actual volume
V_0	Theoretical volume
$\mathbf{E}$	Electric field
$\mathbf{D}$	Dielectric displacement
$\mathbf{P}$	Polarization
$\mathbf{P}_\infty$	Induced polarization
$\boldsymbol{\mu}$	Permanent dipoles
ε^*	Complex dielectric function
ε'; ε''	Real and imaginary part of the complex dielectric function
$\Delta\varepsilon$	Dielectric strength
F	Onsager's parameter
g	Kirkwood-Fröhlich correlation factor
ω	Angular frequency
f	Frequency
U_R	Amplitude of the complex differential voltage
φ	Phase angle of the complex differential voltage
θ	Contact angle
γ	Interfacial energy
d	Film thickness

List of Constants

k_B	Boltzmann constant ($k_B = 1.381\times10^{-23}$ m^2 kg s^{-2} K^{-1})
R	Ideal gas constant ($R = 8.314$ $Jmol^{-1}K^{-1}$)
ε_0	Dielectric permittivity constant in vacuum ($\varepsilon_0 = 8.854\times10^{-12}$ $AsV^{-1}m^{-1}$)
N_A	Avogadro number ($N_A = 6.022\times10^{23}$ mol^{-1})

LIST OF PUBLICATIONS

Publications related to thesis

Peer-reviewed journal articles

1. **H. Yin;** S. Napolitano; A. Schönhals, *Molecular Mobility and Glass Transition of Thin Films of Poly(bisphenol A carbonate).* **Macromolecules,** 2012, 45 (3), pp. 1652–1662.
2. **H. Yin;** A. Schönhals, *Calorimetric Glass Transition of Ultrathin Poly(bisphenol A carbonate) Films.* **Soft Matter,** 2012, 8, pp. 9132-9139.
3. **H. Yin;** A. Schönhals, *Calorimetric Glass Transition of Ultrathin Poly(vinyl methyl ether) Films.* **Polymer,** 2013, 54, pp. 2067-2070.
4. **H. Yin;** D. Cangialosi; A. Schönhals, *Glass Transition and Segmental Dynamics in Thin Supported Polystyrene Films: The Role of Molecular Weight and Annealling*. **Thermochimica Acta,** 2013, 566, pp. 186-192.
5. **H. Yin;** A. Schönhals, *Glass Transition and Segmental Dynamics of Ultrathin Poly(bisphenol A carbonate) Films*. VI International Conference Times of Polymers (TOP) and Composites, June 10-14, 2012, Ischia (Na), Italy, **AIP Conference Proceedings,** Volume 1459, 2012, pp. 64-67.
6. V. M. Boucher; D. Cangialosi; **H. Yin;** A. Schönhals; A. Alegria; J. Colmenero, T_g *Depression and Invariant Segmental Dynamics in Polystyrene Thin Films*. **Soft Matter,** 2012, 8, pp. 5119-5122.
7. **H. Yin;** A. Schönhals, *Calorimetric Study of Miscible Polymer Blend Confined in Ultrathin Films*, In Preparation.

Book chapter

1. **H. Yin;** A. Schönhals, *Glass transition of ultrathin polymeric films - A combination of relaxation spectroscopy with surface analytics* in **Dynamics in Confinement,** Series: Advances in Dielectrics, Series Editor: Friedrich Kremer, Springer, 2014.

Other publications

Peer-reviewed journal articles

1. **H. Yin;** R. Mix; J. Friedrich, *Influence of Differently Structured Aluminium-Polypropylene Interfaces on Adhesion.* **Journal of Adhesion Science and Technology,** 2011, 25 (8), pp. 799-818.
2. C. Krause; **H. Yin;** C. Cerclier; D. Morineau; A. Wurm; C. Schick; F. Emmerling; A. Schönhals, *Molecular Dynamics of a Discotic Liquid Crystal Investigated by a Combination of Dielectric Relaxation and Specific Heat Spectroscopy.* **Soft Matter,** 2012, 8, pp. 11115-11122.

Book chapters

1. **H. Yin;** A. Schönhals, *Dielectric properties of polymer blends* in **Polymer Blend Handbook,** Charles A. Wilkie, L. A. Utracki (eds), Springer, 2014.
2. R. Mix; **H. Yin;** Jörg F. Friedrich, *Aerosol-based DBD—A simple way to provide polymers with functional groups for adhesion promotion* in **Recent Advances in Adhesion Science and Technology**, Wojciech (Voytek) Gutowski, Hanna Dodiuk (eds), CRC Press, 2014.

Contributions to conferences

Oral presentations

1. **H. Yin;** A. Schönhals, *Molecular Mobility and Glass Transition of Thin Poly(bisphenol A carbonate) Films,* Spring Meeting, German Physics Society (DPG), Berlin, Germany, 2012.
2. **H. Yin;** A. Schönhals, *Glass Transition and Segmental Dynamics of Ultrathin Poly(bisphenol A carbonate) Films,* 6th International Conference on Times of Polymers (TOP) and Composites, Ischia, Italy, 2012.
3. **H. Yin;** A. Schönhals, *Glassy Dynamics of Ultrathin Polymer Films Investigated by a Combination of Complementary Methods,* Broadband Dielectric Spectroscopy (BDS) and its Application, Leipzig, Germany, 2012.
4. D. Cangialosi; V. M. Boucher; **H. Yin;** A. Schönhals; A. Alegria; J. Colmenero, *Are the Thermal T_g and the Segmental Dynamics in Polymer Thin Films Fully Interdependent?* Broadband Dielectric Spectroscopy (BDS) and its Application, Leipzig, Germany, 2012.
5. **H. Yin;** A. Schönhals, *Calorimetric Glass Transition of Ultrathin Films of Homopolymers and Their Blends,* Spring Meeting, German Physics Society (DPG), Regensburg, Germany, 2013.
6. C. Krause; **H. Yin;** A. Wurm; C. Schick; A. Schönhals, *Glassy-like Dynamics in a Discotic Liquid Crystal Revealed by Broadband Dielectric and Specific Heat Spectroscopy,* 7th International Discussion Meeting on Relaxations in Complex Systems, Barcelona, Spain, 2013.

Poster presentations

1. **H. Yin;** A. Schönhals, *Glass Transition of ultra-thin Polycarbonate Films* 11th Lähnwitzseminar on Calorimetry*,* Rostock, Germany, 2010.
2. **H. Yin;** A. Schönhals, *Calorimetric Glass Transition of Thin Poly(bisphenol A carbonate) Films,* Spring Meeting, German Physics Society (DPG), Dresden, Germany, 2011.
3. **H. Yin;** A. Schönhals, *Glass Transition of Thin Poly(bisphenol A carbonate) Films Studied by Dielectric Spectroscopy,* Spring Meeting, German Physics Society (DPG), Dresden, Germany, 2011.

4. **H. Yin;** A. Schönhals, *Molecular Dynamics of Miscible Polymer Blend Thin Films,* Spring Meeting, German Physics Society (DPG), Berlin, Germany, 2012.
5. **H. Yin;** A. Schönhals, *Specific Heat Spectroscopy on Thin Films of Miscible Polymer Blend (PVME/PS),* 12th Lähnwitzseminar on Calorimetry*,* Rostock, Germany, 2012.
6. **H. Yin;** A. Schönhals, *Calorimetric Glass Transition of Thin Miscible Polymer Blend Films,* 15th International Conference "Polymeric Materials", Halle, Germany, 2012.
7. **H. Yin;** A. Schönhals, *Dielectric Study of Miscible Polymer Blend Thin Films,* 7th Conference of the International Dielectric Society, Leipzig, Germany, 2012.
8. **H. Yin;** D. Cangialosi; A. Schönhals, *Glass Transition and Segmental Dynamics of Ultrathin Polycarbonate and Polystyrene films,*7th International Discussion Meeting on Relaxations in Complex Systems, Barcelona, Spain, 2013.
9. **H. Yin;** A. Schönhals, *Calorimetric Glass Transition of Ultrathin Films of Homopolymers and Their Blends,* 7th International Discussion Meeting on Relaxations in Complex Systems, Barcelona, Spain, 2013.